Biophysical Investigation of *Acanthamoeba castellanii* Interactions with Target Cells and Biomimetic Materials.

Dissertation

submitted in fulfillment of the requirements for the degree of
doctor of engineering sciences (Dr.-Ing.) to the Faculty of Engineering of the
Christian-Albrechts-Universität in Kiel

submitted by

Sören Björn Gutekunst

from Berlin

24. November. 2015

Everything we hear is an opinion,
not a fact.
Everything we see is a perspective,
not the truth.

(Marcus Aurelius)

Dedication:

In deepest love to my family.

1st Reviewer:	Prof. Dr. Christine Selhuber-Unkel
2nd Reviewer:	Prof. Dr. Rainer Adelung
Day of defense:	Wednesday, 27.01.2016

Declaration:

I declare, that I have produced the Dissertation "Biophysical Investigation of *Acanthamoeba castellanii* Interactions with Target Cells and Biomimetic Materials." independently and without improper external assistance and that I have identified all word-for-word quotations of other authors, as well as comments based closely on other authors' ideas, and I have listed the relevant sources.

I am aware that, unless agreed otherwise, the Dissertation produced under supervision represents a group achievement and forms part of the overall research of the supervising institution. As a result, none of the co-authors (e.g. authors of text, creative project staff, co-supervisors) may use passages from the thesis for commercial purposes or make them accessible to third parties without the (written) approval of all those involved due to reasons of copyright. Particular note must be taken of the "Arbeitnehmererfindergesetz" (German Employee Invention Act), according to which pre-publication of patent-related content is prohibited.

Kiel, 24. November. 2015

Sören Björn Gutekunst

Zusammenfassung

Untersuchungen zu Wechselwirkungen zwischen pathogenen Erregern und ihren Wirtszellen sind von großer Bedeutung und deren Verständnis kann dazu beitragen, die medizinische Forschung zu verbessern und neue Heilungsmöglichkeiten zu entwickeln. Eine Infektion, verursacht durch Akanthamöben (*A.*), lässt sich in vier Stufen unterteilen; die Adhäsion, Migration, Phagozytose und Zellteilung. In der vorliegenden Arbeit sollen diese Infektionsstadien mittels biophysikalischer und materialwissenschaftlicher Methoden untersucht werden.

Die ubiquitären *A.*-Spezies sind in der Lage durch Enzystierung widrige Umstände zu überdauern, um später in aktiver Form gefährliche Infektionen, wie *A.* keratitis und granulomatöse Amöben-Enzephalitis (GAE), hervorzurufen. *A.* keratitis ist eine Infektion der Augen, während bei der GAE Bereiche im Gehirn betroffen sind. Diese Organe (Augen und Gehirn) bestehen aus weichem Gewebe mit einem hohen Wasseranteil und einem niedrigen Elastizitätsmodul. Um das Wissen über die Pathogenizität der *A. castellanii* zu vertiefen und neue Heilungsmethoden sowie Forschungsanwendungen zu entwickeln, wurde die Eigenschaft verschiedener Elastizitäten aufgegriffen und untersucht.

So wie eine Infektion, beginnt auch diese Arbeit mit dem Vorgang der Adhäsion. Polydimethylsiloxansubstrate wurden mit einem Elastizitätsmodul von 4 bis 128 kPa hergestellt, um Experimente mit *A. castellanii* durchführen zu können. Das Adhäsionsverhalten der *A.* auf weichen Substraten wurde mit einer vergrößerten Adhäsionsfläche verifiziert und somit besonders bevorzugt. Dies lieferte erste Beweise für das mechanosensitive Verhalten humanpathogener Protisten.

Nach der Adhäsion der Amöben an die Hornhaut *in vivo* breitet sich die Infektion durch Migrationsprozesse problemlos auf die umliegenden Zellgewebe aus. Zur Untersuchung dieser Vorgänge wurde basierend auf einer hydrolysierbaren Matrix ein biomimetisches Konzept von 3D Substraten bestehend aus Polyacrylamid erstellt. Im Gegensatz zu konventionellen porösen Materialien, konnte hier durch ein spezielles Design eine durchgehende Vernetzung auch bei niedrigen Porösitäten gewährleistet werden. Die Elastizität der Probe ist frei wählbar und der Zellmaterialkontakt beträgt bis zu 97 %, bei einer gleichbleibenden guten Nährstoffversorgung. Zum einen können mögliche Kavitäten in

diesem labyrinthartigen Material als Zellfalle genutzt werden, da die Bewegungen von *A. castellanii* reduziert werden und zum anderen können chemotaktische Substanzen für eine gezielte Führung der Zellen eingebracht werden.

Es ist bekannt, dass *A.* ihre Zielzellen durch Phagozytose töten. Zur Quantifizierung der dabei entstehenden Deformationskräfte wurden Partikel synthetisiert und Zellen verwendet, die in ihrer Größe den Zielzellen entsprechen. Eine optische Manipulation von Zellen und Partikeln wurde mit einer optischen Pinzette durchgeführt und mithilfe der Fluoreszenzmikroskopie verfolgt. Bei der Aufnahme von roten Blutkörperchen durch *A. castellanii* konnten Deformationskräfte von mehreren hundert pN detektiert werden. Diese Arbeit zeigt einen ersten Versuch den Verlauf einer Infektion mittels mechanischer Kräfte zu beschreiben und darzustellen, wodurch sie neue Möglichkeiten für Therapieansätze liefert.

Abstract

The investigation of pathogen-host interaction is of major importance to understand biological questions, for medical research, and treatment solutions. The four distinct steps of infections for *Acanthamoeba* (*A.*), i.e. adhesion, migration, phagocytosis, and proliferation, were studied in this thesis using biophysical and materials science methods.

Ubiquitous *A.* species resist unfavourable conditions by encystment and can cause severe diseases like the *Acanthamoeba* keratitis (*A.* keratitis) and granulomatous amoebic encephalitis (GAE). *A.* keratitis is an infection of the eye. GAE occurs in the brain. These organs (eye and brain) are soft tissues with a high water content and low Young's modulus of several kPa. Therefore, *Acanthamoeba castellanii* (*A. castellanii*) were investigated to enrich the knowledge about the pathogenicity of *A.* and affiliated cells and to develop new methods for treatment and research applications.

In this thesis the initial step of infections, the adhesion was presented. Polydimethylsiloxane substrates of 4 to 128 kPa were produced, followed by adhesion experiments of *A. castellanii*. The results featured in bigger cell adhesion areas on softer substrates. This was the first evidence for mechanosensing in a human pathogenic protist.

After adhesion of amoeba to the cornea substrate *in vivo* the infection proceeds with migration on and through cells' tissue. This was observed with biomimetic concept of 3D substrates fabricated from polyacrylamide, which were synthesized with a hydrolyzable template. In contrast to conventional porous materials, an interconnectivity can be maintained via its special design even at low porosities. The stiffness can be varied, a high cell-material contact up to 97 % can be realized, and a good nutrient supply can be achieved. Cavities of this labyrinth structured material can act as cell traps as migration is reduced for *A. castellanii* and chemotactic reagents can be implied to guide cells.

A. are known to kill target cells. For deformation force quantification, particles were synthesized and cells in the size range of target cells were used for phagocytosis experiments. Optical manipulation of cells and particles were acquired with Optical Tweezer and observed with fluorescence microscopy. Observation of deformations of red blood cells during uptake by *A. castellanii* resulted in deformation force of several hundreds of pN. To conclude, these results are a first approach to measure and understand the impact of mechanical forces during an infection and show new opportunities in the treatment.

List of Abbreviations

A. *Acanthamoeba*

A. castellanii *Acanthamoeba castellanii*

A. comandoni *Acanthamoeba comandoni*

***A.* keratitis** *Acanthamoeba* keratitis

AFM atomic-force microscopy

APS ammonium peroxodisulfate

BDA bead deformation assay

BFP back-focal-plane

bidest. double distilled

cAMP cyclic 3',5'-adenosine monophosphate

CCD Charged Coupled Device

DMEM Dulbecco's Modified Eagle Medium

E. hystolytica *Entamoeba hystolytica*

ECM extracellular matrix

EPABs elastic polyacrylamide beads

FBS Fetal Bovine Serum

GAE granulomatous amoebic encephalitis

HCEC-12 Human Corneal Endothelial Cells-12

HEMA 2-hydroxyethyl methacrylate

HLB hydrophilic - lipophilic balance

Laser Light Amplification by Stimulated Emission of Radiation

MMA methyl-2-methylpropenoate

OT Optical Tweezers

PAA polyacrylic acid

PAAm polyacrylamide

PBS phosphate buffered saline

PDF phagocytic deformation force

PDMS polydimethylsiloxane

PEG polyethylene glycol

PMMA polymethylmethacrylate

PYG 712 medium peptone-yeast extract-glucose 712 medium

PTFE poly(1,1,2,2-tetrafluoroethylene)

RBC red blood cell

REF52 wt rat embryonic fibroblasts 52 wild type

RICM Reflection Interference Contrast Microscopy

spp. species

TEMED *N,N,N',N'*-tetramethylethane-1,2-diamine

TFM traction froce microscopy

t-ZnO Zinc oxide tetrapod

Contents

1 Introduction

Like a molecule is related to an atom, multicellular organisms are built from single cells. They are microscopic specialized machineries which evolved to make it possible for men to withstand extreme temperature conditions, cancer, injuries and infections through human pathogens or exposition to hazardous materials. Human infections are related to pathogen microorganisms or viruses, which infect the host cells and try to use them as nutrients, as symbiont or just as reproductive incubators. [1]

Life is all about these interactions, death and survival. For survival, life only knows two possibilities. On the one hand, if the conditions are unfavorable organisms developed to stay immortal. Organisms have to withstand extreme changes and conditions. [A] Like the choice of animals to hibernate in winter and withstand unfavourable conditions. On the other hand, for a habitable environment life uses reproduction. Like the growing of nature in spring and the movement of birds to warmer areas in winter. Besides, there are organisms, which lie in-between these states. Human pathogenes, e.g. borrelia, [2] fungi, [3,4] bacteria, [5] and *Acanthamoeba,* [6] with different morphologies [B] for favourable reproductive or unfavourable immortal conditions. The morphology is the biological classification of structure and form of an organism. [8] These transitions are often energy consuming mechanisms as molecules interact and perform reactions resulting in change and force generation.

The aim of this thesis was to investigate pathogen-host interactions and to get insight into one of the smallest life forms - the cell. Therefore, this dissertation is about the pathogenicity of the human pathogen *A. castellanii* and affiliated cells. The main questions were, if *A. castellanii* employ mechanosensing as their infection is based on the initial contact to soft tissue, is it achievable to measure and evaluate the deformation

[A] For example Tardigrade even withstand outer space without any harm and remain alive.
[B] Morphology: *gr. morf* - form or shape, *ologiā* - the study of something. [7]

and therefore force of an phagocytosis event of a target cell or particle, and is there a possibility to produce a biomimetic 3D substrate to culture, investigate or trap cells within *in vivo* inspired materials? For this effort known and new measurement techniques were established and to gain knowledge about the first and most important step of infections - the adhesion, the second part as the cell-host interaction as well as distribution within a host - migration, and the third component the internalization of cells for nutrients and reproduction of pathogens - the phagocytosis. To reveal some of the underlying secrets of these three parts of a human infection might lead to further insight into one of the smallest building block of life.

- The Cell -

1.1. About the Cell

1.1.1. Cell Interior

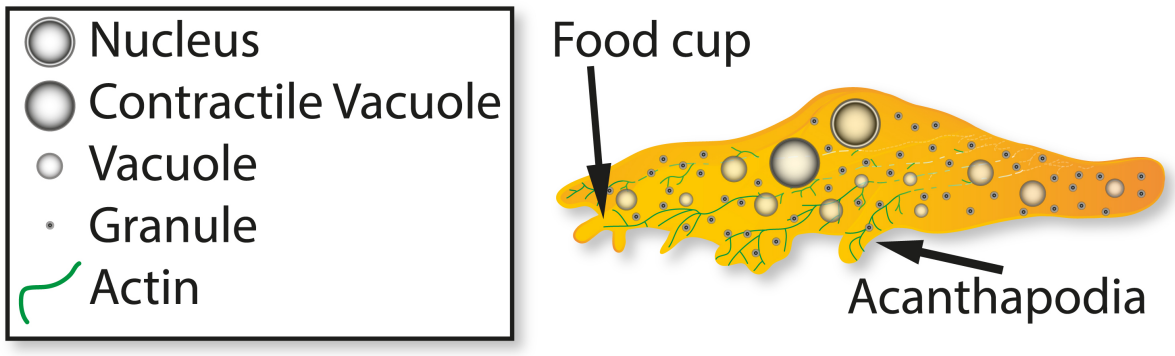

Fig. 1.1.: Cartoon of an amoebic cell structure. The visualized membrane protrusions as the acanthapodia are necessary to sense the environment and are required for cell migration, which is based on actin polymerization. Food cups are utilized for pino- and phagocytosis of liquid and target cells. The nucleus is used for DNA storage and the contractile vacuole equilibrates a cells' water content. Vacuoles contain nutrients as well as lysosomes. [9]

The environmental boundary of a cells' interior to its exterior is its membrane, which is filled with cytosol a visco-elastic fluid. The membrane is used to create a micro-compartment for the intracellular dense and crowded ingredients. [10] A eukaryotic cell[C] is constructed with a nucleus for DNA storage and reproduction (Fig. 1.1). [11]

[C] Eukaryote: eu, *gr. karuōtos* - having nuts, ote.

The golgi apparatus is used for protein vesiculation. The cytoskeleton supports cell shape, function and migration. Vacuoles and particularly the incorporated lysosomes are the counterparts to our gastrointestinal tract and needed for phagocytosis. Mitochondria are discussed as a remaining symbionts' part of evolution from bacteria and produce energy within a single cell.[D]

1.2. Infections

To introduce the three main chapters of this thesis, most important scientific background on adhesion, migration and phagocytosis of *Acanthamoeba* as well as state of the art applications, will be explained in the following sections.

In 1767, Zimmerman published an article about the "Amöbenruhr" in Germany.[12] Nearly 30 years after *A. castellanii* were discovered (Sec. 1.2.1), Culbertson *et al.* found evidence for the cytopathic effects of *Acanthamoeba* on monkey kidney cells and *in vitro* animal killing.[13] This pointed to the findings of GAE by Jager and Stamm in 1972[14] (Fig. 1.3) and further to the identification of *A.* keratitis in 1973. The cyst state of an *A.* keratitis infection in the deep human corneal stroma can resist a treatment with chlorhexidine for more than one year.[15] Drozanski's research related *Acanthamoeba* infections with bacteria in 1956[16] and Krishna-Prasad and Gupta showed pathogenic facultative mycobacteria inside *Acanthamoeba* 1978.[17] Therefore, *Acanthamoeba* are known as the "Trojan Horse" of the microbial environment. Since 1980 it is known through the results of Rowbotham that *Acanthamoeba* and *A. castellanii* are linked to Legionnaires' disease[18–21] as they grow better within *A. castellanii*.[22] In addition, *A. castellanii* adapt over the years to chemicals and become more persistent contrary to heat changes.[23]

These facts and prospects make it important to investigate biophysics of *A. castellanii* for their distinct behaviour and to add potential new treatment strategies for this human pathogen.

1.2.1. *Acanthamoeba*

Complex biological processes involved in pathogenesis of *Acanthamoeba* has been summarized by Khan.[6] These aspects are presented in the following sections for this thesis.

[D] Interestingly, mitochondria are only inherited from our mothers.

Acanthamoeba species (spp.),[24] an overview of many aspects of *Acanthamoeba* biology, and in particular its trophozoites can be characterized with the the aid of the *gr.* prefix "acanth" - spike, which is the so-called acanthopodia from the surface of the *Acanthamoeba* (Fig. 1.1 and 1.2). Acanthopodia or for other spp. named pseudopods are of main importance for adhesion, migration and capturing bait. These spine-like structures are protrusions from the cytoskeleton[25] and maintain amoeboid motion and migration.[26–28] *Acanthamoeba* belong to the kingdom of protists,[E] which means it cannot be restricted to other eukaryotes.

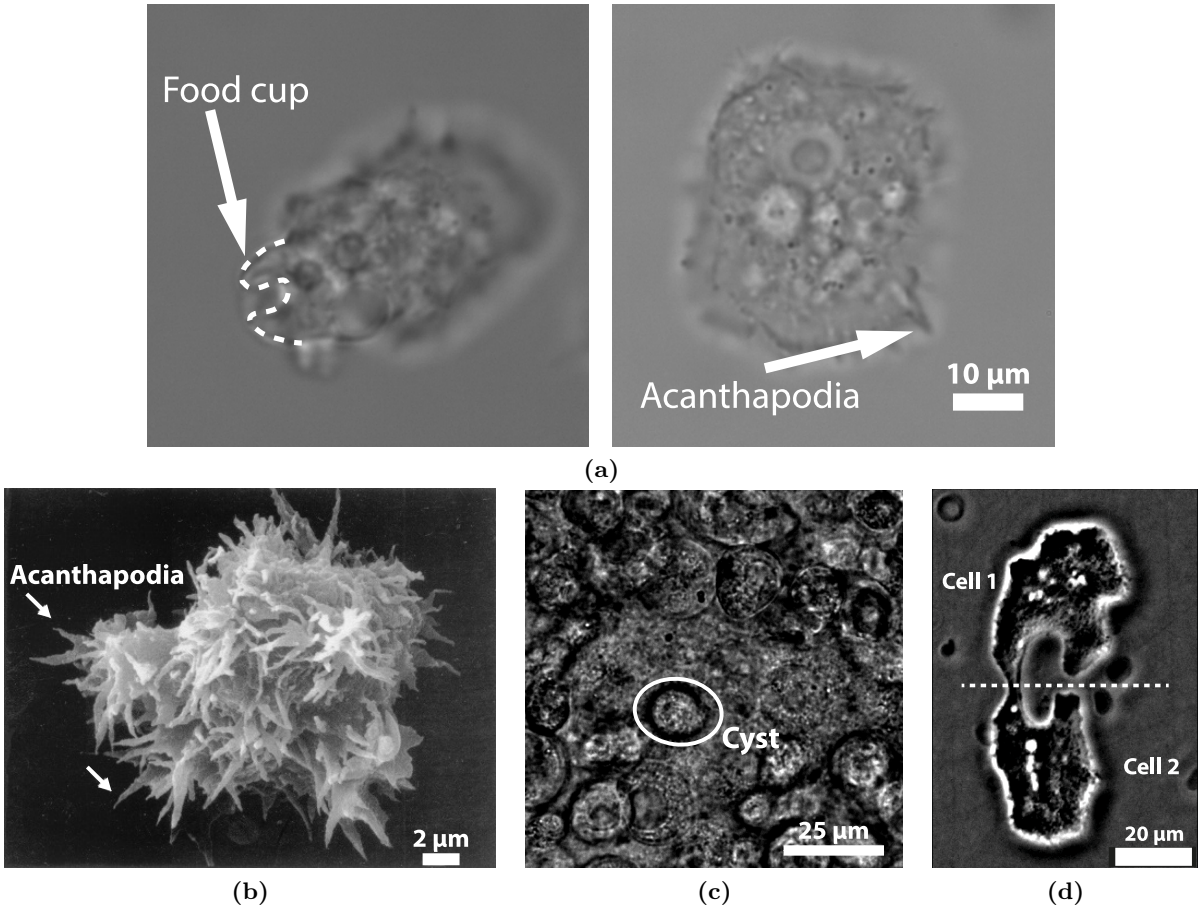

Fig. 1.2.: (a) Bright field image of *A. castellanii* migrating on glass with a formed food cup (left, white dashed line) for medium engulfment and acanthapodia (right). Scalebar = 10 µm (b) SEM image of an *Acanthamoeba* spp. with white arrows indicating Acanthapodia. Scalebar = 2 µm.[29] (c) Phase contrast image of crowded *A. castellanii* cysts under unhabitable conditions (inrease of T, pH, $c_{osm.}$). Scalebar = 25 µm. (d) Mitosis of *A. castellanii* showing the almost separated daughter cells. Scalebar = 20 µm.

[E]Protist: *gr. protiston* - the first of all ones.

The former categories of the sub-kingdom Protozoa[F] and its way to the order of Amoebida with the families of Entamoebidae,[G] Hartmannellidae,[H] and Acanthamoebidae[I] can now be neglected as these traditional classes are only based on morphological characteristics. The new classification is separated by the kingdom of organisms with the five main groups: prokaryotes, fungi, animals, plants and protists. Inside the kingdom of protists are, e.g. Eukaryotes or the Amoebozoa, which are free-living organisms, have a parasitic form like the previously named *Entamoeba*, *Balmuthia* and *Acanthamoeba*.

To understand *Acanthamoeba* morphologies and parts, an illustration of *A. castellanii* trophozoites is presented in Fig. 1.2 (a) and (b). On the left the most important cellular structure for phagocytosis is exemplified - the food cup. A food cup is a membrane deformation and protrusion by involved actin polymerization that is able to include cells or other nutrients as a "membrane mouth".[34–37] The second most important part for phagocytosis and migration are the previously described acanthapodia of trophozoites (Fig. 1.2 (b)). Apart from all of these properties, *Acanthamoeba* spp. have different morphological states with two different morphologies. These states are the active trophozoite as well as the double walled highly resistant cyst state[J] is present under unfavourable conditions (Fig. 1.2 (c)).

Acanthamoeba spp. are divided into 15 genotypes (T1 - T15)[38,39] by means of ribosomal ribonucleic acid (rRNA) sequencing. The gene-specific 18S rRNA (*Rns*) gene[40] amplicon ASA.S1 includes two regions. The conserved stem 29 and highly variable stem 29-1, which is also referred to as the diagnostic fragment 3 (DF3).[41] Moreover, corneal infections are related to T3 - T6, T11 and T15 genotypes, where more than 90 % of isolates of human pathogens belong to the T4 genoytpe.[42,43] Fig. 1.2 (d) demonstrates a proliferation of one *A. castellanii* by mitosis.

Habitat of *Acanthamoeba*

Acanthamoeba spp. are abundant free-living ubiquitous organisms, which can be found in soil[44], drinking-, bottled-, tap-, environmental-water[44], even in dust as well as air,[45,46] and in air conditioner[47] all over the world.[45,48–50]

[F] Protozoa: *gr. proto* - first, *zoa* - animal.
[G] Genus: Entamoeba, *Entamoeba hystolytica* discovered in 1873[30] and named 1903.
[H] Genus: Hartmannella[31].
[I] Genus: Acanthamoeba, discovered in 1930 and named *A. castellanii*[32,33] 1930, and the Genus: Balamuthia.
[J] For social amoeba as *Dictyostelium discoideum* a the third form is the fruiting body.

They survive in dry and cold Antarctica as well as the warm Amazon region. *Acanthamoebae* adhere to many different types of surfaces and can migrate or swim.

1.2.2. *Acanthamoeba* Species, Infection Pathways, and Pathogenicity

Acanthamoeba comandoni (*A. comandoni*) belong to the T9 genotype, were only found in environmental sources and are as far as known no human pathogens.[51] The diameter of a typical *A. comandoni* trophozoite is $30 - 40$ µm and were investigated in this thesis as a control organism for the different behaviour to *A. castellanii*.

The *Acanthamoeba culbertsoni* and *A. castellanii* are human pathogens[29,52] and related to granulomatous amoebic encephalitis (GAE) and *Acanthamoeba* keratitis (*A.* keratitis). The infection pathways of these diseases are graphically displayed in Fig. 1.3.

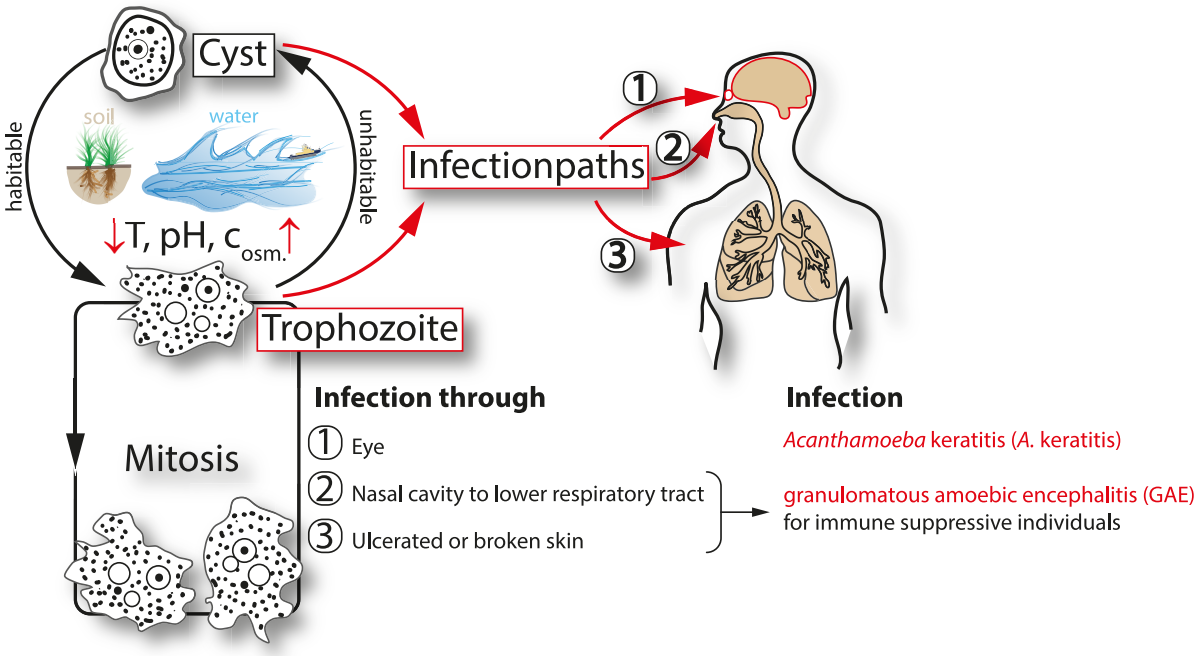

Fig. 1.3.: Distribution and infection pathway of *Acanthamoebae* spp. The *Acanthamoeba* life cycle with the two forms of a cyst and trophozoite. *Acanthamoeba* replicate by mitosis. Infection through the eye (①, *A.* keratitis infection), the nasal passages through inhalation[46] (②, GAE infection), or ulcerated broken skin and skin lesions (③, GAE infection). GAE occurs only in compromised immune suppressive individuals. Adapted form[53].

A. castellanii belong to the T4 genotype[51,54] and therefore are human pathogen and utilize *N*-acetyl-glucosamine on their surface in varying availability and orientation.[55] *A. castellanii* is related to the human pathogen infections *A.* keratitis[56] and

GAE[57] (Fig. 1.3). *A.* keratitis is often connected to eye contact with brackish-water, wrong contact lens use or cleaning procedures.[58] GAE is a serious chronic infection of the brain, but occurs only in individuals with immune deficient systems. Proliferation of *A. castellanii* trophozoites is carried out by mitosis with resulting cells of $20 - 30$ µm in diameter (Fig. 1.2 (d)).

Acanthamoeba spp. have two morphological states. The active trophozoite and inactive doubled walled highly resistant cyst form (Fig. 1.3). Hence, the purpose of a cyst is to resist pH, temperature, osmolality and even ultrasound stress to maintain cell survival. Recent research confirmed that existing and new one-step H_2O_2-based contact lens disinfection solutions does not reliably induce encystment of *A. castellanii* and remains a complex field.[59] Unhabitable conditions are connected with trehalose-6-phosphate synthase necessary for encystment. The resulting encystment is furthermore connected to the cellulose synthase genes for procession of cellulose to build the inner cell wall. This cellulose is linked to the cellobiosidase genes to obtain cellulose degradation to glucose and morphology change under habitable conditions to the active trophozoite state (Fig. 1.3). The infectious *Acanthamoeba* trophozoite states purpose is to adhere, migrate, and proliferate under habitable conditions. Nutrients can either be internalized with pino- or phagocytosis (Sec. 1.4).

1.2.3. Contact Lens and Polymer Adhesion

Contact lenses were developed by Heinrich Wöhlk from Kiel. To increase the wearing ability, he rounded the edge of each lens made of acrylic glass and reduced the size to one of an iris and further optimizations were performed.[60] A major challenge was the reduced oxygen diffusion, wettability and the increased infection possibility.[61] Therefore, the material was later changed to soft hydrogel materials[62] with strict cleaning procedures.[63] This advantages directed to the success for nowadays contact lenses.[64,65] Contradictory, this medical tool increases the chance to infect a hosts eye with *A.* keratitis drastically and gives easier access for human pathogens as *A. castellanii*, because a corneal trauma can be induced due to daily insertion and removing of contact lenses,[66] result of wrong contact lens use, insertion overnight or swimming with contact lenses[67,68] (Sec. 1.2), and especially soft contact lenses.[69] As a consequence of these developed wearable optical aids *A. castellanii* adhesion and migration to comparable materials (Chapter 3 and 4)

and phagocytosis experiments with many altering samples were realized (Chaper 5) (Fig. 1.4).

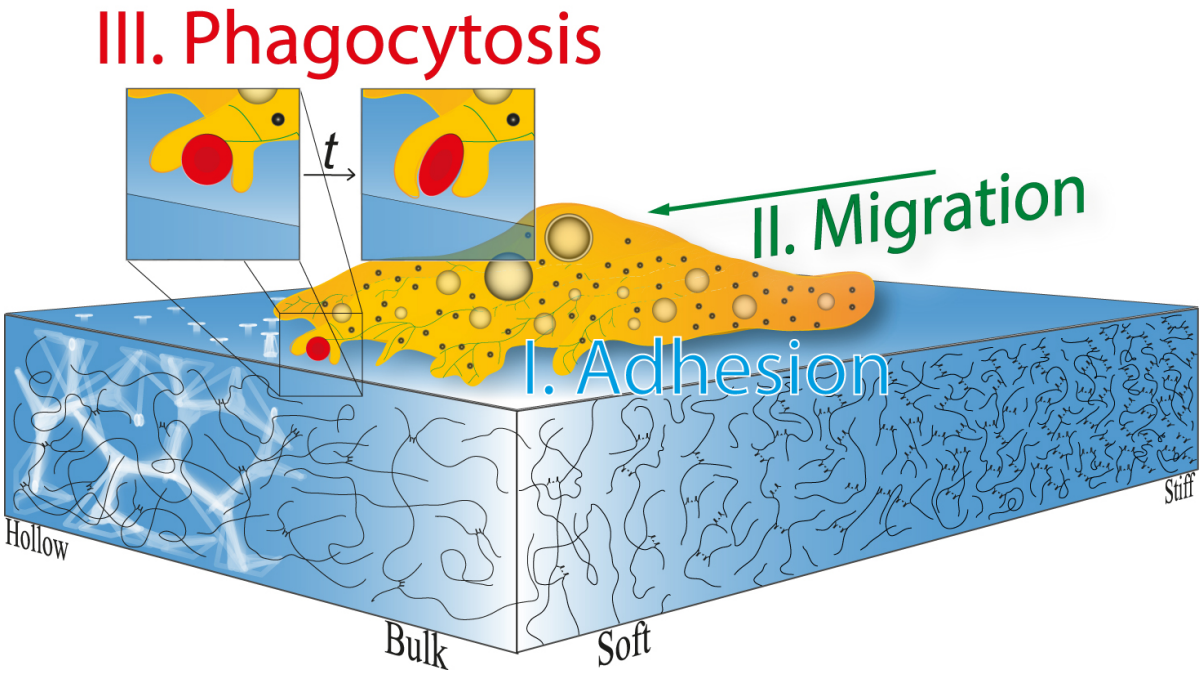

Fig. 1.4.: Graphical abstract of the three main projects of this thesis: adhesion, phagocytosis, and migration of *A. castellanii*. A comparison of soft and stiff as well as hollow and bulk substrates have been conducted with cells for adhesion (Sec. 3) and migration (Sec. 4) studies. The zoom depicts the expected deformation of a sample (red) during phagocytosis (Sec. 5) with a force exerting food cup. The green lines show actin polymerisation and depolymerization at the dorsal end (dotted line) as the cell is migrating towards the lower left corner of the polymer substrate by pushing the ventral part with acanthapodia.

1.3. Migration and Motility

After the initial step of adhesion with its surface interaction and cell spreading, *Acanthamoeba* spp. start to migrate on surfaces. In Fig. 1.5 a strongly visible bright halo around the *Acanthamoebae* is observable, showing that they are not spreading in a flat manner on the surface, but keep an ellipsoidal shape.

The mechanism of amoeboid motion is caused by variations in actin de- and polymerization (Fig. 1.4) and intracellular transport. Actin depolymerisation occurs at the dorsal end of the cell to provide and maintain cell movement. The free actin is transported to the ventral part and consumed to form polymer rods with branches of actin in a 70° angle.[70,71] This pushes the cell membrane towards the ventral edge, while the

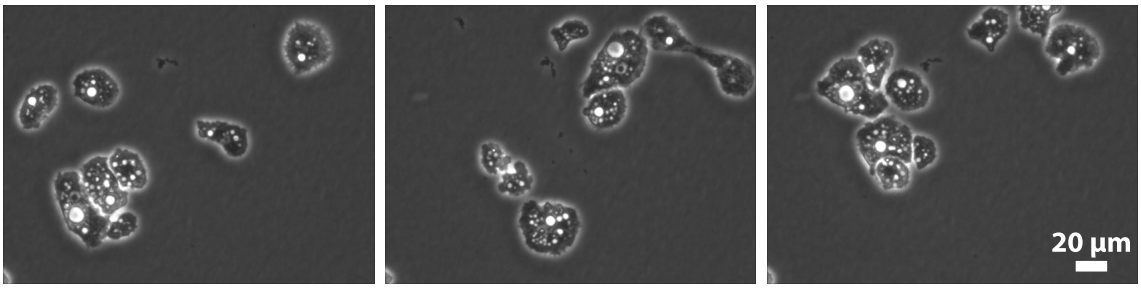

Fig. 1.5.: Phase-contrast images of moving *A. castellanii* on a petri-dish at different time steps. Scalebar = 20 µm.

cytoskeleton and microtubule keep the cells shape. This energy consuming mechanism leads to cell migration and can be used in *Acanthamoeba* to form acanthapodia to reach target cells for phagocytosis (Sec. 1.4).[72]

1.4. Phagocytosis and Target Cell Killing

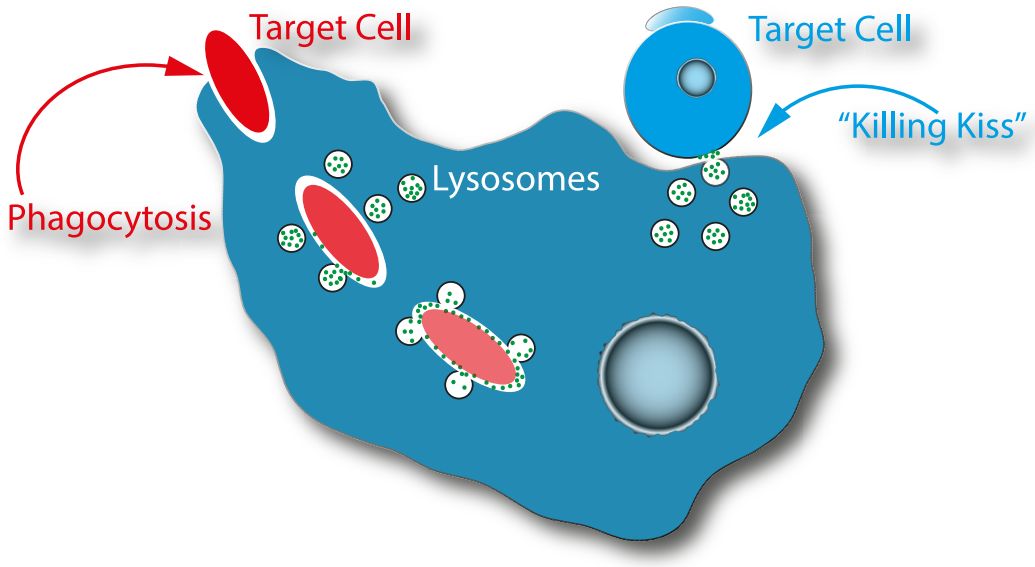

Fig. 1.6.: The two pathways of cell killing in *Acanthamoeba*. The left depicts the phagocytosis event of a target cell (red). The target cell is lysed by enzymes (lysosomes, green granules). On the right, a "killing kiss" is presented, which is an exocytic killing of a target cell (blue) through membrane protruding lysosomal enzymes (green granules). Adapted from[73].

Phagocytosis[K] represents the engulfment of nutrients and target cells into a cell for cell killing and further digestion. For *Acanthamoeba*, there are two known pathways of cell killing.

[K]Phagocytosis: *gr. phagein* - to devour, *gr. kytos* - cell, *gr. osis* - process.

On the one hand, an *Acanthamoeba* can form a so called "food cup" made from the cell membrane to enclose a target cell (Fig. 1.6). Encapsulation and internalization of the target cell into a formed food vacuole. Michalek *et al.* showed that acanthaporines a pore-forming toxin of *Acanthamoeba culbertsoni* is related to cell killing of human neuronal cells [74,75] or for cell death.

On the other hand, a mechanism called the "killing kiss" is a fast exocytosis of a target cell with membrane protruding lysosomal enzymes. Moreover, for *Entamoeba hystolytica* (*E. hystolytica*) another mechanism is hypothesized and is called "trogocytosis" [76,77][L] (Sec. 1.5).[76] The nibbling at target cells by other organisms is not directly connected cell killing. In both cases, of the phagocytosis and the "killing kiss", infections of a human host are caused by *A.* keratitis or GAE (Sec. 1.2.1). The description of the *Acanthamoeba* genome shows it possesses the superoxide-generating NADPH oxidase and lysozyme, which promotes the lysosomal pathway (Fig. 1.6) and is necessary for *Acanthamoeba* phagocytosis and "killing kiss" mechanism.[78] Through intra- and intercellular lysosomal cell killing a target cell starts a programmed cell death (apoptosis) and is digested or nibbled to death in the case of *E. hystolytica*. This lysis mechanism is only accessible for amoeba spp. to target cells and intercellular between *Acanthamoebae* as they might have a different membrane structure not yet observed. Toney *et al.* showed that a treatment of cycloheximide or cytochalasin D in normal human serum increased the susceptibility to complement lysis.[79] Furthermore, *A. castellanii* could have an "transport-dependent extracellular matrix as well as the presence of complement inhibitory surface proteins".[79]

1.5. State of the Art: Methods for Movement, Forces and Optical Manipulation

The opportunistic *Acanthamoeba* spp. are ubiquitous organisms and therefore, as well as increasing infection rates with pathogenic amoebae, it is of great interest to develop curing agents and treatment solutions.[45,49,50] Highest interest should not only lie on treatment solutions but also on the reduction of the infection chance.[44] Infections with *A.* keratitis[56] are strongly related to wearing of soft contact lenses[69,80,81] and in advance to corneal trauma as explained in Sec. 1.2.3. Maybe due to the locomotion and feeding

[L] Trogocytosis: *gr. trogo* - to gnaw or nibble, *gr. kýtos* - bulge, curvature or *anc. gr. kútos* - cell, *gr. ōsis* - to process or action.

of *Acanthamoeba* at the water air-interface,[82] the infection risk increases with the use or swimming in water.

For diagnosis of an infection with pathogenic free-living amoebae[83] different diagnosis tools are possible. Current procedures are the scraping of contact lens cases,[84] making use of the autofluorescence of *Acanthamoeba*,[85] as well as simple morphology analysis from cornea samples. Still an *A.* keratitis can easiliy be misdiagnosed an not linked to amoeba.

Treatment against *A.* keratitis in the encysted stages are propamidine isothionate (0.1 %, every hour to the eye), polyhexamethylene biguanide (0.02 %, drops every hour) with chlorhexidine (0.02 %),[86] gentamicin (1.5 % every hour) with systemic antibiotics ciprofloxacin, intraconazole (~1 month), or topical neosporin.[20,87–94] Some patients may require a corneal graft or in a late resistant stadium full enucleation.[87] The treatment time is in the timescale of about 20 weeks or with the use of topical steroids around 38.5 weeks.[95] These treatments are successful in most cases, when the infection is diagnosed within 1 month.

GAE treatment is performed with a combination of ketoconazole, rifampin, and trimethoprim/sulfamethoxazole[96] or sulfadiazine and fluconazole[97] but in these systemic infections the disease is often incurable. Affiliated cells like *Balamuthia mandrillaris* found in soil[98] or environmental sources[99] and *Naegleria fowleri*[M] are connected to the fatal meningoencephalitis[100] or *Acanthamoeba polyphaga* were related to encephalitis.[101]

A new treatment method could be to exploit the intracellular *A. castellanii* shikimate[N] for aromatic amino acid syntheses and a possible antimicrobial treatment solution.[103] This long time and sometimes useless treatment options, when the infection is too late related to *Acanthamoeba*, make it important to reduce the chance for infections as the infection rates are increasing. techniques for demonstrating cell death.[75,104]

The adhesion of many cells depends on mechanical properties of their natural and artificial tissues.[105–107] As *A.* keratitis is connected to the use of contact lenses and the adhesion of *A. castellanii* has to be linked to the used polymers in contact lenses as hydrogel, silicones or its' composites. Substrates made from the biocompatible polydimethylsiloxane (PDMS)[108,109] have been frequently used in cell culture and therefore are a reliable

[M] *Naegleria fowleri* are also called "brain eating amoeba".

[N] "The shikimate pathway links metabolism of carbohydrates to biosynthesis of aromatic compounds." [102]

tool for cell adhesion on microstructures.[110,111] Glass coatings for PDMS microfluidic channels,[112] PDMS with tunable elastic modulus to study cell mechanobiology,[113] and nanostructuring for a change in wetting, hydrophobic recovery and protein absorbtion [114] was developed.

Cells can react to changes in surface properties[115,116] by active probing of the interface.[117] Surface instabilities may have an influence on membrane substrate interface.[118] Stem cell differentiation[119,120] and tumor cells for example are influenced by surface stiffness (related to Sec. 3).[121] This is one of the reasons why tissue engineering becomes highly relevant for cell culture studies.[122–125]

1.6. Dependence of Substrate Stiffness

Engler *et al.* investigated mesenchymal cell differentiation on polymer samples with different elasticities.[119] They determined cell proliferation from naive cells into certain cell types in dependence of the used substrate, e.g. naive mesenchymal cell lines differentiated with soluble inducing factors to osteoblasts' morphology on a sample of 25 - 40 kPa,[119] which is the natural stiffness crosslinked collagen of osteoids (Fig. 1.7).

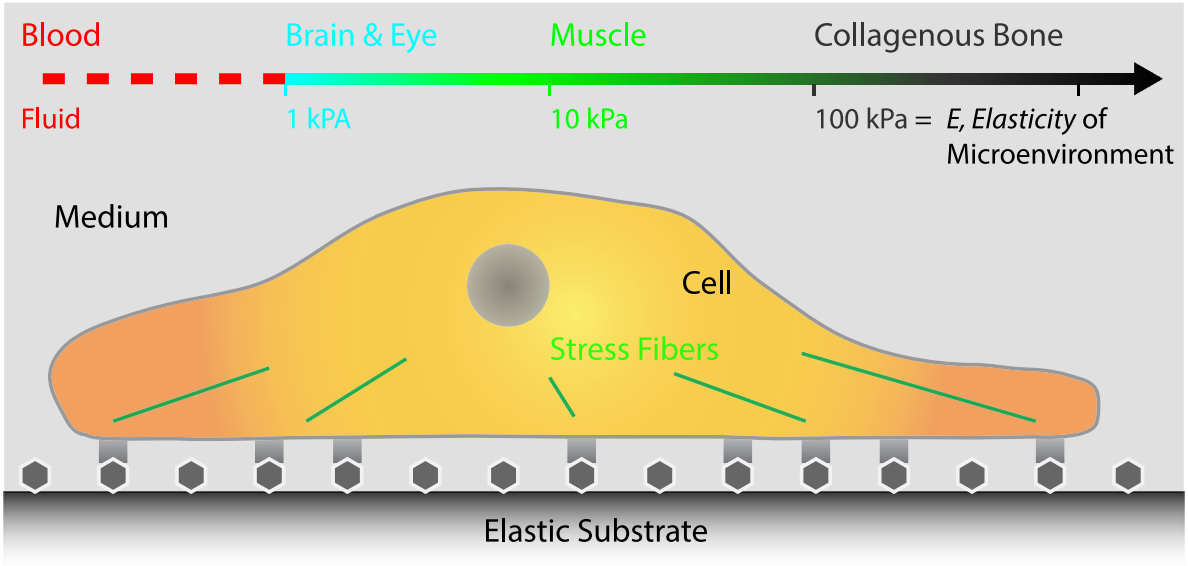

Fig. 1.7.: Influence of substrate stiffness on cell adhesion and spreading. Adapted from Engler *et al.*[119]

This related the stiffness properties of substrates to cell differentiation and therefore leads to investigation into changes of cell properties on polymer substrates. In advance, it gave hints towards the previously described mechanosensing for cells (Sec. 3). Because

A. castellanii adhere to soft substrates due to their infection pathway it was interesting to test if *A. castellanii* have mechanosensing abilities as mechanosensing is not completely understood and not observed in human pathogenic protists.

On tissues, pathogenic cells can not only adhere but also migrate for better proliferation in a host. Therefore, Amoeba and affiliated cells have their own way of migration, which is called amoeboid motion.[126,127] Sackmann *et al.* for example investigated the cell-surface interface of *Dictyostelium Discoideum* and presented the connection between crawling, locomotion and adhesion.[128] Focal sites of *Dictyostelium* were discussed by Gebbie *et al.*[129] Moreover, Amselem *et al.* showed chemotactic migration of *Dictyostelium* cells with microfluidic devices.[130] Viscoelastic fluids[131], intracellular microrheology,[132] "focal contacts" in amoeba locomotion on glass,[133–135] and geometry-driven polarity of amoeboid cells[136] are fundamental to comprehend amoebic adhesion and migration. Mesenchymal stem cells for instance increase their amoeboid migration speed in confinements.[137,138] Zebrafish embryos migrate within a cortical flow in a fast amoeboid motion combining mesenchymal like and blebbing motion due to increasing myosinII activity.[139] This suits to Chan *et al.* recent research as they proved cell softening through myosinII activity,[140] because softer cells might migrate faster as they can deform their membrane more easily. Studies on *E. hystolytica* revealed a big difference in immune responsive cells. Lymphocytes nibble on cells, which does not particularly lead to cell killing but amoebic trogocytosis[76] of *E. hystolytica* does.[77] In addition, it defines its cause as the fatal diarrheal disease (amoebiasis) and its tissue invading abilities, but gives a possibility for treatment.[76] To study amoebiasis by *E. hystolytica* an ex-vivo human intestinal model was designed because humans are the only known host for amoebiasis and therefore no animal tests can be performed.[141] Cell lysis was tested by lactate dehydrogenase, but no colon infection from *Entamoeba dispar* (non-pathogen cell) in contrast to *E. hystolytica* was observed.

This is potentially relevant for *Acanthamoeba* as most of this recent research is not yet connected to *Acanthamoeba*. For several decades, cells have been cultured on 2D substrates as agar plates for bacteria and cells, but it is proven that cells grow more natural on 3D tissues[142,143] as the extracellular matrix (ECM) of cells is often 3D. Many cell types grow in 3D structures as organs like the brain, eye, and liver, when they are not directly involved into interface functions as the lung for carbondioxide exchange

with oxygen or arteries for blood stream distribution. The extracellular environment has a physical influence on cell migration in complex tissues. [144]

To provide 3D biomimetic networks for cell studies, [145] different approaches were utilized as brushes, [146] or pillar structures, [147] although they only represent a topographical structured 2D environment, but not a true 3D environment (related to Sec. 4). [28] Rapid prototyping and other methods used to produce real 3D substrates are summarized in Tab. 1.2. Most of these procedures have in common that they need special equipment, are expensive, and have a high fabrication time. Biomaterials such as matrigel, [148] Poly(Lactide-co-Glycolide) scaffolds, [148–152] 3D alginate hydrogels, [153,154] compressible alginate carboxymethyl copolymers, [155] hydrogels, [156] and biodegradable materials [151,157–161] have proposed interesting strategies and are of major importance for cell studies. The migration of cells through these confinements is probably hindered most by the cells' nucleus, [162] its properties, [163] and deformability. [164] Cells are guided on 2D and through 3D structures by a mechanosensing mechanism, [165] i.e. there is a geometry depending leader cell formation in collective behaving epithelial cells. [166] Therefore, 3D biomaterial scaffolds are promising materials for mimicking the natural environment of many cell types (related to Sec. 4). Interestingly, for *Acanthamoeba* the main target are soft environments like the eye or brain (Fig. 1.3). [53] This observation resulted in studies of *Acanthamoeba* on substrates made of contact lens like materials. [167] Soft substrates or hydrogels are of major use for studies on *Acanthamoeba*. Whereas, most named techniques are not able to manufacture these materials. This is the reason why a new 3D structured material with interconnected channels will result in a more natural analysis technique for biophysical cell investigation as well as cell cultivation, and pathogen cell trapping.

Tab. 1.1.: Comparison of Optical Tweezer and AFM.

	Optical Tweezer	**AFM**
Resolution	$<$ nm	
Force Range	fN - pN	pN - μN
Measurements	intra- and extracellular	extracellular
	vertical and lateral	
Stiffness	$10^{-4} - 10^{-5}$ N/m	$10^{2} - 10^{-3}$ N/m
Size of usable particles	nm - μm	–

Next to adhesion, generated forces by cells, phagocytosis and intracellular movements[168] are in focus of interest and often used with atomic-force microscopy (AFM) or Optical Tweezers (OT). A small comparison of these techniques is given in Tab. 1.1. The trapping efficiency and stiffness of trap has to be calculated[169] to measure these cell-generated forces. Experiments between two DNA strains,[170] stretching[171] and rotation[172] of cells, cell-particle interactions,[173] red blood cell (RBC) rotation,[174,175] and deformation,[176] (visco)-elasticity measurements of cells,[177,178] and new setups like the optical stretcher were realized[171] (related to Sec. 5.4). Until now no 3D investigation with optical manipulation of samples was combined with spinning disc confocal microscopy to test the deformation force while phagocytosis.

Tab. 1.2.: Overview about methods to fabricate three-dimensional polymer substrates reported in literature.

Method	Function	Advantage	Disadvantage	Lit.
Template/salt leaching (sodium chloride) mediated polymerization (PEG)	Bone marrow [122] replacement Bone marrow tissue [122,150]	Relatively easy synthesis Template dissolution with water Interconnected pores	High Template concentration needed for interconnected pores	[122,124,179,180]
Bulk Polymerization	Semi 3D scaffolds are possible for cell experiments.	Easy synthesis Interface investigations are possible Cell film grows between two polymer substrates	uneven pressure on the cell	[181]
Selective Laser Sintering (SLS)	Prototypes	Many different structures are possible. Use of polymers, ceramics and metal powders only which can be melted	Expensive Resolution depends on laser-beam diameter Powder bed-based see STL	[182–185]
Multiphoton Lithography/Direct Laser Writing (DLW)	3D cell culture scaffold with adjustable pore size	Structural diversity	Expensive Slow Material diversity	[186,187]
Stereolithography (STL/SL)	Prototypes	Fast Lacking highly complex structures, multi-material, and multicellular parts	Expensive Photopolymers Liquid a resin see SLS	[188,189]
BioPlotting	Liver/Organ synthesis	Use of ceramic pastes or hydrogels (collagen or alginate) with body own cells	Resolution	[125,190,191]
3D Printing/Fused deposition modeling	Structural and biopolymers, ceramic-polymer, or metal-polymer composites	Easy to use and can be use with a large variety of materials	Only thermoplastics	[191–194]
t-ZnO-mediated polymerization	Cell trap 3D cell culture scaffold	Chemotactic function Tunable channel size (microscopic) Tunable material size (macroscopic) Interconnected pores cheap	Template hydrolysis at pH 1 - 4	[195–197]

2 | General Procedures

In this chapter all methods and procedures are described that have been repeatedly used in different parts of this thesis. Application specific variations are described in the chapters 3, 5, and 4. A list of suppliers is given in Tab. A.3.

2.1. Culture Media

Cell cultivation is associated with the use of the correct medium for each cell type as it is important to generate comparable results. All used culture media were either sterilized by autoclaving or sterile filtrated to sustain habitable conditions as well as infection free organisms. Commercially available media were used as supplied. The sterile media were stored at 4 °C and heated to 25 - 37 °C (Heater 1083) before use. In Tab. 2.1 the related media to cell types are described.

Tab. 2.1.: Culture media and cell type relations.

Cell Type	Medium	Supplier and Sec.
A. castellanii/*A. comandoni*	PYG 712	2.1.1
A. castellanii/*A. comandoni*	Sodium chloride solution	2.1.3
HCEC-12	Ham's F12 + Medium 199 + 5 % FBS	Life Technologies 2.2.4
REF 52 wt	DMEM	Biochrom 2.2.2
RBC	Sodium chloride solution	2.1.3

2.1.1. PYG 712 Medium

Mixture of peptone-yeast extract-glucose 712 medium (PYG 712 medium): Proteose peptone (20.0 g), yeast extract (1.00 g), distilled water (950 mL), magnesium sulfate monohydrate solution (10.0 mL, 400 mM, $MgSO_4 \cdot H_2O$), calcium dichloride (8.00 mL, 50.0 mM, $CaCl_2$), sodium citrate dihydrate (34.0 mL, 100 mM), ammonium iron(II) disulfate hexahydrate (10.0 mL, 5.00 mM, $Fe(NH_4)_2(SO_4)_2 \cdot 6H_2O$), disodium hydrogen

phosphate heptahydrate (10.0 mL, 250 mM, $Na_2HPO_4 \cdot 7H_2O$), and potassium dihydrogen phosphate (10.0 mL, 250 mM, KH_2PO_4) were mixed and sterilized by autoclaving. Then the filter sterilized D-glucose (50.0 mL, 2.00 M) was added to the solution. Adapted from[198].

2.1.2. PBS Buffer

For the preparation of phosphate buffered saline (PBS) buffer sodium chloride (8.00 g, 137 mM), potassium chloride (200 mg, 2.7m mM), disodium phosphate (1.44 g, 10.0 mM), potassium-dihydrogen phosphate (240 mg, 2.00 mM) were dissolved in distilled water (800 mL). The pH was adjusted to 7.4 with hydrochloric acid solution. The total volume was increased to 1 L with distilled water to obtain a 1x PBS buffer. The buffer was sterilized by autoclaving (VX-75) and stored at 4 °C.

2.1.3. Sodium Chloride Solution

Sodium chloride (50 mM) was dissolved in double distilled (bidest.) water and sterilized by sterile filtration.

2.2. Cell Culture

Handling, storage, cell splitting, and cell experiments were conducted under a laminar-flow bench. All microscopical investigations were performed in closed samples to prevent infections.

2.2.1. *A. castellanii* and *A. comandoni*

Trophozoites of *A. castellanii* (ATTC 30234) or *A. comandoni* were cultured at room temperature in PYG 712 medium. In this axenic culture, the PYG 712 medium was exchanged at least once within two weeks in the cell culture flasks (growth area 75 mm^2) in order to avoid encystment of *Acanthamoeba* trophozoites.[167,198]

2.2.2. Rat Embryonic Fibroblast 52 wt (REF52 wt)

For cultivation of rat embryonic fibroblasts 52 wild type (REF52 wt) standard cell culture conditions were used (37 °C, atmosphere of 21 % O_2, 5 % CO_2 and 95 % humidity,

CO_2-Incubator C150). Cell culture flasks (growth area 25 mm^2) were used with cell culture medium Dulbecco's Modified Eagle Medium (DMEM) (450 mL), which included Fetal Bovine Serum (FBS) (50 mL) and was stored at 4 °C. It was preheated to 37 °C in a waterbath right before use. Passaging of cells was performed every three to four days to one fifth of confluency (80 - 90 % → 20 %).

2.2.3. Red Blood Cell (RBC)

The RBCs were conserved with heparin in an isotonic medium. Small amounts (5 - 20 µL) were transferred into a sterile tube, filled with sterile filtrated sodium chloride solution (1 mL) and mixed well. 200 µL from this suspension was stained with anti-GlyA (10 µL, 30 min). From this sample 5 µL were mixed with *A. castellanii* (1 mL, 30,000 amoeba/mL) in a glass-bottom petri dish or 6-well plate for phagocytosis experiments.

2.2.4. Human Corneal Endothelial Cells-12 (HCEC-12)

Human Corneal Endothelial Cells-12 (HCEC-12) (ACC 646) were cultured under ambient conditions in an incubator (37 °C, atmosphere of 21 % O_2, 5 % CO_2 and 95 % humidity, CO_2-Incubator C150) and handled like REF52 wt cells (Sec. 2.2.2) but in a medium mixture recommended by the supplier (95 % mixture of Ham's F12 + Medium 199 (1:1) + 5 % h.i. FBS). After confluency of 70 % was reached (~5 d) the cells were split to maintain a homogenous proliferation behaviour.

2.3. Live Cell Imaging

The setup which was mainly used for image acquisition of this thesis as for bright field, phase contrast, epi-fluorescence, spinning disc confocal fluorescence and optical tweezer, was a custom-modified inverted microscope (IX-81) with an mounted motorized stage (SCAN IM 120x80).

For bright field, phase contrast, and epi-fluorescence, a motorized filter turret with a triple band filtercube (DAPI, FITC, TxRed), a motorized bright field shutter (U-FSHA), a fluorescence burner (MT20E) with included fast changing triple band filters, and a light sensitive camera (XM10) were connected to the microscope.

For spinning disc confocal images a spinning disc confocal unit (Andromeda) and laser combiner (iChrome MLE) with a monochrome digital camera (C-9100-13) were used.

For optical tweezers, a Charged Coupled Device (CCD) camera (602f-2) was connected and in exchange to the 1.6 magnification lenses an infrared reflective filter was mounted to couple the IR-Light Amplification by Stimulated Emission of Radiation (Laser) into the objectives. 60x and 100x oil objectives were immersed with immersion oil (Immersol 518 F or Immersionoil Type-F, $n_e = 1.518$) or a 60x collar corrected water objective was used and immersed with bidest. water. Attachment of one of the following cameras was possible. For bright field, epi-fluorescence and phase contrast the XM10 or MFCool cameras were connected. Optical Tweezers (OT) images were captured with the 602f-2 or XM10 and for spinning disc confocal fluorescence the C-9100-13 digital cameras.

2.4. Spinning Disc Confocal Fluorescence Microscopy

For cell experiments, phase contrast and spinning disc confocal fluorescence microscopy was performed. Advantages of confocal fluorescence microscopy are to filter unfocussed stray light from unfocussed unconfocal points of an image to gain a higher and better three-dimensional resolution. The disadvantages are the longer capture times than epi-fluorescence and higher light intensities on the sample, which could lead to bleaching or even DNA destruction. This is the reason why this technique has to be carefully chosen. To reduce the long captures times a spinning disc (Nipkow disc) can be inserted into the beam path. This reduces the picture resolution compared to a scanning confocal microscope but gains a faster capture times in the lower millisecond range (Fig. 2.1).

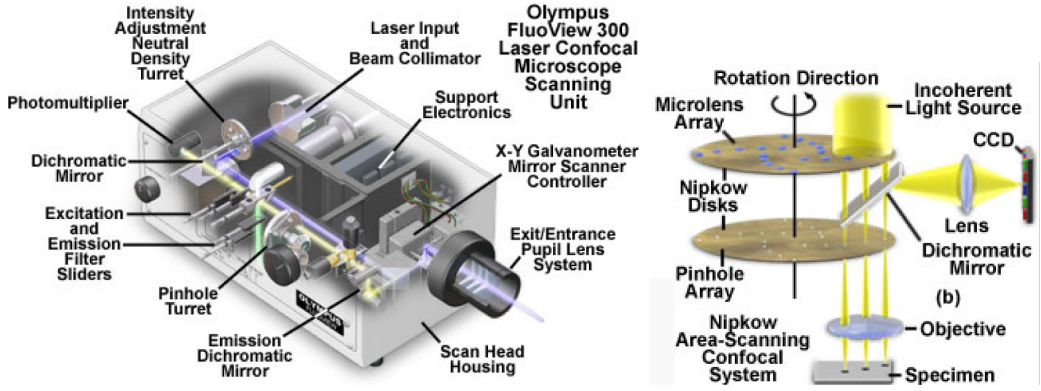

Fig. 2.1.: Example of a Spinning Disc Confocal Microscope and its interior construction. Adapted from [199] and reprinted by permission from Olympus Microscopy Research Center: 01.06.2015.

In this advanced system fluorescence can be observed by using a laser combiner and fitting filters to see fluorescent cells, particles, substrates and many more. Because of the fast capture times it is possible to generate three-dimensional live cell images and to investigate movements and deformations *in situ* (Fig. 4.5).

2.4.1. Amoeba Staining

Acridine orange, a fluorochromatic dye, has been used to stain bacteria or fungi from infectious keratitis.[200,201] With an acidic buffer, acridine orange shows bacteria in orange fluorescence, and human cells or other background materials in green-yellow fluorescence.[202,203]

Acanthamoeba staining was performed for fluorescence visualization in migration studies (Sec. 4). Acridine orange was used to stain the *Acanthamoeba* membrane and cytosol as well as propidium iodide. Contrary to other cell types like fibroblast this was no proof for a dead cell as the membrane of *Acanthamoeba* is different. Therefore, an acridine orange staining solution (1 g/L) was prepared. The sterile filtrated solution was protect from light with aluminium foil and 30,000 *Acanthamoebae* were added into a 6-well plate or petri dish. Either only the sterilized acridine orange staining solution (50 µL) or acridine orange staining solution (50 µL) with sterilized propidium iodide (4 µL, 1 g/L) staining solution were mixed in sterilized PBS (1 mL) in the same container. After dye absorption (5 min, room temperature) the supernatant of the light protected container was exchanged with fresh PYG 712 medium ($1 - 2$ mL).

2.5. Syntheses

The majority of syntheses in this thesis are polymerization reactions of assorted polymers. These were necessary to produce substrates for cell adhesion and migration as well as particles for phagocytosis experiments. All polymers were washed and swollen to equilibrium if applicable. The polymers were disinfected prior to cell experiments.

2.5.1. Polyacrylamide Reaction

The Tab. 2.2 shows different polyacrylamide (PAAm) compositions. The ratio between monomer and crosslinker was changed to produce different elasticities due to different monomer to crosslinker ratios. The polymerization reaction is presented in Fig. 2.2.

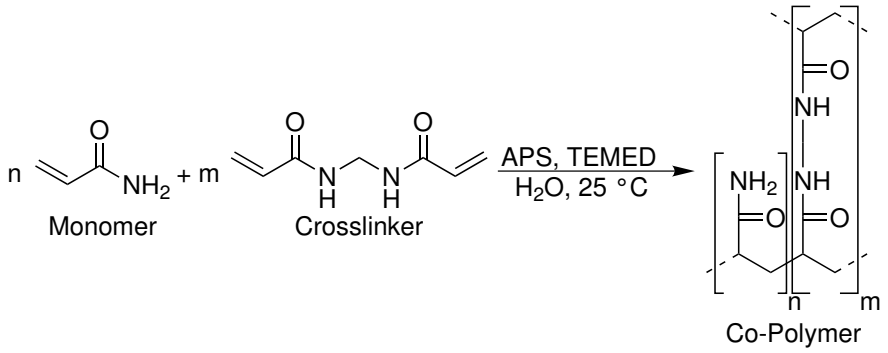

Fig. 2.2.: Polymerization reaction of acrylamide with bis-acrylamide and redox initiation.

The redox reaction induced initiation (Fig. 2.3) of this polymerization is based in the radical decomposition of ammonium peroxodisulfate (APS) and radical transfer reaction to *N,N,N',N'*-tetramethylethane-1,2-diamine (TEMED), which leads to the ammonium hydrogensulfate (A), and the two radicals from sulfate (B) and TEMED (C). The amount of initiator should be in the range of 0.05 % and 10 % eq. as a high amount will lead to shorter polymer chains due to faster chain termination. The HEPES buffer was included to buffer the acidic APS and fluorescein-dextran for fluorescence microscopy experiments.

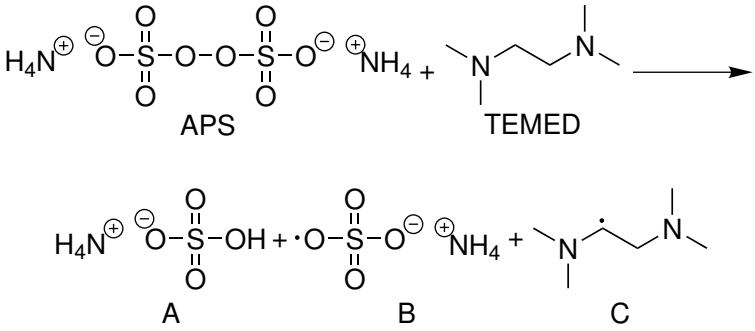

Fig. 2.3.: Initiation reaction of the redox system APS and TEMED.

Tab. 2.2.: Mixtures of used acrylamide polymerization solutions for the experiments.

Compound	**A [µL]**	**B [µL]**	**C [µL]**	**D [µL]**
Acrylamide 40 %	1000	1250	1250	1000
Bis 2 %	200	500	1000	200
HEPES buffer	50.0	50.0	50.0	50.0
Bidest. water	3750	3200	2700	3475
Ammoniumpersulfate 10 %	30.0	30.0	30.0	75.0
TEMED	20.0	20.0	20.0	5.00
Fluorescein-dextran 1.8 wt.-%	0	0	0	200
Young's Modulus [kPa] (Sec. 2.6)	11.3 ± 2.33	33.8 ± 2.76	55.5 ± 9.10	NA

2.5.2. Resin Casting

Different mixtures of acrylamide solution (40 %), *N,N'*-methylene-bisacrylamide (Bis, 2 %), APS solution (10 mg/100 µL) and bidest. water were degassed *in vacuo* for 5 - 30 min depending on volume of the monomer solution (Tab. 2.2). It was well mixed with TEMED to initiate the redox reaction that induces polymerisation at room temperature.

For elasticity measurements, adhesion or migration experiments the mixture was immediately casted into round tablets, or cubic forms made of custom-build poly(1,1,2,2-tetrafluoroethylene) (PTFE), polydimethylsiloxane (PDMS) or stainless steel molds (CAU TF workshop). After 1 - 2 h the polymerized samples were washed with bidest. water ($1 - 2$ mL, three times), or disinfected and washed with appropriate buffer.

2.6. Elasticity measurements

Mechanical properties of PDMS and PAAm were determined by microindentation using a micro-force measurements device (Basalt-BT01).[58] The recorded force-distance curves were used to calculate the Young's moduli of PDMS and PAAm substrates as well as the work of adhesion with the Johnson-Kendall-Roberts (JKR) model.[204] This model is used to characterize the mechanical properties of soft materials in the presence of adhesion, since it takes into account the attractive forces between the microindenter tip and the sample seen in the curves of Fig. 2.4. This exemplary figure presents the derived stress-strain from the force deformation curve of a PDMS substrate. The approach to the sample and complete retraction is not presented here. For all substrates, elastic moduli were determined from the unloading part of the curve to account for only the elastic behaviour and not the plastic deformation of the sample. The measurements were performed at ambient conditions (25 - 26 °C temperature and 40 - 50 % relative humidity). The Young's moduli of the different PDMS and PAAm substrates are presented in Tab. 2.3.[198]

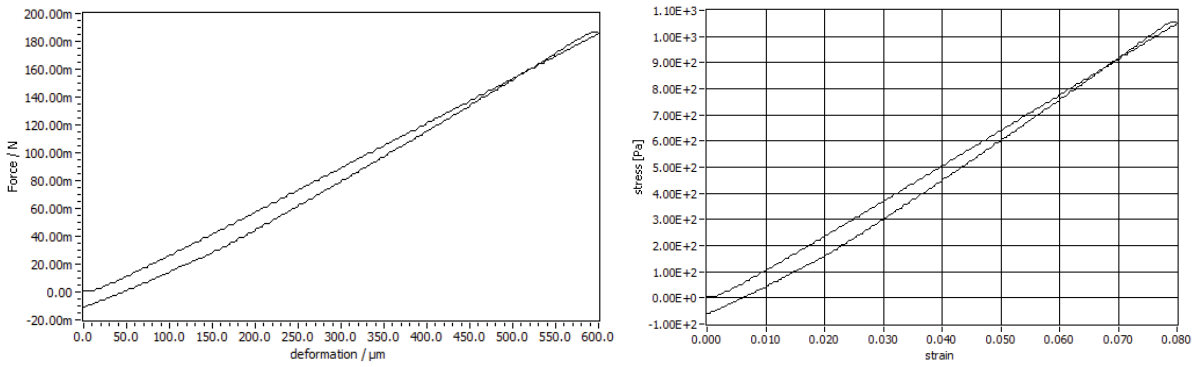

Fig. 2.4.: Example graphs for the determination of the Young's modulus. A force against deformation curve (left) is shown and the resulted stress as a function of strain curve (right). Through the use of the linear regime of the curve the JKR model was fitted to the unloading part of the curve.

Tab. 2.3.: PDMS and PAAm elasticity measurements of different monomer mixtures.

PDMS (base:curing agent)	Young's Modulus [kPa]	Standard Deviation [kPa]
80:1	4.08	1.38
57:1	28.9	3.07
40:1	127	31.5
PAAm Mixture Tab. 2.2	**Young's Modulus [kPa]**	**Standard Deviation [kPa]**
A (unswollen)	17.3	3.63
B (unswollen)	42.7	9.45
C (unswollen)	79.2	17.0
A (swollen to eq.)	11.3	2.33
B (swollen to eq.)	33.8	2.76
C (swollen to eq.)	55.5	9.10

2.7. Significance Tests

To achieve the results of Sec. 3.2 the analyzed data had to be tested with the non-parametric Kruskall-Wallis test for significance where the null hypothesis is not a gaussian distribution (Fig. 3.4) but their mean rank. Next to this a Friedmann test was carried out and showed even some significance after multicomparison test but was not further used because of the need of paired data sets. The results of the Kruskall-Wallis test was further analyzed with the non-parametric multicomparison test which led to the high significance for the examined three independent experiments in triplicate of the four different elasticities (Fig. 3.3).

3 | Adhesion and its Effect on Infection

Adhesion is the initial step the infection pathway cascade in pathogenic cells as it is required to attach to human tissue and target cells. It is fundamental for all cells and is in consequence crucial for the functioning of all biological systems as, e.g. tissue growth. It can be found in fibroblasts, myocytes, and neurons. Adhesion depends on the mechanical properties of the cellular microenvironment [105–107] and this results in adhesion to artificial materials, which mimic the same mechanical properties as their natural equivalent. Cells can respond and adjust their migration direction on materials with constantly changing stiffnesses to more supportive areas, which is named mechanotaxis. [115,116,205] This adaptation is due to an active probing of the cellular microenvironment by nanobiomechanical mechanism in cells, allowing to re-orientate themselves on mechanotactic migration. [117] After cell differentiation on a defined substrate elasticity, the cell responds with intracellular stiffness adjustments. [206] Nevertheless, not only differentiated cells show these consequences, because of the substrate stiffness changes. Stem cell proliferation can be directed towards certain cell types with mechanical property selection of a natural surrounding (Sec. 1.6), [119] also due to stress-fibre polarization. [120] Tumor cell adhesion can be controlled by this phenomenon [121] since pancreas tumor cells tend to be more often softer than their healthy counterparts. [207] Nonetheless, there are several other important effects for adhesion, such as surface functionalization with certain interacting molecules or mechanical anchors. [208] These can enable focal adhesions and build cluster formation which leads to increasing adhesion force, e.g. fibroblast, human osteosarcoma cells (U2OS) [209] or bovine pulmonary artery smooth muscle cells (BPASMC). [111]

Luo *et al.* considered the role of myosin II motor proteins in mechanosensing of social amoeba *Dictostelium discoideum.*[210] Mechanosensing of cells is assumed to be linked to the active force generation in cells by analyzation of traction forces on elastic substrates, by means of traction force microscopy. This gave insight into the underlying executable forces of cells.[211,212]

To conclude, all these evidences report mechanosensing in mammalian cells, but detailed mechanisms are still under investigation. Presently, talin, vinculin, and ion channels are argued to provide mechanosensing of the cellular microenvironment.[213–215] Contrary to mammalian cells, sensing of elastic properties of surfaces resulting in a cellular response is not completely understood and for eukaryotic protists as amoebae not observed yet. Moreover, *Acanthamoebae* adhesion depends on the elastic properties of a substrate. The main targets of *A. castellanii* infections are the eye and the brain, i.e. soft environments of a low Young's modulus between 1 - 15/20 kPa (Sec. 1.6).[53,105]

In the following section, experimental results on elastic properties on adhesion is shown. This is important as these results provide first indications towards the relevance of mechanical aspects for the pathogenicity of eukaryotic parasites. Consequently, the goal was to relate changes of substrate stiffness without any inclination of functionalization, wettability[216], nor water content to the projected adhesion area of *Acanthamoeba.*[167,198] The results of this chapter have been published as Gutekunst *et al.*[198]

3.1. Bulk Substrate Polymerization

Most polymers used in contact lens production are based on hydrogels, silicones or compositions of these.[167] Therefore, bulk silicone based polymers were casted and used to test stiffness dependence of *Acanthamoeba* adhesion. PDMS is neither swollen in water,[217] nor significant wettability changes can be related to stiffness variations.[216][A] PDMS is water-repellant and was tested without any interference or bias in wettability nor functionalization.

To exemplify the complexity of mechanical dependence of adhesion, the elasticity of polymer substrates by varying the amounts of crosslinker in polymer substrates was changed. The used Young's moduli were chosen to cover natural and reported elasticity ranges (Fig. 1.7).[105] To investigate *A. castellanii* adhesion on PDMS substrates

[A] The surface wettability of polymers can be changed by direct corona discharge.[218]

(Sec. 3.1.1), three different Young's moduli were synthesized to investigate the initial step of infections, i.e. the adhesion of pathogenic *A. castellanii*.

3.1.1. Polydimethylsiloxane (PDMS)

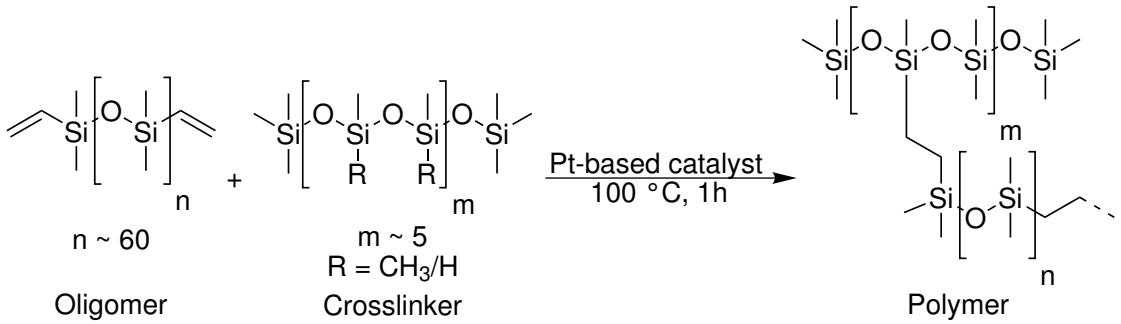

Fig. 3.1.: Assumed organometallic crosslinking/hydrosilylation reaction of the commercial available oligomer Sylgard 184 to PDMS.[219,220]

Silicone base and curing agent (Sylgard 184) were mixed thoroughly in a ratio (m/m) of 80:1 (4.08 ± 1.38 kPa), 57:1 (28.9 ± 3.07 kPa) and 40:1 (127 ± 31.5 kPa) by following the curing procedure given by Trappmann *et al.*[208] Afterwards, the mixtures were poured in sterile 6-well plates up to a thickness of approx. 2 mm for 3.5 h *in vacuo*. Thermal polymerization was carried out for 21 h at 70 °C followed by a cool down to room temperature to receive PDMS substrates.[198] The Young's modulus of each substrate type was measured as described in Sec. 2.6. The organometallic hydrosilylation of dimethyl siloxane oligomers is shown in Fig. 3.1. The Pt-based catalyst might be hexachloroplatinic acid ($(H_3O)_2[PtCl_6]$) as it is used for silane addition to vinyl groups. This reaction can only be assumed as the real chemical composition remains a companies secret. Dow Corning showed hydrosilylation of vinyl-groups and therefore a platinum-based catalysis of vinyl-methylsiloxanes and crosslinker is reasonable to polymerize PDMS as the initiation and reaction time is temperature dependent.[219,220] This reaction mixture should not be mixed with acids, bases, water or moisture as hydrogen can be generated, which is another indication for the hexachloroplatinic acid.

3.2. Adhesion experiments

Synthesized polymer substrates were disinfected with ethanol (70 %, 2 - 3 mL, 1 - 5 min), washed with sterile PYG 712 medium (2 - 3 mL), and transferred into a sterile

6-well plate or petri dish. 30,000 *A. castellanii* trophozoites were transferred onto each substrate and PYG 712 medium (1 - 2 mL) was added. After 1 h images and videos of the adhered *Acanthamoeba* were captured (IX-81, C-9100-13) and further analyzed (ImageJ, Origin, MatLab) (Sec. 2.7). The adhesion experiments were conducted as three single experiments in triplicate.

In Fig. 3.2 randomly chosen phase contrast images of *Acanthamoeba* trophozoites are representing the average cell adhesion area of each substrate type. In these figures halos around the cells are visible as a result of the ellipsoidal shape of *A. castellanii* unlike mammalian cells such as fibroblasts.[221,222]

To quantify the difference in cell adhesion areas image segmentation of 11,438 cells in total was systematically performed. A graphic program (ImageJ 1.46r) was used for manual encircled around the black and white halo edge of *A. castellanii* (Fig. 3.2). This analysis was performed without any bias as the stiffness of the substrates were unkown, while manual encirclement, and only calculated after full acquisition of all data sets. The acquired data was plotted with Origin 9.1G and tested for significance in MatLab R2013a. The mean values of cell area were calculated as 712.59 μm^2 (4 kPa), 666.63 μm^2 (29 kPa), 611.65 μm^2 (128 kPa), and 783.92 μm^2 (control).

The increasing adhesion area as a function of decreasing Young's modulus is contrary to the behaviour of human mesenchymal stem cells[181] but is in good agreement with the trend observed in studies of neural stem cell cultures.[223] This result is reasonable, if considering that the infection pathway is the soft brain and eye with a Young's modulus of 1 - 10 kPa[119], as discussed in Sec. 1.2. *A. castellanii* trophozoites can adhere well to PDMS polymers without further biofunctionalization, as the substrate was used in its hydrophobic, non-functionalized state (Sec. 3.1.1). This is of major importance as previous indications revealed that not only the elasticity of the substrate is an essential parameter for cell adhesion as well as the functionalization of adhesion promoting molecules to the substrate[208] and water content[167]. The usage of non-functionalized PDMS substrates avoid bias by these effects and influences on adhesion by ligands or water content in the performed experiments.

This resulted in a biggest adhesion area for the softest sample (4 kPa) and decreased from the medium sample (29 kPa) to the hardest PDMS (128 kPa). The results refers to a petri dish sample as a control to look for any deviations in natural cell behaviour.

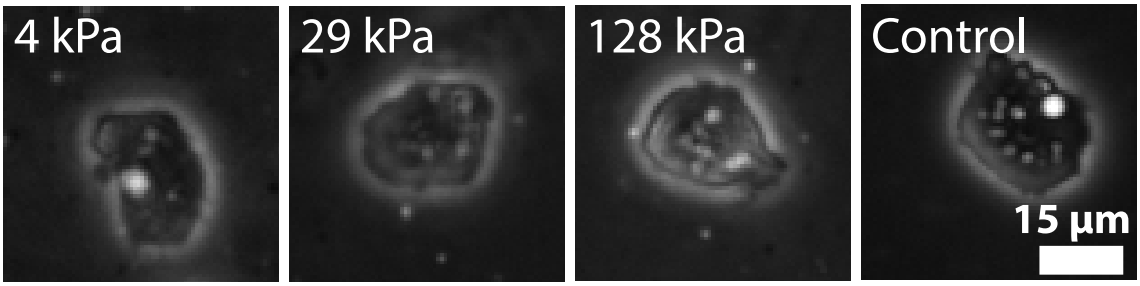

Fig. 3.2.: Phase contrast images of *A. castellanii* trophozoites on PDMS substrates with different Young's moduli and a control after 1 h in culture in PYG medium (4 kPa, 29 kPa, 128 kPa, and control). The adhesion area of *A. castellanii* is influenced by substrate stiffness, i.e. the cell area on the stiff sample (128 kPa) is smaller than on the softer samples (4 kPa, 29 kPa) and on the petri-dish control sample (Control). The comparison of *Acanthamoeba* morphology on PDMS substrates and on the control sample shows that *Acanthamoebae* adhere very well to the non-functionalized PDMS substrates. Scalebar = 15 µm. Adapted from [198] under the terms of Creative Commons Attribution License 2.0.

For the hardest duroplastic cell culture plate a comparable value of adhesion area to the 128 kPa PDMS sample was calculated. This is counterintuitive at first although the cell culture plate has even stiffer material properties as the hardest PDMS substrate but has surface modifications for better cell culturing properties. This paradox is therefore easy to disprove due to its biocompatible surface modulation, functionalization and different hydrophobicity.

Acquisition of the data was quite challenging and to achieve a significant plot of the relative cell count to the cell adhesion area more than 2000 cells had to be measured for each substrate. The analysis of this data set as described in Sec. 2.7 is summarized in Fig. 3.3 and 3.4. Fig. 3.3 depicts the mean projected cell adhesion areas and standard deviations of *A. castellanii* relative to substrate stiffness. These values were determined from in total nine experiments, i.e. three independent experiments each carried out in triplicate. The data reveal that cell adhesion area decreases with increasing substrate stiffness of PDMS substrates. The significance was evaluated (MATLAB R2013a) and graphs were created with Origin 9.1G as described in Sec. 2.7, which revealed that all mean ranks are significantly different at a 0.001 level (***).

To relate the changes of the projected cell area distribution against relative counts to each control sample was compared and plotted as a function of substrate stiffness (Fig. 3.4). The cell count of each stiffness was averaged through the three triplicate in relative to complete cell counts.

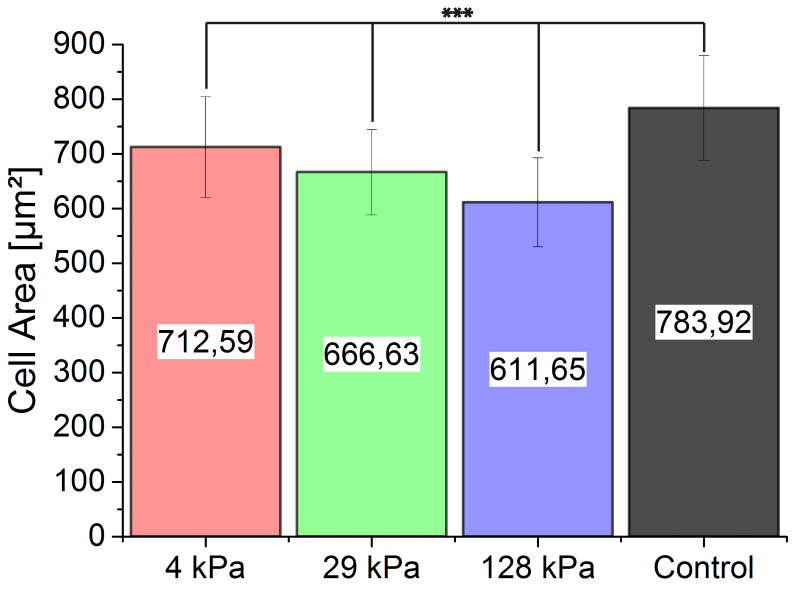

Fig. 3.3.: Cell adhesion area of *A. castellanii* as a function of Young's modulus of the PDMS substrates and in comparison to the control substrate after 1 h of adhesion in PYG medium. These results were obtained from analyzing 3092 amoebae (4 kPa), 3044 amoebae (29 kPa), 3108 amoebae (128 kPa), and 2194 amoebae (control). The bar diagram gives the mean cell area (calculated from the mean of cell adhesion area on each substrate) and standard deviation. This standard deviation is a measure for the differences in cell adhesion area on different individual samples of the same type. The numeric mean values are additionally given inside the bars. The differences of the means are statistically significant (Kruskal-Wallis test; ***, $p < 0.001$, $n > 2194$ cells per substrate type). Adapted from [198] under the terms of Creative Commons Attribution License 2.0.

The bin size of the cell area was also evaluated to the average bin size of three triplicate and related to the overall cell area distribution to equally rate all single experiments of the full data set. This provided the data for Fig. 3.4. The pie plot shows that the area of $600 - 1200$ µm^2 increases with lower stiffness of the PDMS, which is an expected size of the trophozoite stage of an average *A. castellanii* trophozoite from $20 - 30$ µm in diameter. The cell count distribution did not follow a Gaussian distribution function, but showed a long tail towards larger cell areas. This tail is a typical feature of cell size distributions, and has been reported for cell types as mammalian cells [224,225] and *A. castellanii*. [226]

The distribution of cell adhesion areas were compared between each substrate supported by the results from Fig. 3.3 and 3.4. These figures promoted that substrate stiffness influences cell adhesion area.

The difference between the control and PDMS substrate (128 kPa) is noticeable here.

In addition, differences between the PDMS samples of different Young's modulus were observed. Specifically, the pie charts demonstrated the quantity of large and small cell areas changed as a function of PDMS stiffness.

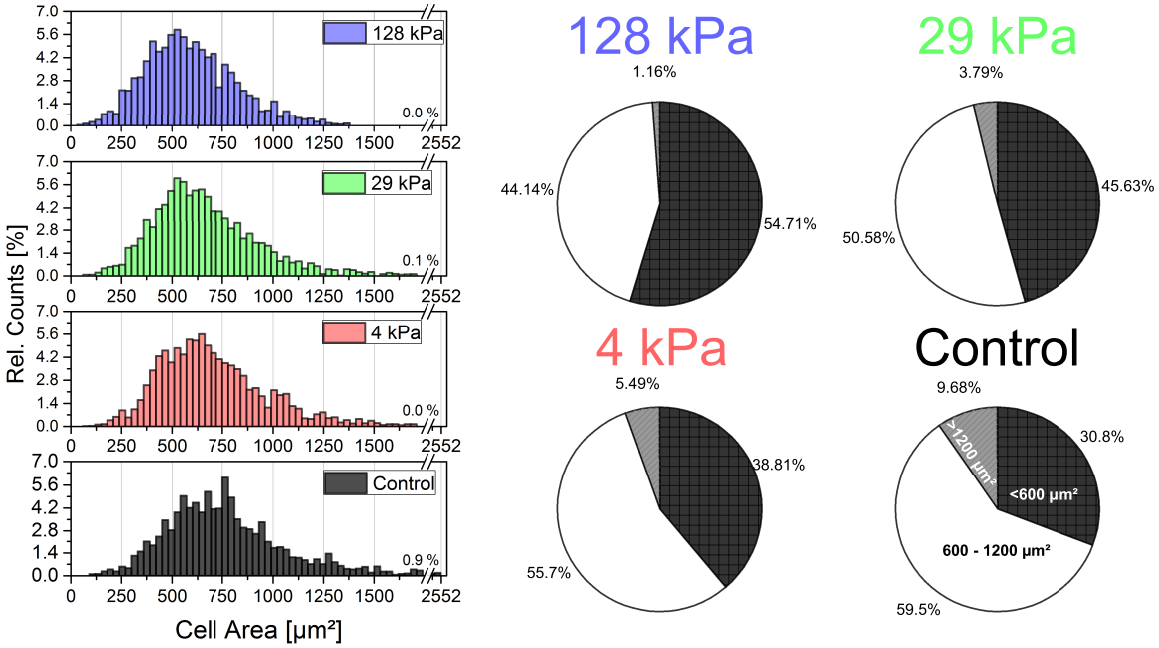

Fig. 3.4.: Average relative counts of projected cell areas of adhering *A. castellanii* on PDMS substrates and on the control substrates. The histograms show that the distribution is slightly asymmetric and can therefore not be fitted with a Gaussian. Average relative counts were calculated by determining the relative counts per sample and generating the average for each bin from all experiments, in order to equally rate all experiments. The value above the interception of the x-axis shows the relative counts of cell adhesion areas larger than 1750 µm^2. Differences in cell area distribution become particularly visible when comparing the pie charts (cell adhesion are in black: < 600 µm^2; white: $600 - 1200$ µm^2; grey: > 1200 µm^2). Adapted from[198] under the terms of Creative Commons Attribution License 2.0.

In contrast, the results of an increasing adhesion area with decreasing substrate stiffness cannot be related to the cell count relative to the control sample (Fig. 3.5). All mean values with their standard deviations overlap and do not lead to a clear conclusion.

The one hour adhesion time chosen here prior to image acquisition before each experiment might be uninfluenced in the cell numbers as the proliferation and doubling time of *A. castellanii* in axenic culture is on the timescale of 24 h at 25 °C,[227] 12 h at 25 °C[228], or 15 h[229]. A grow rate is fast for *Acanthamoeba* spp., when it is below 20 h for a generation time.[230] Thus, it is reasonable that there is no difference in the effect

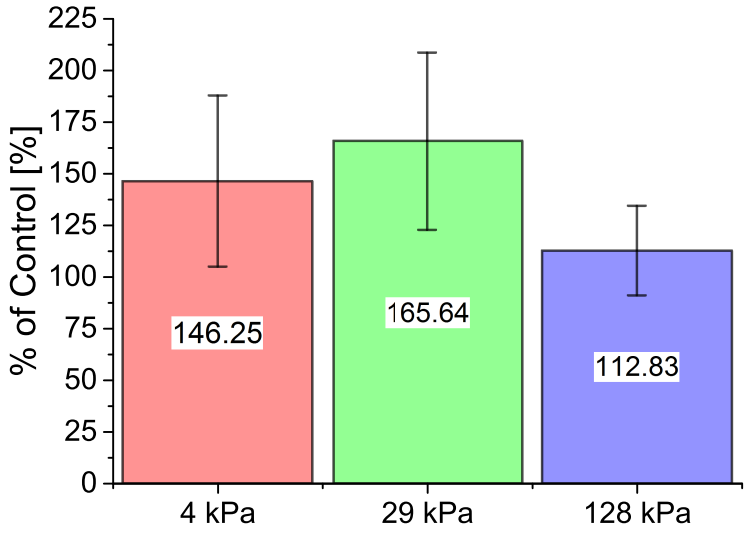

Fig. 3.5.: Numbers of *A. castellanii* adhering to PDMS substrates after 1 h of incubation. The values were normalized to the number of *A. castellanii* adhering to the control substrate. Here, no systematic effect of substrate stiffness on cell number could be observed. Mean values are shown in a bar diagram, where each numeric value is given inside the bar. Error bars denote standard deviations. Adapted from [198] under the terms of Creative Commons Attribution License 2.0.

of stiffness on cell number as amoeba can be cultivated in suspension, [29] so proliferation might not be influenced by the presence of any substrate.

Previously, Reverey *et al.* investigated adhesion of *A. castellanii* to hydrogel materials used for contact lenses. [167] They determined a strong dependence of *A. castellanii* adhesion on the water content of contact lens materials, i.e. a significant increase in adhering trophozoites per area of the substrate (trophozoites/cm^2). Contrary to these contact lens materials the investigated hydrophobic and water repellent PDMS did not show this influence. According to Lee *et al.*, the water content of PDMS is negligible. [217] Therefore, a bias of our data by changes in the water content of the substrates can be excluded for these experiments.

Furthermore, Reverey *et al.* [167] did not find a significant dependence of adhesion on substrate stiffness for the Young's moduli regime between 0.30 and 0.66 MPa but a significant change on water contant. [167] Here, we investigated cell adhesion area at much lower Young's moduli, which are an order of magnitude smaller than the discussed hydrogel material values. However, the substrate stiffness influence on the adhesion of *A. castellanii* observed in this study is not as pronounced as for mammalian cells. [106] Such an extenuated effect is reasonable, as *Acanthamoebae* have to be able to survive

and migrate in very diverse natural environments, ranging from soil to water reservoirs (Fig. 1.3).

3.3. Conclusion and Prospects

The idea behind this project was to relate surface stiffness with projected adhesion areas of human pathogenic *A. castellanii* without any surface modification, functionalization or water-content changes in the substrate. The latter effects were conducted by Reverey *et al.*[167] The water-content difference has a big effect on the adhesion properties of *Acanthamoeba*.

Significant changes in increasing adhesion area of *A. castellanii* as a function of decreasing substrate elasticity was found. However, a growth rate difference has not been observed, which might be due to the short one hour adhesion time. So these studies lead to first indications of mechanosensory mechanism that allows *A. castellanii* to sense and react on stiffness of their microbial environment of *Acanthamoebae* to nothing else but unbiased surface elasticity changes. Interestingly, their major infection pathways are the human brain and eye.[53]

As a solid claim for this idea it was necessary to obtain a very high statistical value (No. of cells analyzed 11438) with highest significance below 0.001 % (Kruskall-Wallis and multicomparison test). To conclude, the results of this project with the aid of fundamental statistical analysis gives the very first indications to the pure unbiased mechanosensory effect of *A. castellanii* to PDMS substrates.

This will be of high importance to contact lens manufactures and the biophysical society and will lead to further investigations in this field. This work was published in the Paper "Influence of Polydimethylsiloxane Substrate Stiffness on the Adhesion of *Acanthamoeba castellanii*",[198] supported by colleagues from Biocompatible Nanomaterials in collaboration with the work group of Prof. Gorb (Zoological Institute, CAU). It provides first indication for the relevance of mechanical properties of cellular microenvironment and associated bionanomechanical cues of a eukaryotic human pathogen. Therefore, a mechanosensory effect for this unicellular eukaryotic human pathogen can be proposed. Furthermore, these results had major influence in the research of porous substrates as well as the phagocytosis experiments described in the following chapters.

4 | Migration and Traps

Most currently used biocompatible biomaterials for cultivating cells *in vitro* are based on 2D substrates due to easy handling, cheap production costs, and commercial availability. In contrast, most cell types are embedded in 3D environments *in vivo* where they are integrated into dense well-structured materials. For mimicking the extracellular matrix (ECM) and bone structures porous materials with broad structural flexibility offer interesting possibilities. Several studies have proven that cells indeed grow more like *in vivo* when cultivated in 3D cell culture model substrates. [142,143]

In order to mimic structural 3D environments in a very simplified way, often brushes [146] or pillar structures are employed, [147] although these structures only represent a topographical structured 2D environment, but no true 3D environment. [28] Still, such quasi-3D substrates can be used as artificial models for the simplified investigation of cellular properties, e.g. studies on cell adhesion and cell migration.In recent years, biomaterials for three-dimensional cell culture and chemotaxis have become relevant in many applications, in particular for tissue engineering [122–125] severall effects have been observed. The use of materials as matrigel, [148] poly(lactide-co-glycolide) scaffolds, [148–152] 3D alginate hydrogels, [153,154] compressible alginate carboxymethyl copolymers [155] and biodegradable materials [151,157–161] are becoming commonly used standard materials in 3D cell culture. Therefore, 3D biomaterial scaffolds are promising materials for mimicking the natural environment, e.g. ECM of many cell types. Confinement and low adhesion of slow mesenchymal cells induces fast amoeboid migration on 3D structured PDMS-polyethylene glycol (PEG) surfaces. [137] Amoeboid motion is the general movement of eukaryotes and amoebocytes, [126,127] but its mechanism is not yet comprehended.

In Tab. 1.2 a variety of techniques are listed for further information as they are used to produce substrates for cell measurements or cultivation. Predominantly, 3D porous structures are developed by pore-leaching techniques, where cavities are introduced into

a bulk material by dissolving salt crystals or other dissolvable particles.[122] The main disadvantage of these techniques are the primarily inverse-opal shaped cavities.[154] This result into enrichment of cells in these cavities, but does not lead to a homogenous locality of cells inside these scaffolds. Thus, cell-cell interactions will be dominant or the cells will adhere in quasi 2D structured manner to the inner side of cavities multiple times bigger than a single cell, because these cavities would not maintain an interconnected structure if the template is chosen too small. However, cell-material interactions are important as they control cell migration direction and controlling cellular behavior including stem cell differentiation and migration.[105,119,181]

To overcome these limitations of conventional 3D porous scaffolds, we fabricated a real 3D network made from a Zinc oxide tetrapod (t-ZnO) template, which mimics a labyrinth-like structure found to the comparable *in vivo* structures, e.g. blood vessels, brain synapses or lung alveoles. A method to generate a 3D biomaterial that contains interconnected labyrinth-like channels in the micro- and nanometer range was developed. These structures are observable, e.g. in the ECM,[156,231] where cells travel through dense fibrous networks.[232,233] Importantly, the structural properties of these scaffolds can be defined as for example the overall shape and size, channel diameter, porosity, scaffold elasticity, density and surface functionalization can be varied independently from each other. This is advantageous to artificial fiber or inverse-opal networks as it maximizes the previously described cell-material contact area as the size is almost equal to a single cell. In advance, the interconnectivity of this porous multi-channel structure is always guaranteed by the fabrication procedure of a seamless interconnected t-ZnO itself. The interconnectivity is independent of channel and pore density. Until now the following experiments are mainly based on hydrogels ensuring that enough nutrients reach the cells even within small channel diameters. Additionally, the cells can be guided through these channels with the help of chemotactic reagents to guide, catch and finally trap cells inside of these scaffolds. Chemotaxis is the reaction of a cell induced by a chemical gradient sense. This phenomenon occurs for predators in the microbial but also in the macroscopic world as they chase their bait in the same manner by leftovers like fragrance, foot steps or tracks. Intriguingly, cells can grow deeply into such scaffold materials and cell migration can be controlled by channel diameter. The parts of the results in this chapter is based on the pending patent (EP 15166793.8).

4.0.1. Zinc Oxide Tetrapod (t-ZnO) Synthesis

For the production of these multichannel labyrinth-like pore structures the published t-ZnO were synthesized in a flame transport synthesis as shown by Adelung *et al.,*[234,235] Mecklenburg *et al.,*[236] and Mishra *et al.*[195–197] as a template material.[A] These tetrapods with dimensions ranging between 100 nm – 10 µm for arm width of a single tetrapod (common used $1 - 8$ µm) were pressed into platelets with a density of $0.1 - 1.4$ g/cm^3 [195] (common used 0.49, 0.70, 0.90 g/cm^3). These t-ZnO tablets were annealed (1150 °C, 1 - 5 h)[195] into a seamless network made from single t-ZnO microparticles. Besides, these tablets can also be provided in a macroscopic form of any shape, which can be sintered, e.g. tablet, disc, or mug shape. It has the magnificent advantage that the t-ZnO network can be fabricated with flexible shape of its single constituents (tetrapod, multipod, sea urchin and platelets), in their vol.-% (1 - 70 %), tunable arm size (even cm tetrapod arm lengths are possible as masterpodes). Most importantly, the templates are hydrolysable and interconnected even with low material concentration.[195] These properties and furthermore flexibility in hydrophilicity with use of UV-light or laurinic acid make a template-mediated polymerization possible in the first place. This is a clear advantage over other approaches that have proven to generate porous 3D polymer structures so far (Tab. 1.2).[192,237]

Therefore, a new method for the synthesis of microporous mazy interconnected hydrogels for the elimination of pathogen microorganisms will be presented. Thanks to hollow interlinked channels inside a hydrogel, which were synthesized with a seamless interconnected t-ZnO tablets as sacrificial material. After polymerization of polyacrylamide and hydrolysis of this template it resulted in a labyrinth-like three-dimensionally structured polymer.

4.1. Template Mediated Polymerisation

4.1.1. Polyacrylamide

The PAAm resins were synthesized as described in Sec. 2.5.2, the elasticity was measured (Sec. 2.6 and Fig. 4.1), and used for cell experiments as a bulk control in contrast to

[A] Cooperation Prof. Rainer Adelung Faculty of Engineering CAU Kiel, Ingo Paulowicz, Iris Hölken and Daria Smazna.

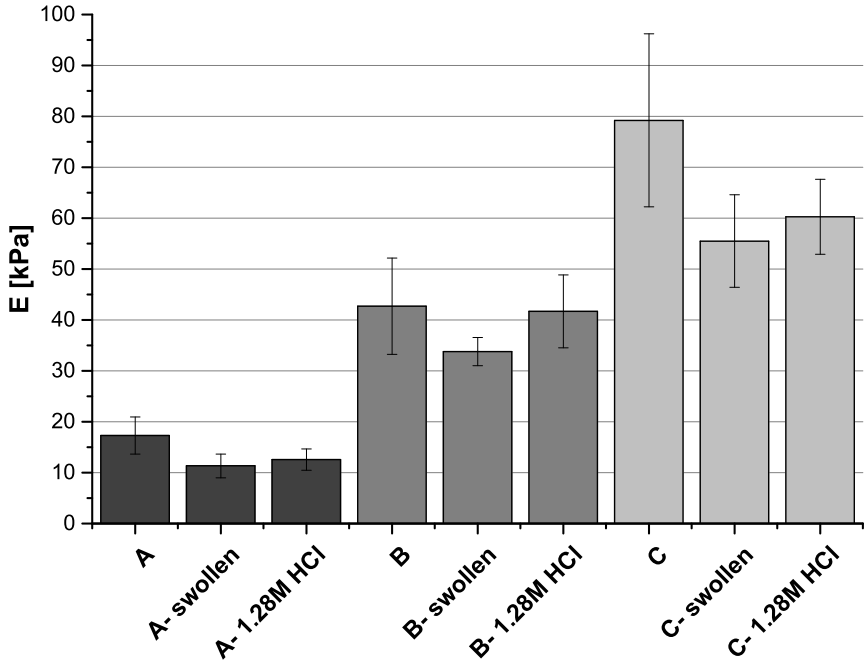

Fig. 4.1.: Elasticity measurements of the three PAAm mixtures (A, B, and C from Tab. 2.2). The samples were measured after polymerization, in a swollen state, and hydrochloric acid solution (1.28 M, 1 d). Each bar derived from 27 measurements and the mean value with standard deviation is shown. Adapted from [238].

3D structured substrates (Sec. 3.2). PAAm ealsticity measurements (Sec. 2.6) led to Young's moduli of 17.3 ± 3.63 kPa (Mixture A), 42.7 ± 9.45 kPa (Mixture B), and 79.2 ± 17.0 kPa (Mixture C) for unswollen substrates and to equilibrium swollen substrates in bidest. water 11.3 ± 2.33 kPa (Mixture A), 33.8 ± 2.76 kPa (Mixture B), and 55.5 ± 9.10 kPa (Mixture C) (Fig. 4.1). [238]

4.1.2. 3D Scaffolds

Template mediated Polymerizaton of Polyacrylamide

The t-ZnOs were synthesized and sintered as in Sec. 4.0.1. Afterwards, the t-ZnO network was used as templates for PAAm polymerization (Fig. 4.2 A). A mixture of acrylamide solution (40 %, 1.00 mL), *N,N'*-methylenebisacrylamide solution (Bis, 2 %, 250 µL), and ammonium persulfate solution (10 %, aq., 30.0 µL) was filled up to a volume of 5.00 mL in a small beaker and degassed for 20 min in a desiccator. The calculated vol. (Eq. 4.1 + 4.2) for complete coverage of the platelets was poured on the t-ZnO tablet with TEMED (10.0 µL). At the end of polymerization (1 - 2 h) the substrate was

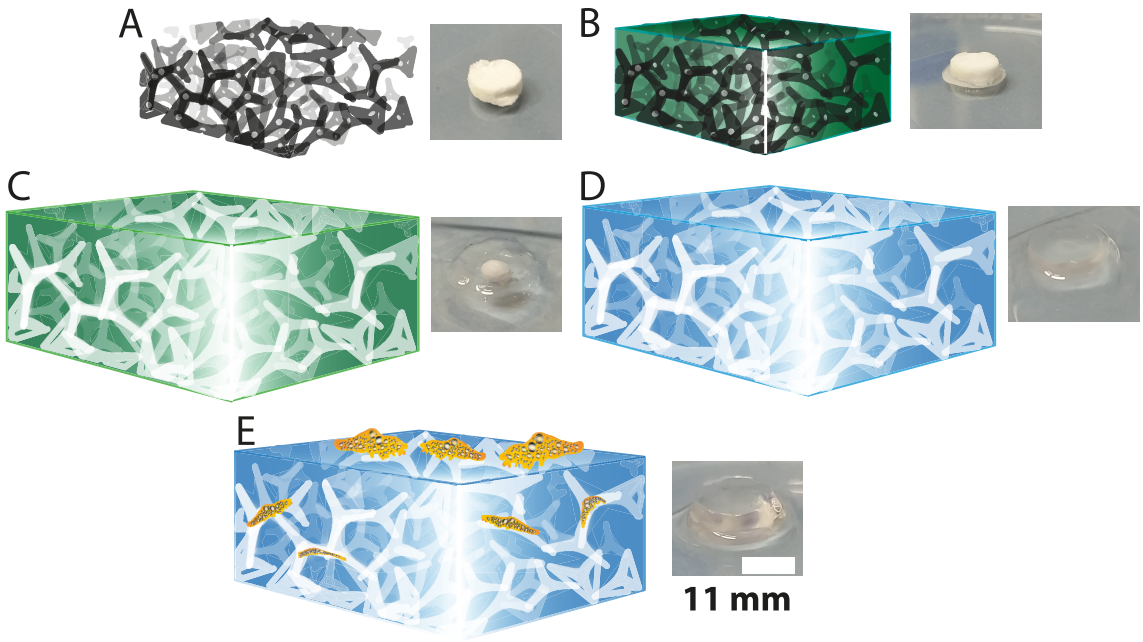

Fig. 4.2.: Synthesis of microchannel-containing polyacrylamide hydrogels. (A) Sintered zinc oxide pellet (black). (B) Zinc oxide pellet embedded into PAAm (green). (C) Hydrolysis of t-ZnO template and swelling of the polyacrylamide substrate. (D) After hydrolysis of the template the PAAm is washed, swollen to equilibrium in cAMP solution and remains with interconnected channels (white). (E) *Acanthamoeba* (orange) are incubated with the microchannel containing material. Scalebar = 11 mm.

washed with bidest. water (Fig. 4.2 B). In advance, other monomer mixtures were used as comparable substrates (Tab. 2.2).

$$V_{tablet} = \pi r^2 h \tag{4.1}$$

$$m_{Mon.sol.} = \rho V_{tablet} \tag{4.2}$$

ρ is the density of the t-ZnO, which was often produced as 0.7 g/cm^3 for higher channel densities to obtain an easily accessible substrate for cells. In contrast, live cell imaging was hindered due to higher stray light inside the sample. This leads to a tradeoff between these factors as a high channel density and less stray light would be beneficial but impossible to produce.

Hydrolysis of the t-ZnO-Template for Microporous Hydrogel Fabrication

The template (1 - 3 x 11 mm) was hydrolyzed with hydrochloric acid (2 - 3 mL, 0.5 - 1.0 M) for 24 - 120 h in dependence of acid concentration, which was exchanged daily

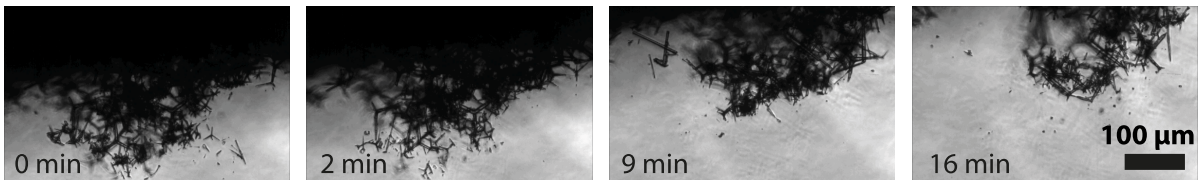

Fig. 4.3.: Phase-contrast images of the hydrolysis of an embedded t-ZnO template in PAAm with hydrochloric acid solution (1.28 M). Scalebar = 100 µm.

(Fig. 4.2 C). A hydrolysis of a PAAm embedded t-ZnO tablet typically takes 2 - 4 d at pH of 4. The macroscopic fabrication and hydrolysis of this template mediated synthesis is shown in Fig. 4.3. After hydrolysis the hydrogel was washed several times with bidest. water until a pH-value above 6 and complete swelling to equilibrium of the substrate was achieved as the a complete mass increase was observed between 48 - 72 h (Fig. 4.4).

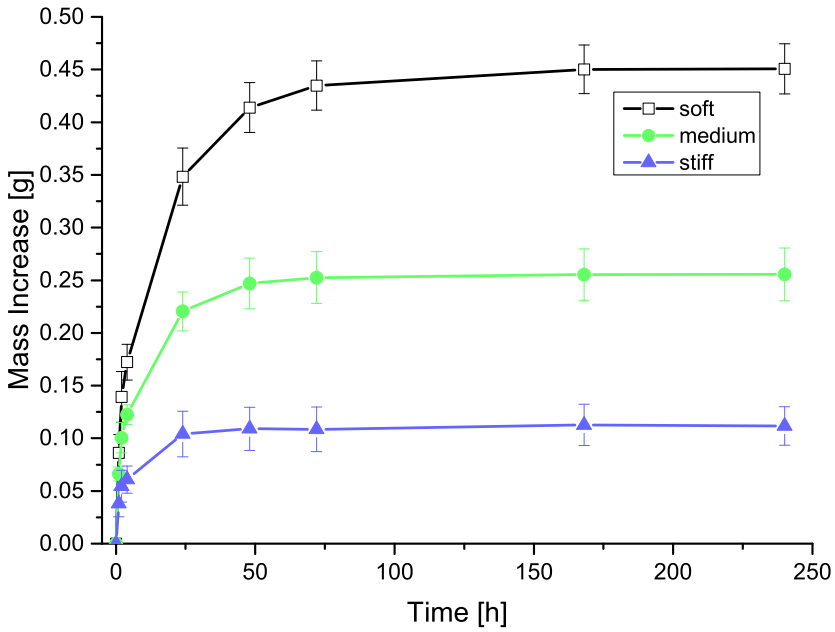

Fig. 4.4.: Graph of PAAm mixtures (n > 3) of Tab. 2.2 were measured for mass increase with given standard deviation. After 48 - 72 h the mass increase reached an equilibrium state. Adapted from [238].

Disinfection with 70 % ethanol and washing under sterile conditions for 24 - 48 h with PYG 712 or cAMP (Sec. 4.2.1) prior to *A. castellanii* or DMEM for REF52 wt experiments was conducted. The cleaned substrates were used within 48 h to maintain sterile, swollen, reproducible and comparable experiments (Fig. 4.2 D).

4.2. Migration Experiments

4.2.1. Chemotactic Substance Absorption of Polyacrylamide

The hydrolyzed PAAm substrate was washed with cAMP (0.01 -10.0 mM) and swollen to equilibrium for 3 to 4 d (Fig. 4.2 D). The cAMP solution was exchanged daily.

4.2.2. Cell Experiments

The sterile substrates were incubated with *A. castellanii* (ATTC 30234, 30.000 cells/mL) or REF52 wt cells (15.000 cells/mL) in a 6-well plate (Fig. 4.2 E). After 0.5 - 2 h of incubation phase-contrast microscope pictures (IX-81/BX-43) and movies were recorded using a monochrome EM-CCD (C-9100-13 or C-9300-221) or a color camera (DFK 31BF03).

Migration of *Acanthamoeba* into Porous Polyacrylamide

Acanthamoebae migrated into the elastic microporous hydrogel substrates filled with cAMP[239] within 15 min up to a depth of $30 - 50$ µm. They quickly moved through the confinements (Fig. 4.5 and 4.6) comparable to the migration in other materials with different cells.[240–242] Experiments with *A. castellanii* showed that the cells were viable as some amoeba still migrated inside the channels in the material after more than 6 d without the exchange of buffer and no encystment was observed.

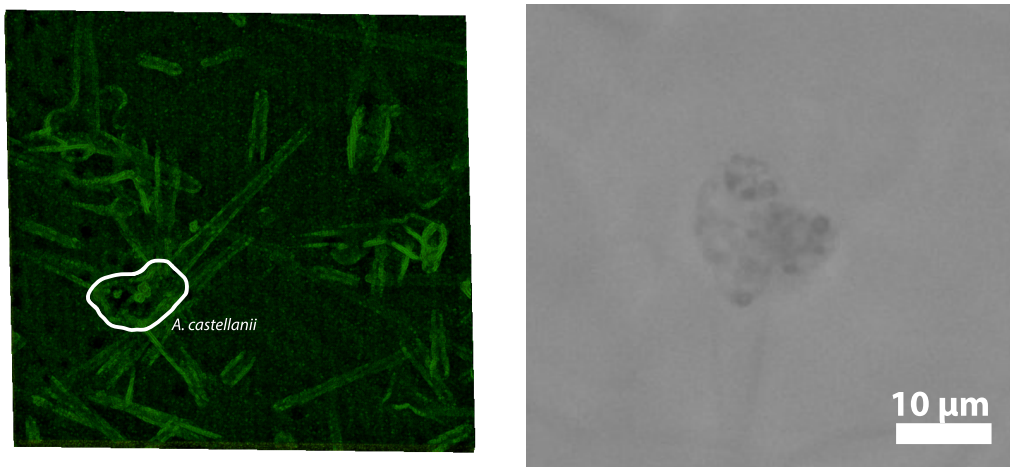

(a) (b)

Fig. 4.5.: (a) Example of spinning disc confocal fluorescence voxel image of *A. castellanii* (white circle) inside the porous channels. (b) A 20 microns deep REF52 wt in a Sulfo-SANPAH fibronectin (20 mg/µL) (as described by A. Möhring[238]) functionalized PAAm (Mix. A Tab. 2.2) channel. Scalebar = 10 µm.

The cells moved to dead ends turned around may be induced to their nucleus [162] and dense packed cytosol, [10] intracellular movements, [243] and went in an amoeboid motion [28] through these channels until they found bigger cavities where they remained at least for some hours (Fig. 4.6). These were our first indications for the potential of this 3D substrate as a possible cell trap.

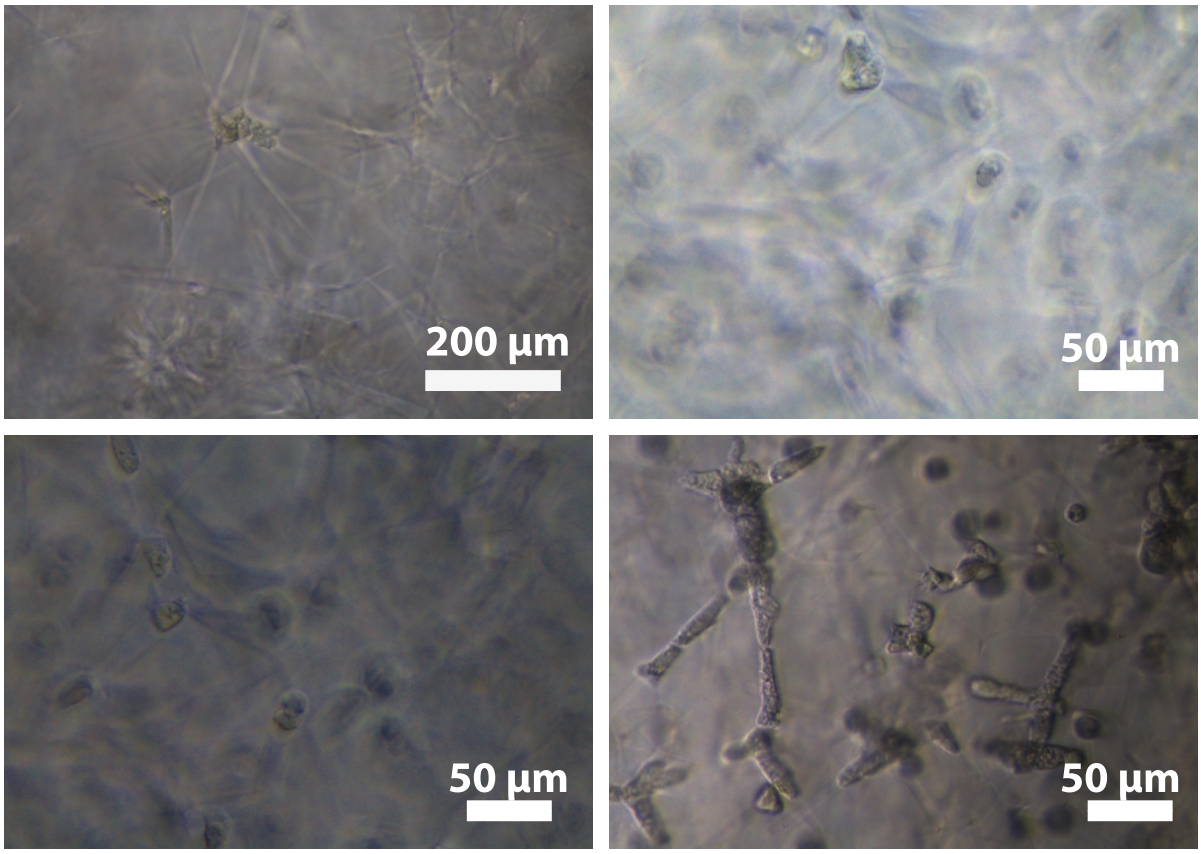

Fig. 4.6.: Phase-contrast images of *A. castellanii* in channels and cavities of the porous PAAm. Scalebar = 200 (upper left image) or 50 µm.

4.2.3. Migration Analysis

The behavior of *A. castellanii* in the porous hydrogels was recorded with phase contrast microscopy (10x objective, BX43) with an acquisition time of 5 sec per frame. The images were analyzed using a graphical software (ImageJ) to obtain the resting time, the speed, and the direction of the *Acanthamoeba* movement. Long term experiments (6 d) were conducted with phase-contrast or spinning disc confocal microscopy (IX-81). The distance of the cells movement and the cell diameter was measured perpendicular to the channel direction. The diameter of the cells in the junction of the porous 3D substrate

were measure parallel to the X axis due to no observable global movement (Fig. 4.7). A definitive cell speed reduction inside the channels in comparison to a bulk substrate was observed. Migration is reduced from $10 - 600$ nm/s for the bulk substrate of the same elasticity to $50 - 340$ nm/s for the channel system. The effective cell diameter adapted to the channel diameter and many resting cells inside the cavities were observed. This leads to the assumption that the porous PAAm substrate acts as a good cell trapping material and will be used for future projects.

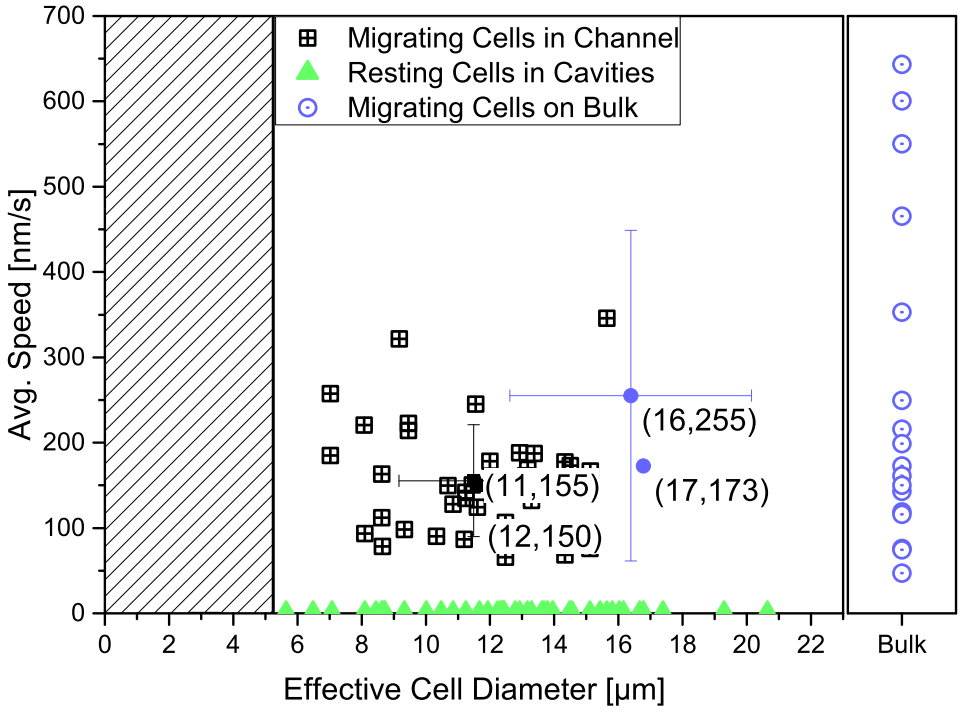

Fig. 4.7.: Graph of *A. castellanii* migrating (black quadric cross) and resting in porous PAAm (green triangle) in comparison to a bulk substrate (blue circle with dot) of the same stiffness. Filled marker show the mean values with standard deviation and median.

For long term experiments z-stacks were captured on an inverted microscope (IX81). The acquisition time was set to one stack per 30 min to obtain focussed images of the moving cells. Z-axis focus changes were noted and a combined into a time and z-focussed video, which was analyzed using the microscope software (XcellenceRT). Marks of the cell edges were measured with the pointfunction and saved as image sequences of the focussed cell (Fig. A.1). Through this, viable and mobile cells for more than 6 days inside the channel network were observed, but A significant number of cells had accumulated in larger cavities.

4.3. Conclusion and Prospects

The focus of pending patent (EP 15166793.8) was to elucidate the interaction of human pathogen *A. castellanii* with hydrogels, i.e. PAAm. These hydrogels are used as contact lens materials and lead to eye damages of contact lens users, which may result in infections and vision loss, known as the *A.* keratitis induced by *A. castellanii* (Sec. 1.2.2). Through previous studies of Reverey *et al.*[167] a higher adhesion behaviour to contact lens materials with a water content above 60 % was observed. Therefore hydrogels were promising substrate candidates as cell traps in medical containers for *Acanthamoeba*. Through the findings of the group of Adelung *et al.*, inclusion of the acidic hydrolyzable t-ZnO network as a template into PAAm was tested. The main challenging of this template mediated synthesis was to find the optimal pH range of the acidic hydrolysis. The t-ZnO are dissolvable with pH values below four in an acceptable time range. On the other hand the PAAm can not resist pH values below two to three even if it's built from low reactive amide groups it may fracture the polymer. Variations between one to four in pH would result in a hydrolysis time of 2 h - 10 days. The acid concentration decreases over time of hydrolysis like shown in the chemical equation 4.3.

$$\mathrm{ZnO} + 2\,\mathrm{HCl} \xrightarrow{c,t,T} \mathrm{Zn}^{2+} + 2\,\mathrm{Cl}^{-} + \mathrm{H_2O} \tag{4.3}$$

The zinc chloride is easy soluble in water and can easily be removed from the system by washing. In advance the acidic concentration will be reduced over time which will decrease the chance of a hydrolysis break of the polymer chains. In advance it PAAm integrity was tested with hydrochloride solution (1.28 M).[238] It resulted in an intact swollen PAAm even after 1 day. This threshold was set and lowered for future hydrochloric acid hydrolysis of the t-ZnO networks.

With this in mind it was possible to build the first seamless interconnected maze like tunnels within a hydrogel. This is advantageous to other inverse-opal like structures or quasi 3D materials where the cell material interaction is reductant and a cell-cell interaction is predominant. With the use of channels the material-cell interactions up to 97 % is given at all time, which can be found in dense structures like the brain, skin or blood vessels. Furthermore, the hydrogel gave the opportunity to use chemotactic reagents and nutrient supply. Cavities of a size above two *A. castellanii* act as cell traps

due to a cells nucleus,[162] its properties,[163] and deformability.[164] Through possible occurring masterpodes of the t-ZnO or probable air bubbles, larger cavities could be implemented into the material. It will further be investigated in future research with these novel 3D supportive substrates.

Adhesion, migration and cell capturing in these channels could be observed. The following experiments showed its suitability for cell culture studies, including chemotactic applications and further possible improvements for cell capturing. This will guide to new technologies to measure cell forces, capture pathogens, and cultivate stem cells in a natural 3D environment.

5 | Phagocytosis and Particles

Phagocytosis is an important mechanism found in many cell types like neutrophile granulocytes, natural killer cells, lymphocytes, macrophages, *Entamoebae*, or *Acanthamoeba.*[244] It is critical for the functioning of biological systems and tissues and plays a significant role for the immune response, because pathogenic parasites are phagocyted by T-Lymphocytes.

For *Acanthamoeba,* it is essential to feed on target cells like yeast or bacteria. The cell killing is induced by lysosomes.[11][A] Lysosomes are a mixture of acid hydrolases, proteins, DNA, RNA, and lipids. The acid hydrolase breaks large organic molecules inside a target cell and leads to programmed cell death (apoptosis).[244,245] Through the following digestion process, the food vacuole will supply nutrients for the amoebae. Besides, from the digested organisms, the gained nutrients are used to produce energy for adhesion, migration, and proliferation as well as membrane synthesis and many more processes in amoebae.

Within this work, it was observed that *Acanthamoeba* exert comparably large forces during target cell uptake. It is known that the energy consuming actin polymerisation guides the membrane protrusions (acanthapodia) in direction of a target cell, which surround and merge into complete engulfment of a target cell. The phagocytic uptake rate for *Acanthamoeba* is higher compared to macrophages. For example, the exchange rate at 30 to 37 °C of internalized polymer particles is 10 to 50 % within one hour.[246,247] As a reference, the exchange rate for a comparable macrophage is 50 % two to five hours.[248]

To decode the complexity and to gain further insights into underlying processes of this uptake event and probable trogocytosis, different particles like elastic polyacrylamide beads (EPABs), stiff polystyrene, and TMOS silicone based[249–251] were used.

[A]Lysosome: *gr. lysis* - destruction, *gr. soma* - body.

The particle size ranged from one to five micrometers, which is the size known for *Acanthamoeba* target cells. Target cell size ranges from one to two microns in width and two to ten microns in length. Literature showed that phagocytosis is only preferred at a size above one micron for *A. castellanii*.[252,253] Smaller particles or fluids are internalized by pinocytosis in *A. castellanii*.[246] This mechanism is necessary for cell growth before mitosis and tends to be generously observable in ubiquitous cell types.

The measurement of forces exerted to a surface of a substrate can be conducted with traction froce microscopy (TFM), where the localization of embedded fluorescent particles into a elastic substrate is related to the traction forces due to known properties of a substrate. To this end, the transfer of the concept of TFM on 3D substrates and synthesize fluorescent EPABs by means of inverse-emulsion polymerization was tested. The elasticity of the EPABs can be controlled by varying the amounts of crosslinker.

The goal was to relate changes in sample shape to forces exerted by cells in a bead deformation assay (BDA). In particular, the method of BDA to study the phagocytotic uptake of EPABs and related samples by *A. castellanii* in a simulated target cell killing experiment was used. Moreover, manipulation of cells with OT for phagocytosis experiments and investigation of the deformation of RBC was conducted, since these cells are biophysically well studied regarding their mechanical properties.

5.1. Particle Polymerisation

A major challenge of an inverse-micelle polymerisation is the produced size distribution of synthetic particles and the choice of surfactant. Many processes were used to manufacture particles of different shapes, sizes, properties, and compositions. A huge variety of techniques, which utilize molds, micelles, templates, or microfluidics were attempted. Either thermodynamical or kinetical effects lead to particle sizes above 10 microns or below 500 nm. In the range between these particle sizes, both thermodynamics and kinetics make it challenging to produce monodisperse samples in the first place. In advance, changes in temperature, concentration of an educt or other chemicals, the use of a surfactant, rotation speed and even the shape of a magnetic stirrer bar direct a synthesis to completely new particles with different size distributions. With this vast variety, only some researcher groups are able to produce monodisperse particle distributions with micelle synthesis. In this case, one task was to produce elastic particles of the

target cell diameter range of one to three micrometers. Therefore, inverse-micelle, and microfluidic based polymerisation was used, which lead to hard reproducible results and will be discussed in the following sections.

5.1.1. Inverse-Micelle Synthesis

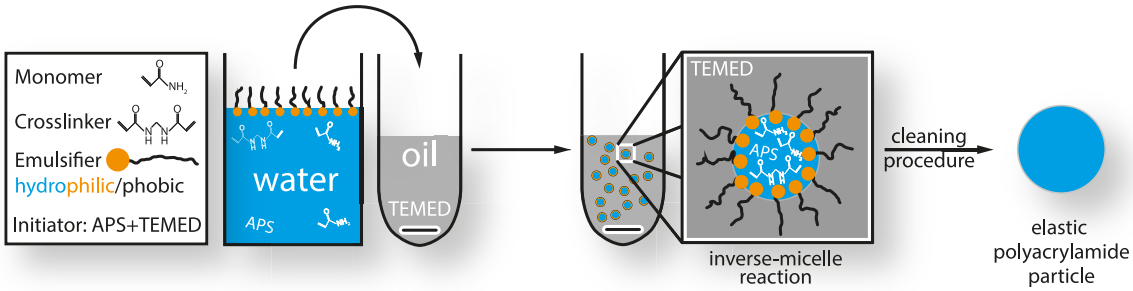

Fig. 5.1.: Scheme of an inverse-micelle reaction with the use of micelle formation induced by emulsifiers, which provide a reaction chambers for particle polymerization in a size range of the micelle. After cleaning of the suspension particles can be achieved.

Chemical mixtures from Tab. 2.2 (1 - 20 vol.-%) were poured into a test tube under inert gas atmosphere with 90 vol.-% of toluene (99.9 %) and dissolved with dodecyl sulfate sodium salt (1 - 20 %) under stirring at rates ranging from 300 to 1200 rpm with different shaped magnetic stirrer bars for at least 1 hour (Fig. 5.1).

This mixture could include fluorescein-dextran (50000 kDa) for fluorescence microscopy. When polyacrylic acid (PAA) was used, further surface functionalization was possible due to free acid groups on the particles' surface with EDC-coupling and free amine terminated molecules. The acrylamide monomer could be exchanged with 2-hydroxyethyl methacrylate (HEMA) or methyl-2-methylpropenoate (MMA) for different compositions in other applications.

The resulting opalescent micellar mixture was cleaned by centrifugation (8 - 10k rpm, 5 - 20 min, 1 - 3 times, Mikro 220R), decantation and resuspention in bidest. water or buffer referring to following cell experiments (Tab. 2.1). Phase contrast and fluorescence microscopy images were acquired (IX-81) for particle verification. As a result of the inverse-micelle polymerisation only hardly reproducible particles were obtained and therefore other monomers and systems were tested.

5.1.2. Fluorescent Polymethylmethacrylate (PMMA) Particle Synthesis

Fluorescein *O,O'*-Dimethylmethacrylate Synthesis

This reaction was performed comparable to Hyun-Ho Sim.[254] Fluorescein (2.50 g) and methylmethacrylate (20 mL) were mixed in a flask with trimethylamine (1.55 g) and cooled in a water-bath (< 7 °C). Methylacrylicacid chloride (2.70 g) was solved in methylmethacrylate (35.0 mL) in a dropping funnel. Under constant mixing (300 rpm) the methylacrylicacid chloride and methylmethacrylate solution was dropped (1 h) into the reaction mixture. After 3 h at low temperatures (<10 °C) the reaction was mixed (18 h) at room temperature. The mixture was washed with dest. water (60 mL) first and then with hydrochloric acid (5 mL, 1 M). The washed reaction mixture was precipitated in sodiumcarbonate solution (25 mL, 5 % in dest. water). The opalescent slightly yellow solution was dried with magnesium sulfate (10 g) and filtrated.[B]

PMMA Particles Synthesis

Cyclohexane (120 mL) and the stabilizer α,ω-methacrylicpolydimethylsiloxane (0.95 g, 130 chain length) were mixed under inert atmosphere and heated to boiling temperature. Dimethyl 2,2'-azobis(2-methylpropionate) (186 mg) was mixed with methylmethacrylate (8 mL) as well as the previously synthesized fluorescein solution. This mixture was poured into the reaction flask at once and heated to stronger reflux (125 °C) for 2 h. Monodisperse fluorescent polymethylmethacrylate (PMMA) particles were obtained.[255][C] These thermoplastic PMMA particles were cleaned with centrifugation (8000 rpm, 10 min, 3 times, Mikro 220R), and resuspension in bidest. water (1 mL), which resulted in floating fluorescent particles in water (Fig. 5.2), which could not further be used for cell experiments.

The following microfluidic technique with inverse micelles was chosen to simplify and produce elastic particles, because all previously described particles were either not homogenous, monodisperse or solid particles nor usable for cell experiments.

[B] Cooperation with Merz Dental, Sebastian Pflesser and Katharina Göpfert.
[C] Cooperation with Merz Dental, Sebastian Pflesser and Katharina Göpfert.

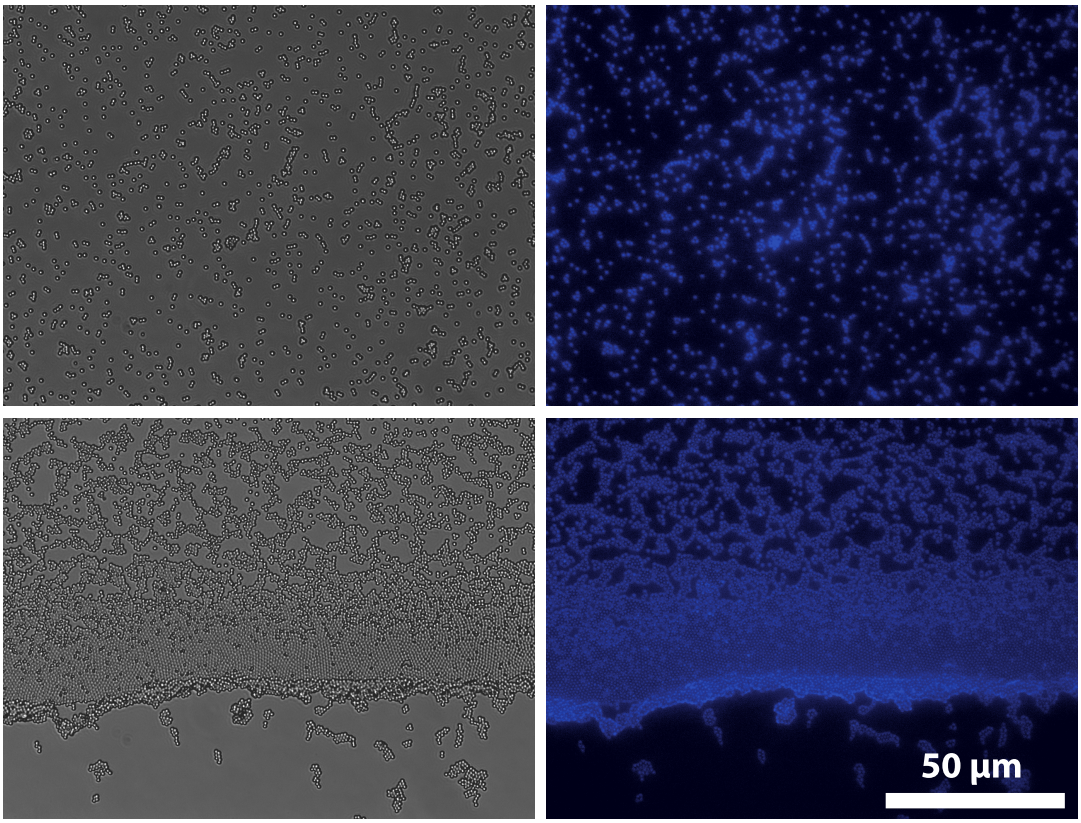

Fig. 5.2.: Phase contrast and fluorescent images of monodisperse PMMA particles. Scalebar = 50 µm.

5.1.3. Microfluidics

Because of the indifferent results in Sec. 5.1.1, a microfluidic apparatus and syntheses were developed. Different chip designs (Fig. 5.3) were tested for their micelle formation ability.

The use of specially designed microfluidic chips[D] was tested with various surfactant, oil, and water mixtures (Surfactants: Tween 20, Span 80, Triton-X 100, SDS, Docusate sodium salt; Oil: Siliconöl M520, Novec 7500, Castor oil). The most promising micelle formation of docusate sodium salt, Triton-X, and SDS (Fig. 5.4 (a)) did not lead to solid particle formation, but only micelles were obtained (Fig. 5.4 (b)).

Even the introduction of light induced radical polymerisation initiator based on hydroquinones into the reaction inside the channels and UV light (OmniCure Series 2000) induced initiation was not convincing (Fig. 5.3 (b)).

[D] Cooperation with Prof. Jakob Kjelstrup-Hansen from University of Southern Denmark, Casper Kunstmann-Olsen (Fig. 5.3 (a,b)) and Jong Wook Noh (Fig. 5.3 (c,d)).

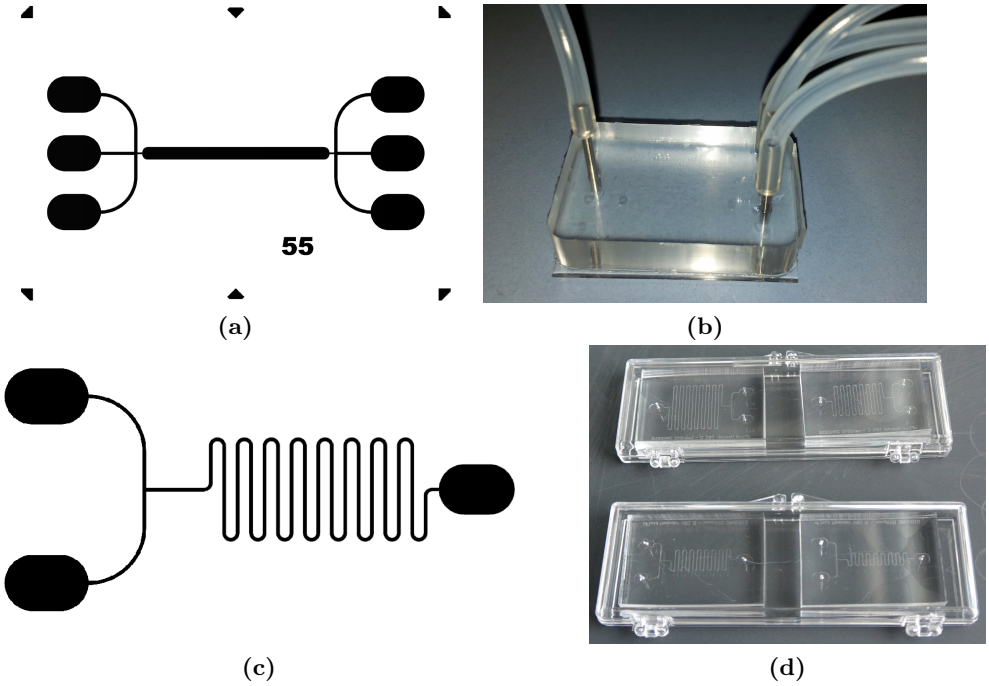

Fig. 5.3.: Schematic of the microfluidic chip design for microfluidics (a) and light induced polymerization with different channel lengths of the snake like structure (c). Images of the fabricated chips (b,d).

Hydrophilic - Lipophilic Balance (HLB)

However, to understand the microfluidic synthesis, the importance of the HLB index for micelle formation described by Griffin[256,258] have to be taken into account. Griffins empirical studies were used to find better surfactant mixtures and to define possible compositions of an emulsifier by means of a single value (Eq. 5.2).[259–261] Furthermore, Davies improved Griffins research into a calculable HLB value by determining and adding numbers for each molecular group.[262] A high HLB index means a good water solubility and leads to an oil-water immersion and *vice versa* (Tab. 5.1).[263]

The HLB index is calculated as

$$HLB = 20(1 - \frac{V}{S}),\ ^{[259]} \tag{5.1}$$

where V is the saponification and S the acid number. Equation 5.1 can be modified to

$$HLB = 20(1 - \frac{M_0}{M}),\ ^{[264]} \tag{5.2}$$

where M_0 is the molecular weight of the hydrophilic part of the surfactant and M the

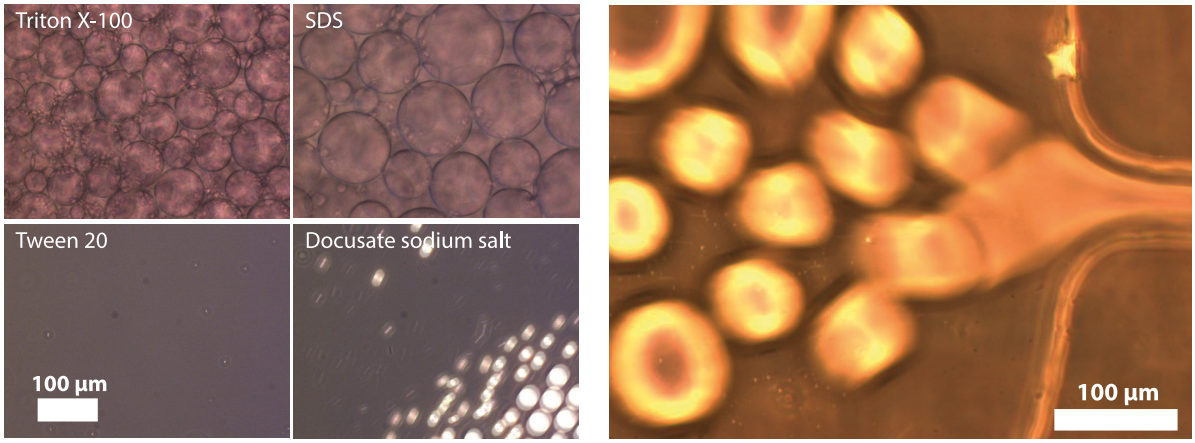

(a) (b)

Fig. 5.4.: Micelle formation of novec oil with water and four different surfactants (Upper left Triton X-100, Upper right SDS, lower left Tween 20 , and lower right docusate sodium salt) (a). Scalebar = 100 µm. Microfluidic mixture of novec oil and water with docusate sodium salt in microfluidic chip 55 (b). Scalebar = 100 µm.

whole molecular weight of the surfactant. So the HLB values summarizes interfacial and stabilizing properties of an emulsifier. This knowledge facilitates a more simplified surfactant choice for an easy, cheap and commercially available T-junction microfluidic synthesis of PAAm particles. A surfactant mixture needed for W/O emulsions and correlated HLB values was used (Polysorbate 80 HLB = 15 [265], Tween 20 HLB = 16.7 [266]).

The surfactant mixture of Polysorbate 80 and Tween 20 was used to gain a stronger micelle formation and to ensure a higher emulsion stability. This was tested and verified with a mixture of Polysorbate 80 and Tween 20 (1:1, 50 µL) in castor oil (4950 µL) or isopropylmyristate (4950 µL) due to the promising HLB values (Fig. 5.5). In conclusion, increased thermodynamical stabilized emulsion systems can be achieved, which resulted in stable W/O droplet formation. Hereafter, following preparations of the liquid phases were performed for microfluidic synthesis.

I. Preparation of Water Phase

1. Ammonium persulfate (64.51 mg) was solved in bidest. water (645 µL).

2. Fluorescein-dextran (7.10 mg, 50000 kDa) was solved in bidest. water (500 µL).

For the microfluidic synthesis the mixture given in Tab. 5.2 was degassed for 20 min *in vacuo* and filled into a two mL syringe for microfluidic synthesis (Fig. 5.6 Water Phase).

Tab. 5.1.: Surface active agent (surfactant) correlations in terms of HLB index. Adapted from [256–259].

HLB range		Use [256]
4 - 6		W/O emulsifiers
7 - 9		wetting agents
8 - 18		O/W emulsifiers
13 - 15		detergents
15 - 18		solubilizing
HLB range	State of the surfactant in water	Corresponding application [256–259]
1.5 - 3	non-dispersible	anti-foaming agent
1 - 4		emulsifier for W/O emulsions
2 - 6	poorly dispersible	
6 - 8	turbid unstable dispersion	wetting agent
8 - 10	turbid stable dispersion	
10 - 13	semi-transparent dispersion	emulsifier for O/W emulsions
13 and more	transparent solution	
13 - 15		detergent
15 - 18		solubiliser

Tab. 5.2.: Microfluidic PAAm mixture.

Compound	**Amount [µL]**
Acrylamide 40 %	2000
Bisacrylamide 2 %	400
HEPES (pH 8.5)	100
Bidest. water	6950
1. APS in bidest. water	150
2. Fluorescein-dextran in bidest. water	400

II. Preparation of Oil Phase

1. Polysorbate 80 and Tween 20 (each 500 µL, 1:1) were poured into a beaker.
2. 50 µL of this solution was mixed with isopropylmyristate (4950 µL) and TEMED (10 µL).

For microfluidic synthesis the mixture was filled into a five mL syringe (Fig. 5.6 Oil Phase).

Microfluidic Synthesis (I. and II.)

These two syringes were mounted into a syringe pump (PHD Ultra 4400) and the silicone tubes were filled bubble free with the liquid phases. The amount of oil phase was set higher (5:2) to gain single micelles within the tube system. Via a T-junction made

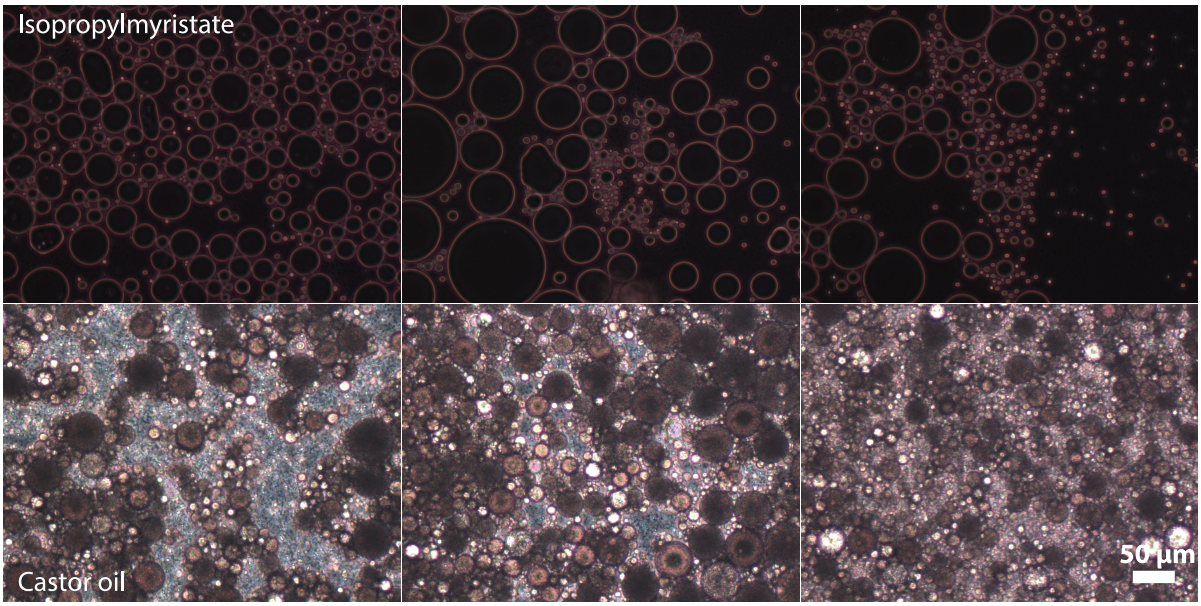

Fig. 5.5.: Image of micelle formation in isoproylmyristate and castor oil with a surfactant mixture of Polysorbate 80 and Tween 20 (1:1, 50 µL) after 3 min in vortex (Vortex Genius 3). Scalebar = 50 µm.

from PTFE the tubes were connected. Settings of the syringe pump was "infuse only", the diameter of the five mL syringe was measured and set to 12.45 mm for accurate flush rate (20 µL/min) calibration. The received micelles, within the oil phase, had a droplet size in the lower micrometer range due to a concentration above critical micelle concentration (c_{cmc}) and detergent properties to form stable micelles. At the end of the tubing, a gel-like mixture was received in a catch reservoir and cleaned via repeatedly centrifugation (8000 - 10000 rpm, 5 - 10 min, 25 °C, 3 - 5 times) with bidest. water (1 mL).

The first stable non agglomerating particles usable for cell experiments were successfully produced with this easy microfluidic T-junction synthesis. The incorporation of the fluorescent dye was not a problem as mentioned by Janiesch *et al.*[267] A major challenge was the imperfect cleaning procedure. The particles still remained in a partly oil phase instead of pure water or buffer and had to be cleaned later on. An idea to solve this problem would be the use of different detergents to get rid of the liquid isopropylmyristate wax or a dialysis of the resulted solution. These methods have not been tested yet, but preliminary cell experiments were conducted with the synthesized mixture as isopropylmeristate is widely used in pharmaceuticals and should therefore be harmless to cells.

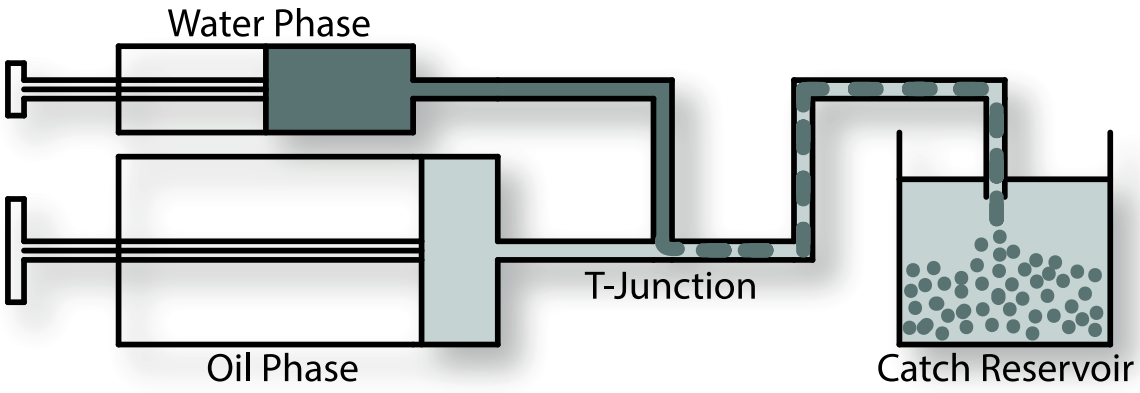

Fig. 5.6.: Scheme of a microfluidic T-junction synthesis. The water phase contains monomers, crosslinker, dyes, and peroxodisulfate as radical initiator. The excessive oil phase is containing detergents and a radical redox initiator partner. Both phases are combined in a T-junction and further stored till the end of the reaction in a big catch reservoir.

5.2. Phagocytosis Experiment

5.2.1. Experiment with Polyacrylamide Particles and *A. Castellanii*

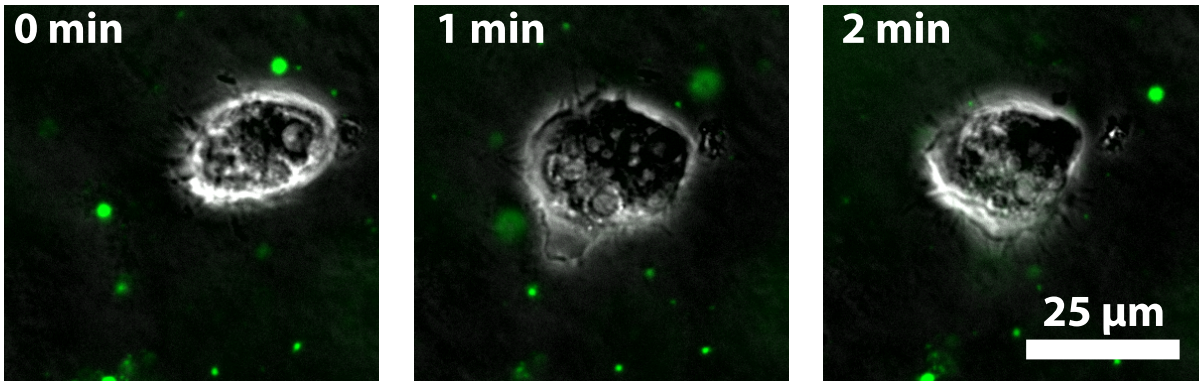

Fig. 5.7.: Merged fluorescence (FITC) and phase-contrast images of *A. castellanii* moving through a polyacrylamide particle solution without internalization of any particle (green). Scalebar = 25 µm.

To test the effect and phagocytosis of *A. castellanii* with deformable PAAm particles. Cell experiments were conducted. *A. castellanii* were cultured as described in Sec. 2.2 in a glass-bottom petri dish. The PAAm particles (100 µL aq.) were resuspended and homogeneously transferred into the petri dish. Fluorescent images (FITC) and videos were captured (IX-81) after 30 min under ambient conditions (25 °C). The *Acanthamoeba* remained unharmed and no encystation or cell death could be observed by microscopy within observation time. Probably, the remaining liquid wax prevented particle phagocy-

tosis and bead deformation (Fig. 5.7). The *A. castellanii* were swimming and migrating inside an oil-water suspension like a baby in a ball pit. To improve phagocytic uptake of these particles, a better cleaning procedure has to be found like described previously. The formation of elastic fluorescent beads with the easy T-junction microfluidic synthesis is a great start for future projects as it could lead to a true BDA and 3D TFM of phagocytosis events.

5.2.2. Polystyrene Particle Phagocytosis

To measure the phagocytic uptake rate of *A. castellanii* and to provide a comparison for the EPABs, polystyrene particles ($0.06 - 4.95$ µm, 1 - 3 % solids, Tab. A.4) were repeatedly centrifuged with 8000 rpm for 5 - 10 min. The supernatant was exchanged with fresh solution (water, buffer, medium) and resuspended with a vortex (Vortex Genius 3) for 1 - 5 min and additionally 30 sec - 5 min with an ultrasonic bath (RK 52) if necessary. Particles of a final concentration of 300 - 1000:1 were added to adhered *A. castellanii* (2 mL, PYG 712 medium) in culture plates at ambient conditions. Some of the experiments were conducted at 37 °C as a comparison because the phagocytosis rate increases drastically with temperature. [246]

5.2.3. Elastic Silicone based Particles

Particles of two different silicone polymers (made from trimethoxymethylsilane (TMOS), Bulk modulus K = 2.49 GPa, or mixtures of vinylmethyldimethoxysilane with tetramethoxysilane [24:1, K = 1.03 GPa; 100:1, K = 0.61 GPa]) with three different compressibility modules (K) were used. [251][E] The incorporation of the hydrophilic fluorescent dye (Nile Red) to the stiffer particles were ten fold higher than into softer ones. Best phagocytosis results were achieved with stiff highly fluorescent particles as they were relatively easy to observe (Fig. 5.8). Intracellular movements of these particles were observed but due to their high bulk modulus no bead deformation was present. Therefore, new samples were chosen to improve phagocytic uptake as well as deformability, which is described in the following section.

[E] Cooperation with Prof. Gabriel Lopez and Wyatt C. Shields from Duke University, U.S.A.

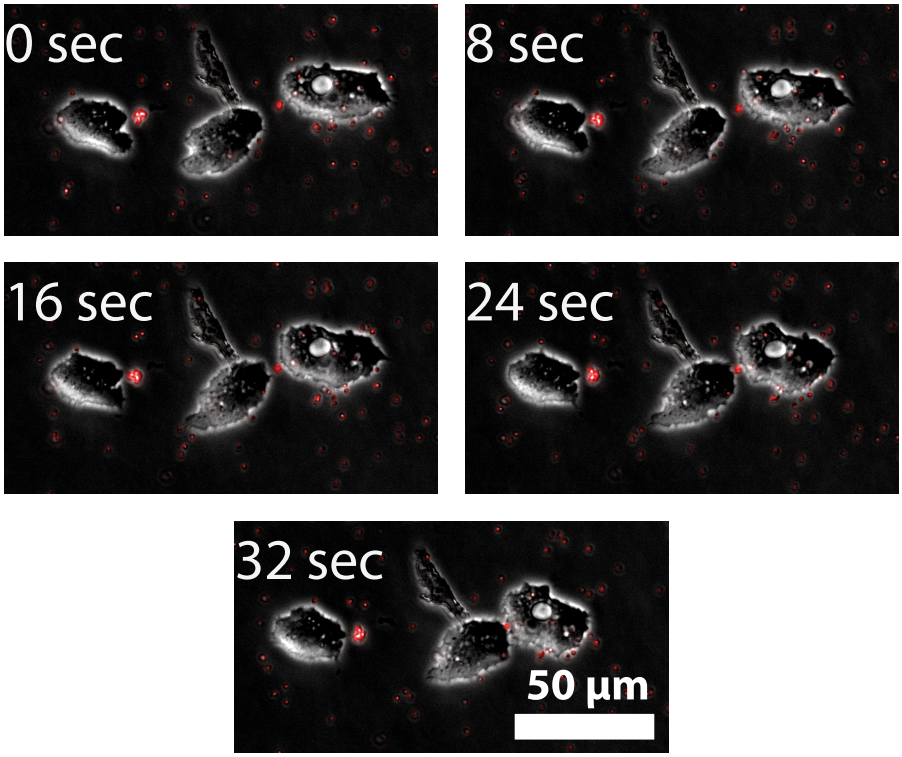

Fig. 5.8.: Resulting fluorescence (TxRed) merged with phase-contrast images of TMOS particles with *A. castellanii*. Scalebar = 50 µm.

5.3. Deformation Measurements

After the promising results in PAAm particles synthesis and silicone based particles, but a lack of phagocytic uptake events, the first biophysically well analysed cells, the RBCs were used to measure a deformation of phagocytosed samples. These cells were used as a comparable elastic deformable cell for deformation measurements. Cultivation of RBC and *A. castellanii* were conducted at ambient conditions. *A. castellanii* (30k amoeba/well) were transferred into a 6-well plate or petri-dish containing sodium chloride solution (50 mM, $2-3$ mL). RBCs were stained with anti-GlyA (Sec. 2.2.3) and controlled by phase-contrast and fluorescence microscopy (IX-81).[F]

5.3.1. Red Blood Cell Deformation

The RBC area and shape deformation was analyzed using the Xcellence RT Software. An observed shape change was orbited with the magic wand tool with best suited settings (tolerance: 50, smoothing: 0, RGB mode). Following properties were determined for

[F] In collaboration with Prof. Dr. Matthias Peipp, Medical Faculty, CAU Kiel, Germany.

further analysis.

- Cell area for 2D assumption on RBC deformation.
- Center of mass x und y to compare position changes relative to *A. castellanii* movement.
- Convexity and Sphericity to evalute shape changes of RBCs.
- Perimeter and Diameter: mean, min, max to relate results with undeformed RBCs.
- Max x and y position in an image, Convex area, Orientation, Orientational aspect ratio, and Elongation.

The most important results were the cell area, sphericity and convexity. To understand these values, some fundamental ideas have to be explained.

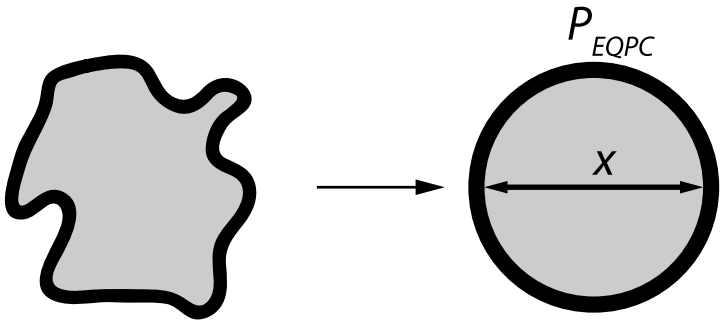

Fig. 5.9.: Graphical scheme of the equivalence perimeter (x) of a circle (P_{EQPC}) resulting in the same projection area like an observed particle. [268]

The area of an observed object can be calculated with the equivalence perimeter of a circle P_{EQPC}, which has to be determined and optimized with the Feret-perimeter to calculate the best fitting diameter (Fig. 5.9). The Feret-perimeter is the calculated group of the tangential measured lengths of a particle (Fig. 5.10 (a)). It is comparable to the measurement with a caliper, e.g. for the thickness of a metal sheet.

The sphericity is calculated by

$$S = \frac{P_{EQPC}}{P_{real}} = \frac{2\pi\sqrt{\frac{A}{\pi}}}{P_{real}}, \tag{5.3}$$

where P_{real} is the circumference of the observed object and A the equivalence area of circle. S can range from 0 (irregular shape) to 1 (perfectly round) due to irregularities of

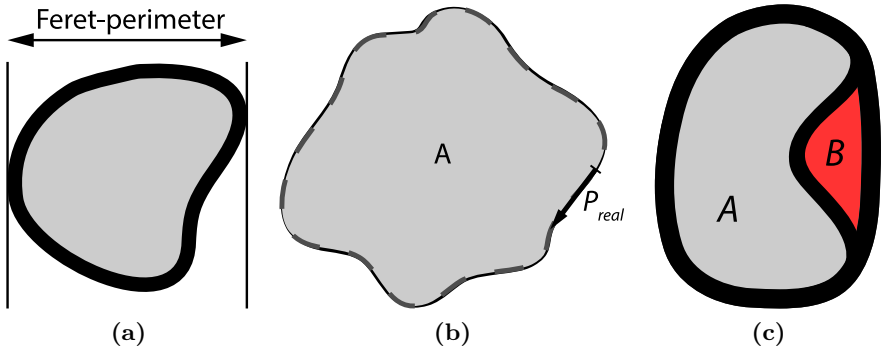

Fig. 5.10.: (a) Scheme of a measured Feret-perimeter. (b) Measurement for Sphericity analysis. (c) Definition of Convexity and meaning of concave area B.[268]

a sample, which lead to a bigger perimeter. The comparison of the smallest possible area is connected to smallest possible projection area A. S derives from the Feret-perimeter, which is shown in Fig. 5.10 (b).[268]

The convexity Ψ_c is displayed in Fig. 5.10 (c) and defined with

$$\Psi_c = \frac{A}{A+B} \tag{5.4}$$

where A is the real projection of a shape and $A+B$ the area of its convex hull. For example, a maximal value of only $\Psi_c = 0.99$ can be achieved using a CCD camera due to the quadratic form of a digital pixel of a camera, which induces slightly concave irregular parts in every captured image.

Tab. 5.3.: Calculated average changes of RBC deformation.

	Start	Change	Deformation	Change	End
RBC Area [μm^2]	37.3 ± 3.01	51 %	56.4 ± 12.1	-21 %	29.6 ± 7.64
Sphericity	0.628 ± 0.126	-53 %	0.293 ± 0.324	-59 %	0.255 ± 0.158
Convexity	0.945 ± 0.024	-14 %	0.810 ± 0.134	-17 %	0.788 ± 0.111
Time [sec]	0.00 - 15.0		15.0 - 37.5		37.5 - 67.5

The deformation data was stored as an image sequence for better visibility (Fig. 5.11). As a control, the cell area of undeformed RBCs were used in all three dimensional orientations (Image analysis: setting of reference cell tolerance = 35). The experiments showed first erythrophagocytosis events of *A. castellanii*. Moreover, cell deformation was observed and validated in Fig. 5.12. The RBC projected cell area as a function of time was plotted for changes in cell area, sphericity and convexity (Tab. 5.3). A change of 51 % in cell area was observed within 22.5 sec of cell-cell contact. The change in the

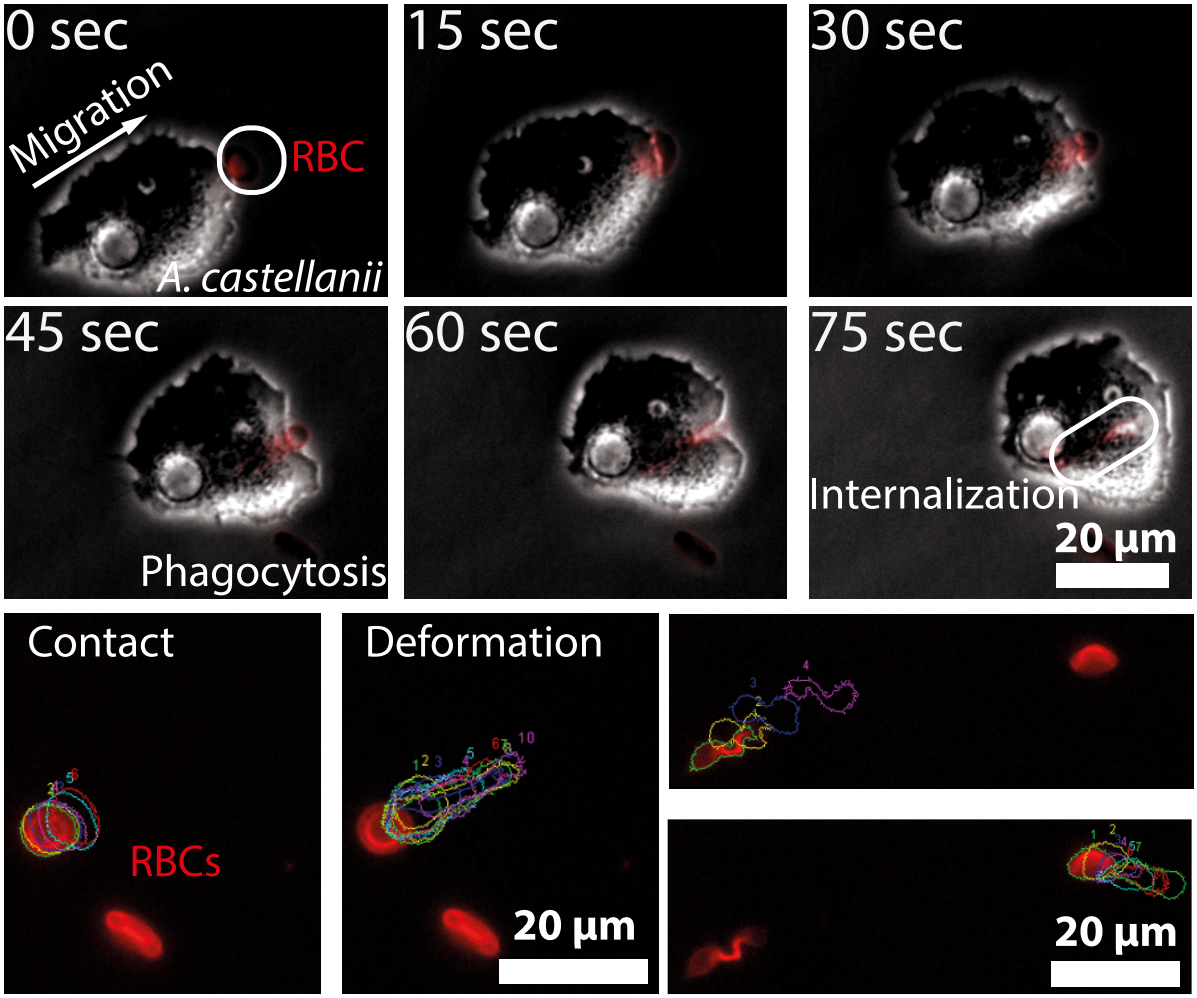

Fig. 5.11.: Merged phase-contrast and fluorescence (TxRed) images of RBC deformation during *A. castellanii* contact. Scalebar = 20 µm.

projected cell area could be assumed as a turning of the RBC but is not probable as the RBC stayed in its shape after deformation. In addition, a simple stretching of RBC by crawling of the *A. castellanii* over the RBC can be neglected as the cell diameter parallel to the phagocytosis direction increased about more than 10.1 µm. Not only phagocytosis but also transportation of RBCs by *A. castellanii* was observed (Fig. 5.13). The *A. castellanii* moved several minutes with the RBC fixed to its membrane. A lysis of the RBC can not be neglected yet and is discussed in Sec. 5.3.2. The force of a phagocytic uptake event was estimated as follows.

Dao *et al.* investigated the deformation of RBCs in OT with two bound particles (contact area 2 µm) connected to the membrane.[270] A maximal deformation of 50 % in axial and -40 % in transversal orientation at 340 pN was observed. A change from the

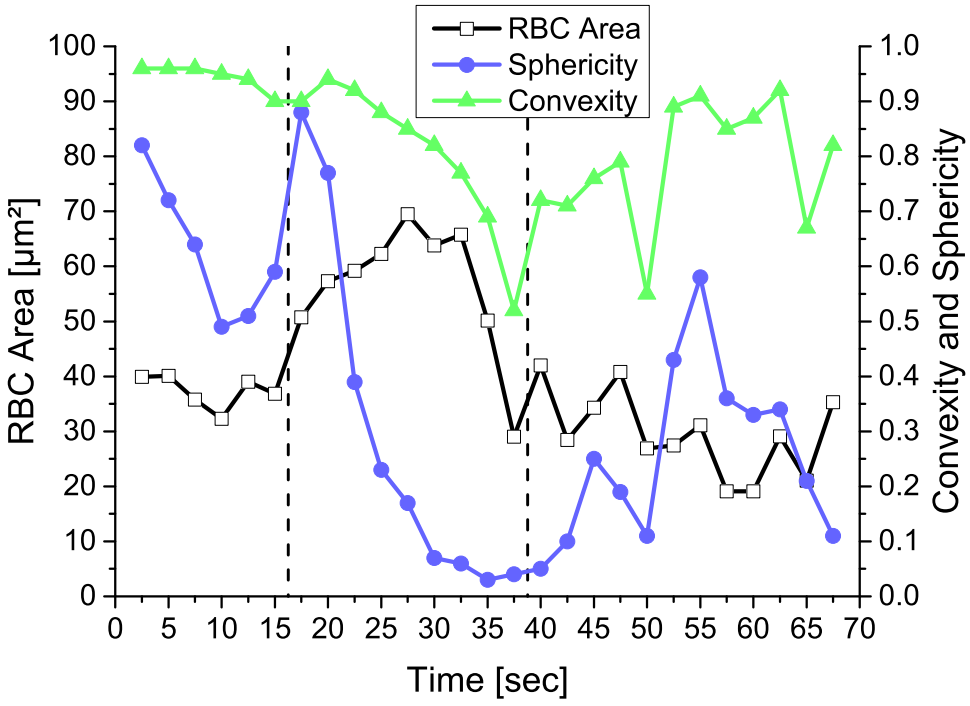

Fig. 5.12.: Graph of the deformation analysis of RBC while *A. castellanii* phagocytosis presented in Fig. 5.11. Dotted lines indicate the start and end of deformation.

initial RBC diameter $d_{Lit.0}$ 7.82 µm was calculated as $d_{Lit.axial}$ 11.73 µm and $d_{Lit.trans.}$ 4.66 µm. These changes were linear extrapolated, plotted (Origin 9.1g) with the observed d of RBC experiments (Fig. 5.15), and resulted in calculated force values for the observed d. From the initial diameter d_0 of 7.76 µm to d_{axial} 17.9 µm with a phagocytic deformation force (PDF) 886 pN and $d_{trans.}$ 3.98 µm with 415 pN. In addition, the values for 886 pN in the transversal deformation was estimated as −0.318 µm and for the 415 pN the estimated axial deformation was 12.5 µm. Obviously these last values are false, as a negative diameter is impossible, but from the linear extrapolation in Fig. 5.15 a qualitatively good agreement is valid.

To support these values the comparison to the optical stretcher experiments of Guck *et al.* was performed.[269] This calculation was performed in the same way as the previously discussed PDF estimation of the RBC deformation. The initial radius $r_{Lit.0}$ 3.13 µm was deformed in the optical stretcher to $r_{Lit.axial}$ 3.57 µm, which is a change of 14.1 %, and $r_{Lit.trans.}$ 2.77 µm, which is a decrease of 11.5 %, with a stress peak (σ_0) of 1.47 N/m^2. After calculation of the equation, adaptation to the initial experimental RBC radius r_0 3.88 µm, and extrapolation to the observed values the following values

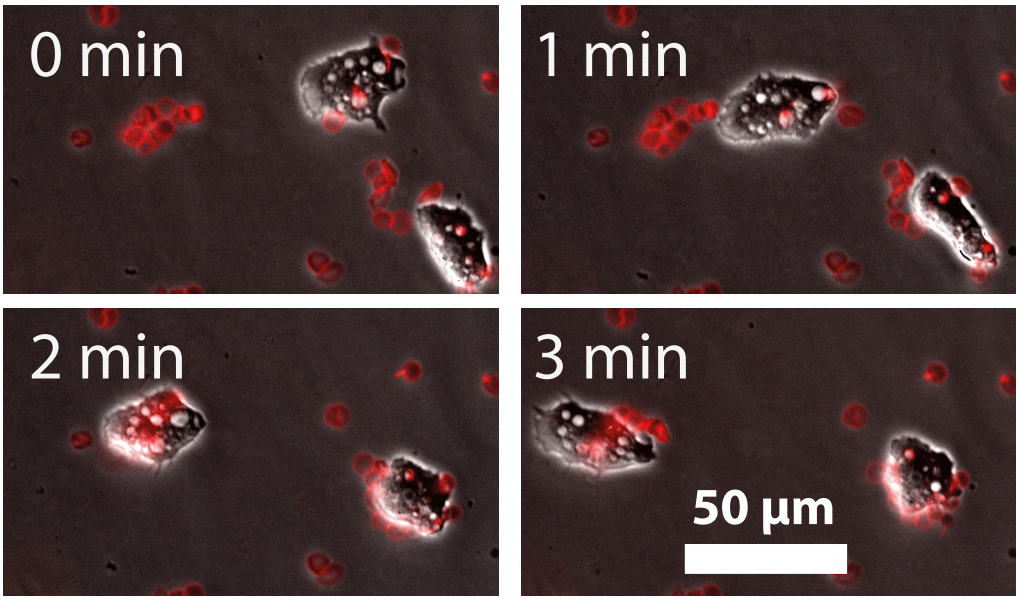

Fig. 5.13.: Merged phase-contrast and fluorescence (TxRed) images of *A. castellanii* transporting some stained (anit-GlyA) RBCs. Scalebar = 50 µm.

were achieved. r_{axial} 8.95 µm is connected to σ_{axial} 5.95 N/m^2 and $r_{trans.}$ 1.99 µm lead to $\sigma_{trans.}$ 2.86 N/m^2. Moreover, the values for r_{axial} at 2.86 N/m^2 were estimated as 4.95 µm and $r_{trans.}$ at 5.95 N/m^2 as 2.05 µm for better comparison. These estimated values are interesting as *Guck et al.* showed that the linear regime of their calculations are only given till a value of 2 N/m^2 for σ_0 and lead to rupture above 3 N/m^2 as presented in Fig. 5.14. This is in good agreement as a probable rupture of an estimated axial diameter of 5.00 µm at 3 N/m^2 for the extrapolated axial curve is actually shown at the second encirclement of the deformation image (yellow 2) in Fig. 5.11. Therefore, the force as well as the stress peak estimations are reasonable as the force is multiple orders of magnitude higher as well as the maximum stress.

5.3.2. Reflection Interference Contrast Microscopy (RICM)

RICM was used to observe whether the RBC deformation is a lysosomal leakage of the cytosol, rolling or real phagocytic uptake event of the *A. castellanii* interaction. Observations under the same conditions as the deformation experiment revealed that *A. castellanii* never migrated or rolled over any RBC and the deformation observed in Sec. 5.3.1 has to occur either as a lysosomal leakage or a real deformation event. RBCs (Fig. 5.16 (a) red circle) can be observed as special round doughnut shaped interference pattern, when the cell lies parallel to the surface. In any other orientation the RBC

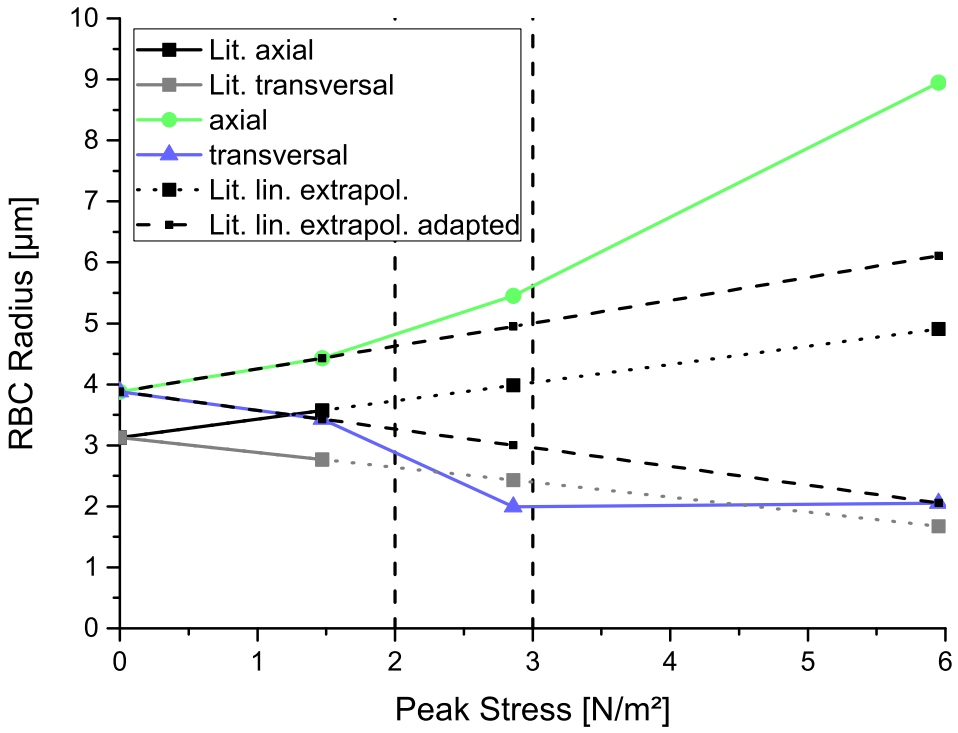

Fig. 5.14.: Graph of the adapted RBC radius as a function of peak stress according to the data shown by Guck *et al.* in an optical stretcher experiment (black and grey square) [269] and its linear extrapolation (dotted lines). The acquired deformation data (green dot and blue triangle) and its estimated values of a peak stress with the adjusted extrapolation to the initial experimental RBC radius (segmented line).

has a spot pattern. *A. castellanii* (Fig. 5.16 (a) white ellipsoid) a complete adhesion pattern can be observed with a periodic changing migration pattern and sometimes in black interference its nucleus or contractile vacuole.

A strategy to proof this difference could be to stain the cytosol of the RBC and test if there is any fluorescent leakage. The major challenge of these experiments will be exclusive staining of RBC cytosol by staining the whole culture medium, which could react with leaking cytosol from RBCs. This will probably be unrealizable with the cellular design of *A. castellanii* as it might lead to cell staining of both cell types. Presumably, with a change of RBC deformation of 51 - 53 % in projected cell area as well as sphericity and convexity alterations of 14 - 17 % at the time of internalization, the deformation can be estimated as a force of 880 pN, when compared to the results of Guck *et al.* [269]

With these experiments, first indications of a phagocytic force generation have been performed but have to be further verified with special staining procedures for this phagocytosis experiment. Furthermore, other erythrophagocytic cells could be analyzed with

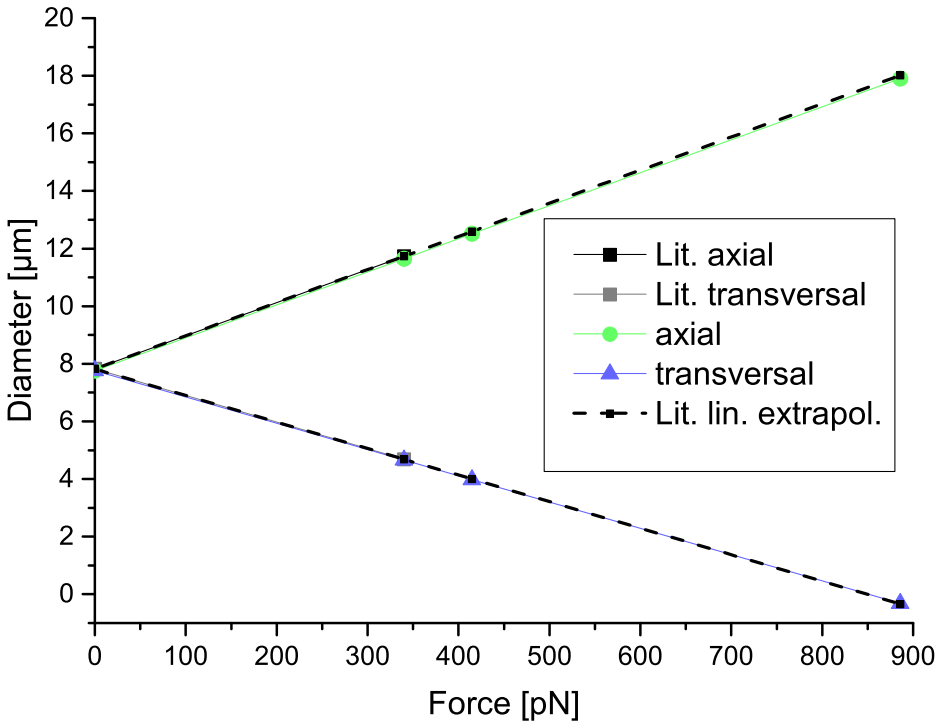

Fig. 5.15.: Extrapolated graph (segmented line) of force against diameter change of an OT experiment by Dao *et al.*[270] (black and grey squares). The positive slope is connected to an axial and negative slope to a transversal deformation of a RBC. The data of the deformation experiments with *A. castellanii* (green dot and blue triangle) is shown as well as estimated values.

this technique. Although manual analysis has to be improved with modeling procedures.

As a prospect of this project, experiments with rod-shaped particles (Sec. A.1) and target cells (Sec. 5.3.3) were performed.

5.3.3. Target Cell Killing Experiment of HCEC-12 with *Acanthamoeba Castellanii*

To test the main infection pathway of *A. castellanii* through the eye and to investigate a real target cell killing experiment of Human Corneal Endothelial Cells-12 (HCEC-12) a culture of *A. castellanii* and HCEC-12 was performed. Therefore, the HCEC-12 were incubated (37 °C, CO_2-Incubator C150) in a glass-bottom petri dish in cell medium ($2-3$ mL, Ham's F12 + Medium 199 + 5 % FBS). After 1 d *A. castellanii* (30k amoeba/well) were transferred into the the same petri dish and experiments were conducted with an incubator (37 °C, MI-IBCD-F1-AF). Adherent HCEC-12 were cultured with *A. castellanii* and followed by phase-contrast microscopy (IX81). The experiments showed at ambient temperatures that *A. castellanii* were migrating in circles

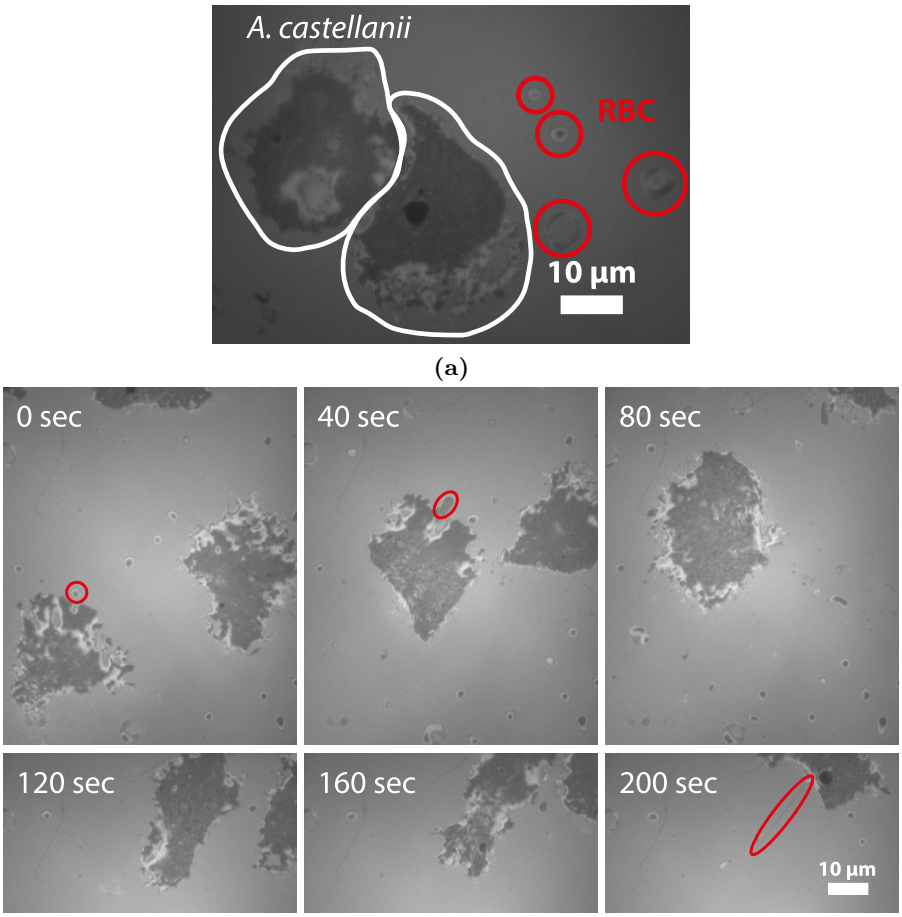

Fig. 5.16.: RICM images of *A. castellanii* (white circles) culture with RBC (red circles) (a). Timelapse of an *A. castellanii* and RBC experiment for verification of the deformation without rolling over the RBC. Scalebar = 10 µm (Zeiss 63x).

around HCEC-12 but no apoptosis of HCEC-12 was observed. At normothermia (37 °C, MI-IBCD-F1-AF) the amoeba lysed the target cells with a "killing kiss" and probable phago- or trogocytosis as the target cell volume decreased within 200 min (Fig. 5.17). Indications of trogocytosis, which have to be verified with cell staining and fluorescence microscopy were monitored (Fig. 5.17, 100 min at the bottom of the image). This is unknown to literature. Further experiments in these projects will maybe proof these assumptions.

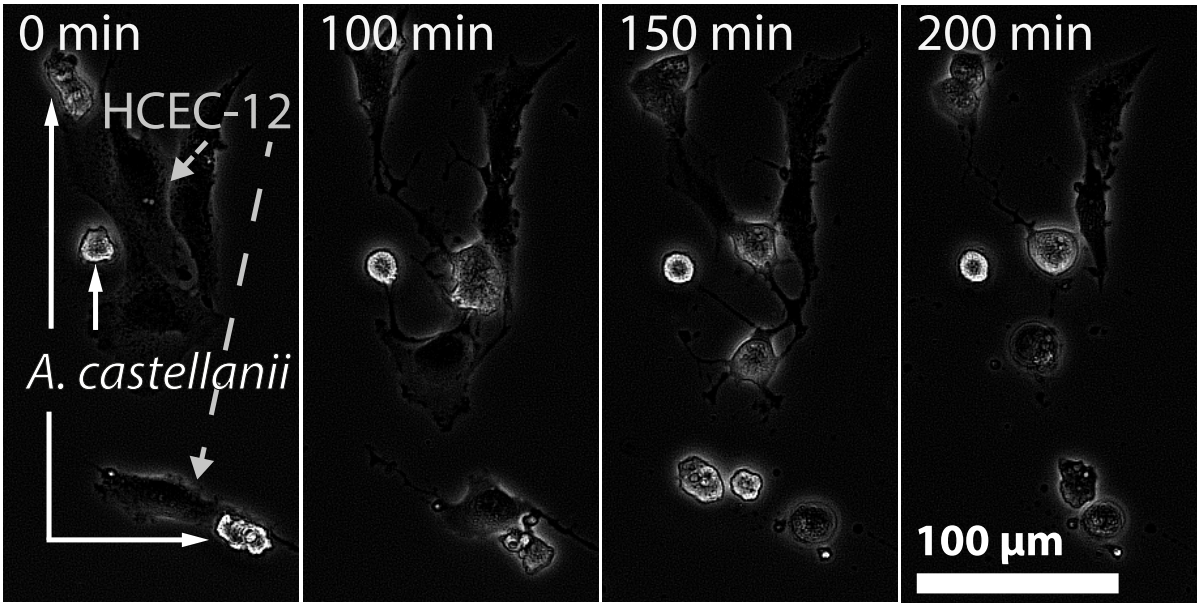

Fig. 5.17.: Culture of adherent HCEC-12 (dotted grey arrows) with addition of pathogenic *A. castellanii* (white arrows) at normothermia (37 °C) in HCEC-12 medium. The *Acanthamoeba* killed most of the target cells within 200 min as then all HCEC-12 had a round shape. Scalebar = 100 µm.

5.4. Optical Tweezers

The background and applications of OT were collected and well explained by Padgett *et al.*[271] and Urban *et al.*[272] The fundamental requirements for a working OT is the momentum transfer between photons and matter. This is counter intuitive to the every day life and contradictory to self-experienced knowledge about light. Although, a radiation pressure was shown even for macroscopic bodies with an electrical field.[273] This phenomenon was first observed by Kepler[274] inspired by Apians observation on the Halleys comet[275]. Kepler observed that a comets tail points into the opposite direction of the sun. This was further hypothesized and developed by Euler,[276,277] Crook,[278] Lebedev,[279] and Nichols with Hull.[280,281] A comet tail will be bent away from the sun by solar winds and therefore photons must transfer a momentum on matter.[282–284] Maxwells electromagnetic theory[285] and Bartoli[286] stated that light performs radiation pressure, which is known as the Maxwell-Bartoli force.

These findings guided to the invention of OT. OT are used to trap, manipulate and measure interactions of particles inside a focussed laser beam. OT were an unique idea of Ashkin in the 1970s, who worked at "Bell Labs" and was therefore able to use the advantageous technique of Laser.[287,288] He and his coworkers were the first people, who were able to explain the interaction of light with particles that have a different optical density than their surrounding and accordingly, the Laser light can act as an optical trap.[289] Based on this, Ashkin was able to construct and measure the interaction of light with particles[290] and even viruses and bacteria.[291] These different spherical shaped objects sense the exerted net force of OT, which is the result of gradient and scattering force (Fig. 5.18). These forces equilibrate with each other, when calibrated correctly on the sample, and will allow to trap particles in three dimensions. 20 to 30 years later, this method made it possible for Grier[170] and many other scientists to determine forces between two DNA strains,[292] stretching[171] and rotation[172] of cells, cell-particle interactions,[173] RBC rotation[174,175] and deformation,[176] as well as (visco-)elasticity measurements of cells.[177,178] Moreover, new setups like the optical stretcher were build to measure deformations of cells within a focused beam[171] or holographic OT were combined with microfluidics and used to manipulate two actin filaments and to measure a 0.2 pN Force for bundle formation.[293]

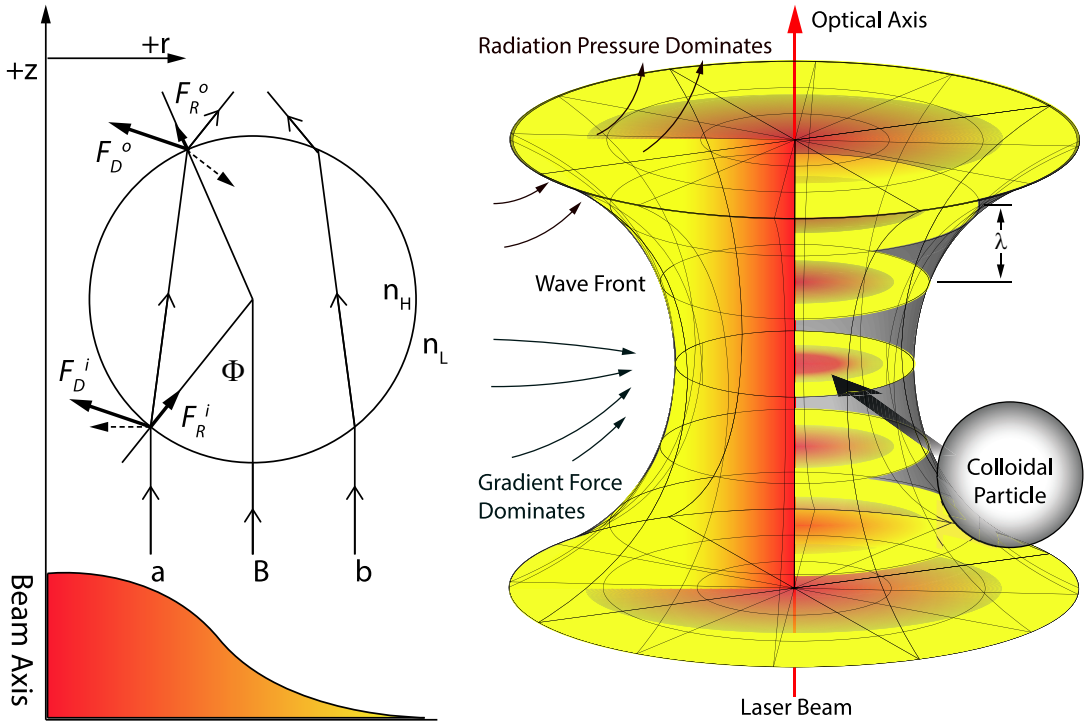

(a) A dielectric sphere situated off the axis A of a TEM_{00}-mode beam and a pair of symmetric rays a and b. The forces due to *a* are shown for n_H (refractive index of the particle) > n_L (refractive index of the medium). The sphere moves toward +z and -r. Adapted from [289].

(b) Schematic illustration of trapping a particle inside an optical tweezer. Adapted from [170].

Fig. 5.18.: Fundamental forces in optical tweezer.

To understand an optical trap, it is necessary to consider the underlying force parallelograms. Therefore, Fig. 5.18 (a) shows the Gaussian intensity profile of a laser beam as the y-axis. The beam a undergoes Fresnel reflection ($_R$) and deflection ($_D$) at both particle interfaces (^{i} for input and ^{o} for output), which results in angular dependent (Φ) forces of radiation pressure (F_R^i/F_R^o) and deflection (F_D^i/F_D^o). The particle will be directed in both cases in positive z but for the deflection in negative r direction. The same but weaker beam b acts as beam a but in positive r direction with less force. [289] This experiment of Ashkin *et al.* explains the centering of a particle inside a focussed laser beam in a liquid.

To focus and trap a particle in z-direction of the optical axis a dominant gradient force is needed contrary acting to the radiation pressure, which is induced by absorbed momentum of the photons. This is achieved with the use of a high numerical aperture objective as the beam is rapidly diverging after the focal point and results into a force

in the objective direction as well as momentum conservation. Fig. 5.18 (b) presents the intensity maxima in z direction (circles). The combination of the scattering and gradient force leads to a slightly higher trap above the focus point. Complex interaction of these forces result in a stable optical trap (Tab. 5.4).[294] Furthermore, the important Mie scattering, which acts at similar length relations of a particle with the interacting light, has to be included.[295]

The force ratio (R), which has to be greater than the unity for an optical trap, can be described by the following equation:

$$R = \frac{F_{grad}}{F_{scat}} = \frac{3\sqrt{3}}{64\pi^5} \frac{n_b^2}{(\frac{m^2-1}{m^2+2})} \frac{\lambda^5}{r^3 w_0^2} \geq 1 \text{ [290]} \tag{5.5}$$

λ is the wavelength in the medium w_0 the focal spot size, which results in axial locations of $z = \pi w_0^2/\sqrt{2}\lambda$. m is the ratio between the refractive index of the bead (n_b) divided by the medium (n_{med}) as $m = \frac{n_b}{n_{med}}$. To understand the method and possibilities of OT a comparison to AFM was carried together in Tab. 1.1.

Tab. 5.4.: Overview about the force parallelogram in optical tweezers.

Gradient force	Different refractive index of the particle to its surrounding
	Axial intensity gradient
	Dielectric material
Scattering force	Electro magnetic wave force transfer
	Acts on the lateral axis of a particle

5.4.1. Construction of an Optical Tweezer Setup

Following the path of the laser beam from the bottom left in Fig. 5.19. The beam of a diode-pumped neodymium-doped yttrium vanadate laser (106-C) provides an infrared wavelength in the transversal electromagnetic $_{00}$-mode (1064 nm, TEM_{00}). Infrared light is used, because the particles in this project will have a perfect size relation to wavelength for strong Mie interaction. In addition, Svoboda and Block showed the relative weak interactions of infrared light with biological samples and water.[291,296] There is no DNA destruction (UV induced), no photoreceptor trigger (visible light induced) but only a small heat transfer and probable metabolism changes within cells[297] from the infrared light.

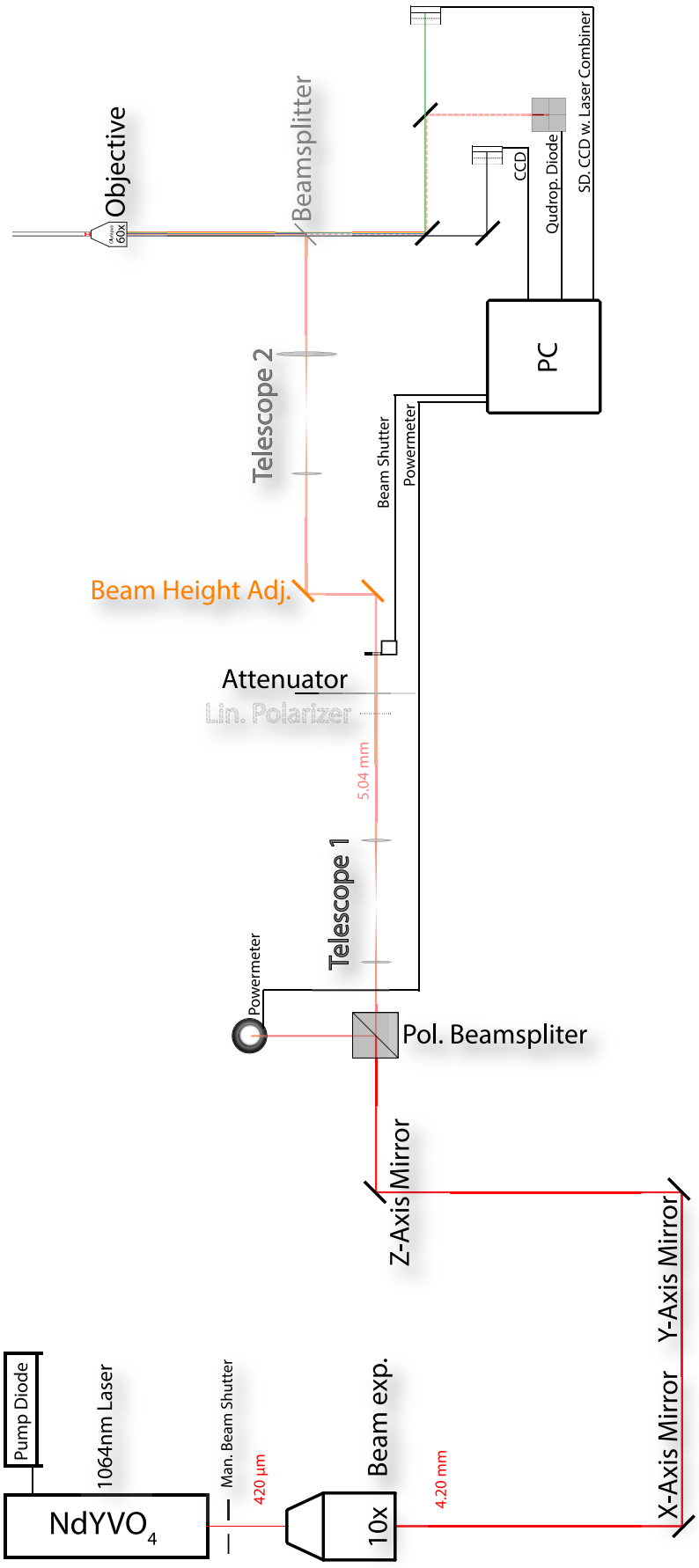

Fig. 5.19.: Scheme of the custom build optical tweezer setup with implemented laser confocal spinning disc fluorescence microscopy.

The initial beam diameter was diverged by a 10x beam expander and reflected with infrared anti-reflective coated mirrors for x, y, and z adjustment. A polarized beamsplitter induced the ability for constant power measurements and logging of intensity variations during measurements with a powermeter. The beam diameter was finally set to 5.04 mm by using a second telescope to fill the back-focal-plane (BFP) of the objectives, which is calculated as

$$BFP_{diameter} = 360 \frac{NA_{Objective}}{Magnification} \tag{5.6}$$

with $NA_{Objective}$ as the numerical aperture of the objective and its magnification. For OT the numerical aperture should be high of a value above 1.2 to increase the light intensity at the focus point and for strong trapping. [290] A rotatable linear polarizer was used to produce a higher beam quality, because every light interaction with a mirror can lead to depolarization the the light. The following attenuator gave the ability to reduce the intensity in a stable way without time consuming current changes of the pump Laser. After height adjustment with two pyrex mirrors, the beam enters the second and more important telescope 2. The first lens can be moved in three dimensions to center the focussed laser spot and correct the z-height of the image focus to the laser focus. This offers the possibility to make exact and precise observations of a laser manipulated sample with an EM-CCD camera and makes this method *a priori* useful. With the aid of the infrared reflective beamsplitter the beam is focused with a water or oil collective objective onto a sample, resulting in a functioning optical tweezer. For optimization of vibrational decoupling of the system, it was mounted onto a stabilization table (Stabilizer High Performance Laminar Flow Isolator S-2000 Series). To readout the force exerted to the trapped sample, the backscattered IR-light with further IR-beamsplitter is lead onto a custom build quadrupole diode. All of the electronic devices are connected to the PC used to observe and store all data as processing, manipulation of the beam shutter, different combinations, and overlays of pictures for further analysis.

5.4.2. Optical Tweezer Manipulation

Cell and Particle Manipulation

HCEC-12 or *A. castellanii* were cultured as described (Sec. 2.2). The cells were incubated in a glass bottom petri dish and immediately manipulated with OT at normothermia

(37 °C, MI-IBCD-F1-AF) before cell attachment occured. Attached *A. castellanii* could be detached from the glass for further experiments with some tapping of the hand to the bottom of it. Experiments with HCEC-12 without CO_2 revealed at 37 °C healthy cell behaviour for several days.

Polystyrene microspheres ($1.00 - 4.95$ µm) were cleaned as described in the suppliers information.[298] Various experiments for laser focus adjustment, confocal adjustment of the EM-CCD with the laser focus, were performed in either bidest. water or sodium chloride buffer (Sec. 2.1.3) to keep particles swimming in the solution. However, also combined *A. castellanii* and particle experiments were realized, which are represented in Fig. 5.20, where a polystyrene particle (4.95 µm) was moved to the membrane edge of an *A. castellanii*. The particles remained inside the trap and after blocking of the laser

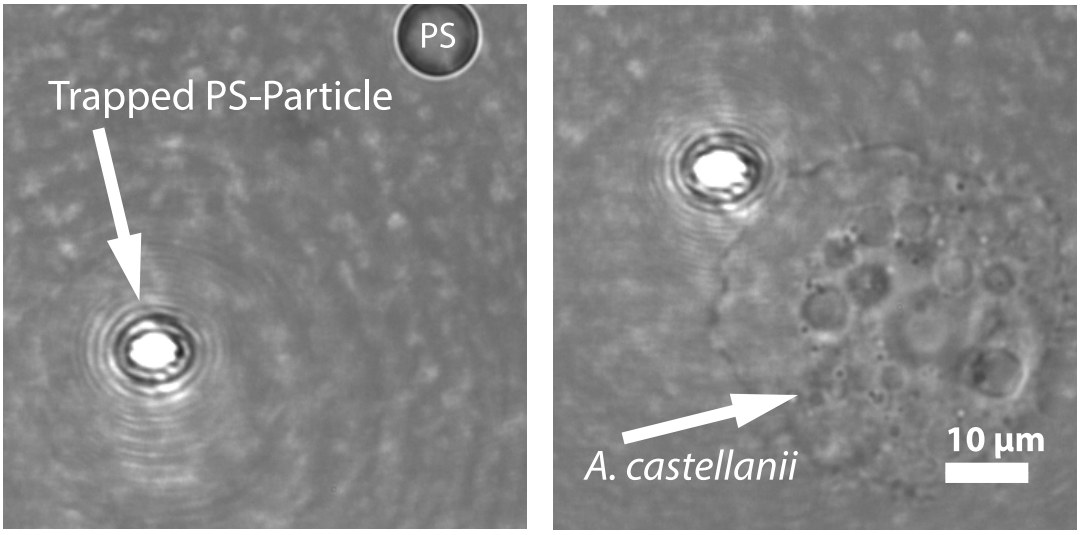

Fig. 5.20.: Optical manipulation and movement of a trapped polystyrene bead (4.95 µm) to an adherent *A. castellanii*. White spot refers to the IR-Laser light. Scalebar = 10 µm.

light the *A. castellanii* did not move or interact with these polystyrene particles. These experiments still showed high potential for future studies on particle-cell interaction and is a basis for further manipulation and force detecting research. The particle phagocytosis has to be improved with surface functionalization and size reduction of the particles and use of the synthesized elastic PAAm particles. In advance, RBCs could not be trapped and moved yet maybe due to their discoid shape, as the manipulation relies on shape, optical density, and size of the sample.[299–301]

5.5. Conclusion and Prospects

In this chapter various particles as made from polystyrene, PMMA, TMOS, or PAAm were used to investigate the phagocytosis event as well as the phagocytic deformation force (PDF) of *A. castellanii*. Especially the synthesis of elastic PAAm particles (EPABs) was challenging as in terms of size dependence for a target cell size of one to three microns, synthesis with inverse-micelle polymerization, and microfluidic synthesis with its special fluid dynamics, HLB index, use of mixed micelles for stronger micelle formation, and chip design. Phagocytosis was observed only for stiffer particles (TMOS and polystyrene), which is in agreement with literature, but the thermoplastic and elastic particles were not incorporated. The use of surface functionalization with binding proteins and an improved cleaning procedure will guide future projects and probable calculations of PDF.

This results led not the predicted bead deformation assay (BDA) but still was achieved as a RBC deformation while phagocytosis. Through the use of literature known data sets about RBC a force regime of 415 - 886 pN as well as a stress peak regime of $2.86 - 5.95\ \mathrm{N/m^2}$ was estimated.

For future projects a functioning OT was established and tested with the manipulation of particles as well as complete cells. Therefore, future projects will benefit from these methods and will lead to new inventions and investigations in the biophysical field.

6 | Final Conclusion and Prospects

Experiments on the three infection steps adhesion, migration, and phagocytosis, which enhances proliferation, of the human pathogenic *A. castellanii* were conducted to understand pathogenic behaviour in all its facets. This thesis revealed some secrets of pathogenicity, gave clues for treatments against the severe disease caused by *Acanthamoeba* and to developed new methods for the investigation of human pathogens.

We started from adhesion, the first step of the infection pathway of human pathogens, i.e. *A. castellanii*, the unicellular organism of the year 2012,[302] and learned about the significantly increasing projected cell adhesion area from 611.7 μm^2 (128 kPa) to 712.6 μm^2 (4 kPa) to soft PDMS substrates and *vice versa*. The higher adhesion area is related to better adherence and can lead to faster migration of cells, which results in greater infection possibilities. Therefore, this study gives the first indication of human pathogens other than mammalian cells to show mechanosensing behavior. In order to avoid an *A.* keratitis infection, contact lenses with lower water-content and higher Young's modulus might be advisable.

Furthermore, the second part of the infection cascade is the migration of *A. castellanii* in 3D structures as it migrates into the deep corneal stroma through lens lesions. Studies on porous biomimetic PAAm substrates could serve as cell traps for medical container due to its ability to accumulate *Acanthamoeba* in larger cavities and its labyrinth like structure interconnected. Through the channels, *A. castellanii* migrates slower than on comparable 2D bulk substrates with similar properties. These substrates showed good potential as a more natural 3D cultivation substrate for cells. The substrate provides good nutrients supply, guided migration pathways with the use of chemotactic agents, and a high cell-material contact area of up to 97 %, which could mimic a cell-host interaction better than conventional substrates. This reveals the opportunity for future stem cell proliferation studies, using biodegradable polymer to observe migration behavior in

complex systems or to realize a setup of a 3D traction force microscopy method.

Investigations in the last part of this work on amoebic infections - the cell killing and phagocytosis, connected *A. castellanii* and related cells with erythrocytosis, trogocytosis, and cell killing. Cell experiments were conducted with synthesized deformable samples to measure 3D forces, while phagocytic uptake was performed. The fabrication of particles was based on a variety of techniques, e.g. microfluidics, inverse-micelle polymerisation, and etching. This demonstrated an easy to use prototype - the RBC. Deformation of these cells were observed and partly proven with RICM. These deformations are related to the PDF range of 415 – 886 pN. In order to extend these phagocytosis studies and to control the cell-particle interaction, a functioning completely custom-build OT was developed and tested. This setup is a useful base for future studies on cell-particle interaction due to its built-in features as incubator, epi-fluorescence, phase-contrast, and spinning disc confocal fluorescence microscopy for fast 3D image acquisition. OT will be a powerful tool for upcoming experiments in this field.

Parts of this work was published as peer-reviewed journal or patented and is a great benefit for the scientific community as it will lead to future projects and hopefully new medical containers for contact lenses, new cell culture substrates and further method development as the material was tested as a proof of concept. Verification of the porous PAAm for cell traps could include tests with synthetic corneal skin to validate prototypes on their cell trap efficiency. This labyrinth like structure could further be employed as a test protocol for experiments, if a single cell can solve a labyrinth and therefore own a memory or to manufacture 3D-TFM samples.

A | Appendix

A.1. Supplementary Information

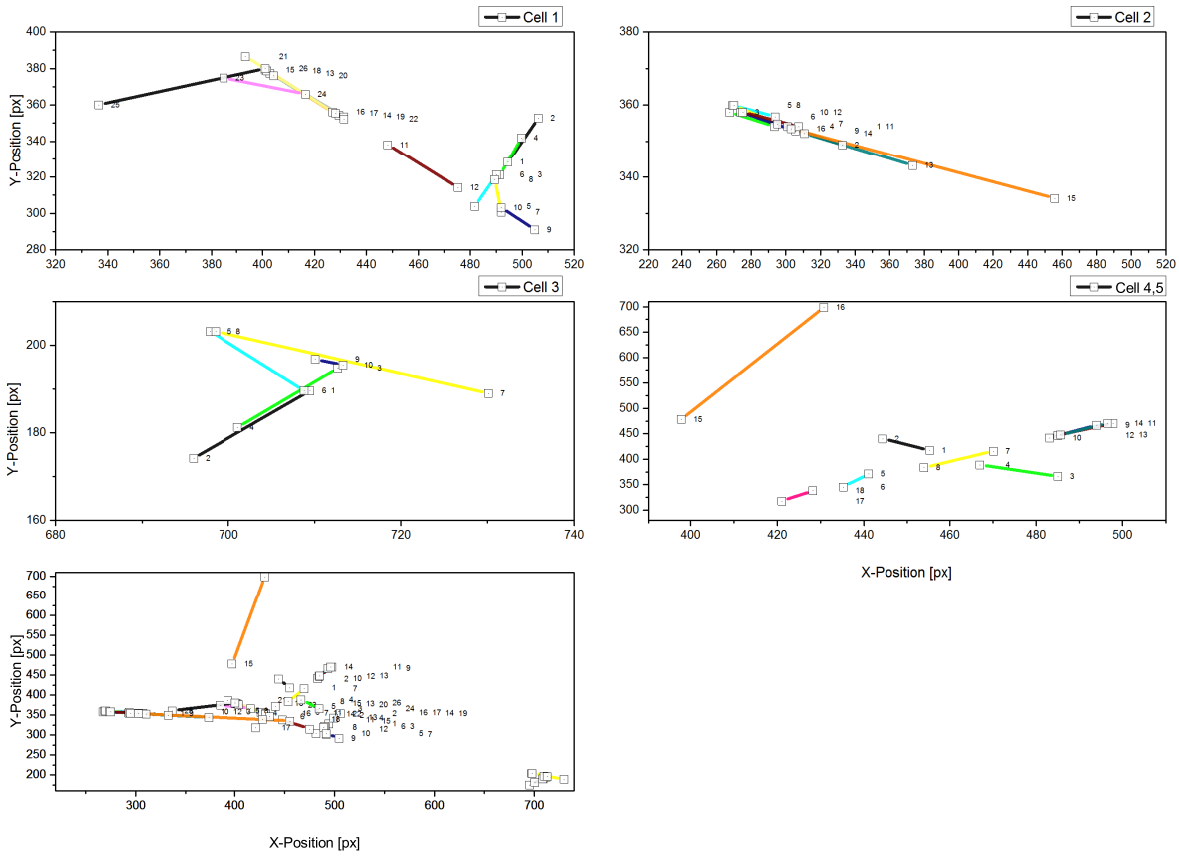

Fig. A.1.: *A. castellanii* moving through the channel system. Every line represents the diameter of a cell measured parallel to a channel. Images were acquired every 30 min. All odd numbers represents the dorsal and even numbers the back of a cell.

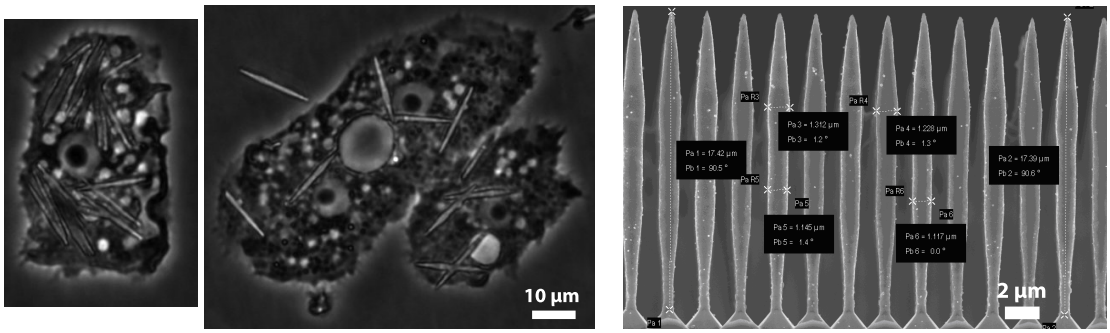

(a) (b)

Fig. A.2.: Phase contrast images of *A. castellanii* with engulfed silica-rods (a). Scalebar = 10 µm. (b) SEM image of silica-rods after the etching process. Scalebar = 2 µm.

Silica-rod Phagocytosis

Champion *et al.* proved that cells can not feel a particles size but its curvature during phagocytosis. The phagocytosis was highly angular and geometry dependent.[303] Preliminary results of the phagocytic uptake of specially designed silica rods (Fig. A.2) were performed.[A]Massive amounts up to 18 silica rods were found in *A. castellanii* (Fig. A.2 (a) and (b)) under ambient conditions after 1 - 2 h.

[A]Cooperation with Prof. Helmut Föll and Dr. Enrique Quiroga-Gonzalez.

A.2. List of Chemicals, Devices and Software

Tab. A.1.: Companies of Chemicals and Cells Part 1.

Chemicals and Cells	**Company**
6-well plates	Sarstedt
acrylamide solution 40 %	Bio-Rad
Ammonia persulfate	Bio-Rad
ammonium iron(II) sulfate hexahydrate	AppliChem
ammonium persulfate	Sigma-Aldrich
anti-GlyA (Anti-glycophorin A Pe with gelantin)	Becton Dickinson
Arcidine orange base	Aldrich
bidestilled water (bidest. water)	AppliChem
calcium dichloride	AppliChem or Sigma
cAMP	Sigma-Aldrich
Castor oil	Henry Lamotte
Cell culture flask	Sarstedt
Cyclohexane	GPR Rectapur
Dimethyl 2,2'-azobis(2-methylpropionate)	Wako Chemicals GmbH
disodium hydrogen phosphate heptahydrate	Roth
DMEM	Biochrom
dodecyl sulfate sodium salt	Merck
FBS	Biochrom
Fluorescein free acid	Fluka
fluorescein isothiocyanat-dextran 50000 conjugate	Sigma-Aldrich
HCEC-12 (ACC 646)	DSMZ
D-glucose	Sigma-Aldrich
Ham's F-12 Nut mix	Life Technologies
hydrochloric acid 37 %	Sigma-Aldrich or Merck
Immersionoil Type-F	Olympus
Immersol 518 F	Zeiss
Isopropylmyristate	Cognis
Lysotracker red DND-99	Thermo Fischer
magnesium sulfate monohydrate	AppliChem or Roth

Tab. A.2.: Companies of Chemicals and Cells Part 2.

Chemicals and Cells	**Company**
Medium 199	Life Technologies
N,N'-Methylenebisacrylamide	Bio-Rad
methylmethacrylate	Sigma-Alrdich
methylmethacrylate >99 %	Evonik
Methylacrylicacid chloride >97 %	Alfa Aesar
Novec 7500 >99 %	3M
PAA 99 %	Alfa Aesar
Polysorbate 80	BASF
Polystyrene microspheres $1 - 4.95$ µm	Bangs Laboratories Inc. Polysciences Inc. (Tab. A.4)
potassium dihydrogen phosphate	Roth
potassium peroxodisulfate	Sigma-Aldrich
Proteose peptone	BD, Sparks
PVB	Mowital®, kuraray
Silicone elastomere base	Sylgard 184, DOW Corning
Silicone elastomere curing agent	Sylgard 184, DOW Corning
Silicone oil M520	Roth
sodium chloride	Roth
sodium citrate dihydrate	Merck
Span 80	Sigma
N,N,N',N'-Tetramethylethane-1,2-diamine	Bio-Rad
toluene EMPlura or SeccoSolv	Merck
Triton-X 100	Sigma
trimethylamine 99 %	Acros Organics
Tween 20	Sigma
yeast extract	BD, Sparks

Tab. A.3.: Companies of Devices and Software.

Device and Software	**Company**
106-C	SpectraPhysics
602f-2	Basler
Andromeda	Till Photonics
Basalt-BT01	Tetra GmbH
BX-43	Olympus
C-9100-13	Hamamatsu
C-9300-221	Hamamatsu
CO_2-Incubator C150	Binder
DFK 31BF03	Imaging Source
Heater 1083	GFL
iChrome MLE	Toptica Photonics AG
IX-81	Olympus
MATLAB 2013a	MathWorks®
MI-IBCD-F1-AF	Tokai HIT
Mikro 220R	Hettich
Motorized Stage SCAN IM 120x80	Merz
MT20E	Olympus
RK 52	Bandolin electronic
Stabilizer High Performance Laminar Flow Isolator S-2000 Series	Newport
Syringe Pump PHD Ultra 4400	Harvard Apparatus
Technote	BangsLabs
U-FSHA	Olympus
Vortex Genius 3	IKA®
VX-78	Systec
Xcellence RT	Olympus
XM10	Olympus

Tab. A.4.: List of particle manufacturer and related particles.

Bangs Laboratories Inc.:	**Dye**	**Size [µm]**	**Inv. #**
P(S/V-COOH)	Dragon Green (480/520)	0.06	L110105B
P(S/V-COOH)	Glacial Blue (360/450)	0.2	L110805D
P(S/6 %DVB/V-COOH)Mag	Dragon Green (480/520)	0.90	L130314B
(P(S/V-COOH)	Glacial Blue (360/450)	1.04	L120209B
P(S/5 %-MAA/5.5 % DVB)	Dragon Green (480/520)	4.95	L100928A
Polysciences Inc.:	**Cat. #**	**Size [µm]**	**Lot #**
Polybead® Amino	17144	0.75	601778
Polybead® Amino	17010	1.0	611485
Polybead® Amino	17145	3.0	611486

A.3. Danksagung

Mein Arbeitstag fängt mit einem Gruß des freundlichen Pförtners an. Am Schreibtisch angekommen erwarten mich bereits dringende E-Mails mit dem Absender Prof. Christine Selhuber-Unkel mit Inhalten über Konferenzvorschläge, neuen Projektideen oder Fragen von 22:56 Uhr. Weitere Nachrichten sind von Prof. Leippe, dass ich gerne weitere Amöben abholen könne, von Prof. Gorb mit Alexander Kovalev im CC, dass Sie die Messungen von Anneke fertig ausgewertet haben sowie einer positiven Rückmeldung von der PVA-SH Mitarbeiterin A. Baumgartner und D. Gieseler. Außerdem schreibt mir Sabrina von der Gruppe von Prof. Gerken, wann ich nochmal Zeit für weitere Fluoreszenzmessungen hätte.

Dabei fällt mir nach dem Gruß von Hannelore ein, dass ich nochmal zur quirligen stets gut gelaunten Ellen müsste, da ein neuer Vertrag für mich bereitsteht, wobei ich mich auf die Stelle beim ERC Starting grant no. 336104 freue. Auf dem Weg grüßen mich die hilfsbereiten Biobliotheksangestellten. Nach dem kurzen Intermezzo und einen freundlichen Gruß an Prof. McCord (Howdy/Moin Jeff), gehe ich zu unseren fleißigen HiWis und frage nach den neuesten Stand oder den längst überfälligen Auswertungen.

Die aufkommenden Probleme können mal wieder nur mit Spezialanfertigung aus der Werkstatt in den Griff gekriegt werden. Schnell zu Matthias oder Bernd, welche mir sagen, dass Sie dieses mal viel zu tun haben und deshalb zwei Wochen brauchen werden. Auf dem Rückwege schaue ich bei der guten gewaltfreien Seele Manuela und meinem groß gewordenen Padawan Phteven vorbei, um sie in die Mittagsessenrituale einbinden-zukönnen.

Dann heißt es auf ins Labor und Suppattra sowie Kathrina neue Ideen für die Proben des Arbeitskreises von Prof. Adelung und Iris, Ingo, Dasha mitzuteilen. Nun geht es an die Synthesen für Fabian oder Victor, wobei ich die Proben aus den U.S.A. der Duke University von Prof. Lopez und Wyatt finde mit denen ich noch einiges geplant habe.

Es ist schon fast Mittag und die wichtigen Essensentscheidung, ob nun weiß oder rot, werden mit dem "Gourmett" Michael, Britta aka Tobi II und dem altbekannten Gesicht Julia entschieden. Nach einem kurzen Benzingespräch mit Hendrikje komme ich gut genährt ins Büro, wo bereits nach größter Spock-Manier die Werkstücke der Werkstatt auf mich warten.

Nach getaner Arbeit warte ich mal wieder auf den freudigen Laith und kriege einige Nachrichten von meinem Matrosen Timmchen und den Wendtlern, welche Fragen, ob sie Svenno und Pödel morgen zum Grillen mitbringen können. Nach dem üblichen Wahnsinn mit den Kollegen der BNanos geht es endlich zum Sport. Eine tolle Kletterpartie mit der aufmerksamen, hilfsbereiten stets gut gelaunten Dori, welche mir von der tollen Pharmazeutischen Technologie mit Regina Scherließ, Judith und Ann-Kathrin erzählt. Anschließend öffne ich daheim den Briefkasten und finde eine Einladung vom Best Buddy, auch Zertifikatsammler gennannt, und seiner Zukünftigen, dass ich bald meine BAGS packen soll für einen Besuch. Freudig gehe ich Zähneputzen und denke an die Hilfe von Merz Dental mit Sebastian Pflesser und Katharina.

Nach Betrachten der Kontaktlinsenlösung und dem Wissen morgen weiter machen-zukönnen, schweift mein Blick über Bilder meines größten Hab und Gutes und ich schlafe gelassen und zufrieden ein.

. . . ***Danke****. . .*

List of Figures

List of Tables

Bibliography

[1] F. E. G. Cox,
Clinical Microbiology Reviews **2002**,
15, 595–612.

[2] E. Aberer, P. H. Duray,
Journal of clinical microbiology **1991**,
29, 764–772.

[3] B. H. Bowman, J. W. Taylor, T. J. White,
Molecular Biology and Evolution **1992**,
9, 893–904.

[4] D. Kadosh,
PLoS pathogens **2013**,
9, e1003795.

[5] S. S. Justice, D. A. Hunstad, L. Cegelski, S. J. Hultgren,
Nature reviews. Microbiology **2008**,
6, 162–168.

[6] N. A. Khan,
Acanthamoeba: Biology and pathogenesis,
Caister Acad. Press, Norfolk **2009**.

[7] Robert M. W. Dixon,
Making New Words: Morphological Derivation in English,
First edition Aufl.,
Oxford University Press **2014**.

[8] Johann Wolfgang von Goethe,
Versuch die Metamorphose der Pflanzen zu erklären,
Ettinger **1790**.

[9] B. Bowers, E. D. Korn,
The Journal of Cell Biology **1969**,
41, 786–805.

[10] D. Arcizet, B. Meier, E. Sackmann, J. O. Rädler, D. Heinrich,
Physical Review Letters **2008**,
101.

[11] C. Chapman-Andresen,
Annual Review of Microbiology **1971**,
25, 27–48.

[12] Johann Georg Zimmermann,
Von der Ruhr unter dem Volke im Jahr 1765, und denen mit derselben eingedrungenen Vorurtheilen: nebst einigen allgemeinen Aussichten in die Heilung dieser Vorurtheile,
Orell, Geßner, Füeßlin und Compagnie **1767**.

[13] C. G. Culbertson, J. W. Smith, J. R. Minner,
Science **1958**,
127, 1506.

[14] B. V. Jager, W. P. Stamm,
The Lancet **1972**,
300, 1343–1345.

[15] P. Gooi, M. Lee-Wing, S. Brownstein, S. El-Defrawy, W. B. Jackson, G. Mintsioulis, *Cornea* **2008**, *27*, 246–248.

[16] W. Drozanski, *Acta microbiologica Polonica* **1956**, *5*, 315–317.

[17] B. N. Krishna-Prasad, S. K. Gupta, *Current Science* **1978**, *47*, 245–247.

[18] J. F. Moffat, L. S. Tompkins, *Infection and Immunity* **1992**, *60*, 296–301.

[19] J. D. Cirillo, S. Falkow, L. S. Tompkins, *Infection and Immunity* **1994**, *62*, 3254–3261.

[20] T. J. Rowbotham, *Journal of Clinical Pathology* **1980**, *33*, 1179–1183.

[21] R. Michel, K.-D. Müller, R. Amann, E. N. Schmid, *Parasitology Research* **1997**, *84*, 84–88.

[22] E. Schunder, N. Gillmaier, E. Kutzner, W. Eisenreich, V. Herrmann, M. Lautner, K. Heuner, *The Journal of Biological Chemistry* **2014**, *289*, 21040–21054.

[23] M. Koehsler, D. Leitsch, M. Duchêne, M. Nagl, J. Walochnik, *FEMS Microbiology Letters* **2009**, *299*, 121–127.

[24] K. Jeon, *The Biology of Amoeba*, Elsevier Science, Oxford **1973**.

[25] B. Bowers, *The Journal of Cell Biology* **1968**, *39*, 95–111.

[26] E. E. Klein, A. Kollmann, *Grundzüge der Histologie*, Dt. autorisierte ausg., nach d. 4. engl. aufl. / bearb. von A. Kollmann Aufl., Arnold, Leipzig **1886**.

[27] E. Klein, M.D., F.R.S., *Elements of Histology*, Fourth edition Aufl., Lea Brothers & Co, Philadelphia **1889**.

[28] D. Arcizet, S. Capito, M. Gorelashvili, C. Leonhardt, M. Vollmer, S. Youssef, S. Rappl, D. Heinrich, *Soft Matter* **2012**, *8*, 1473–1481.

[29] F. Marciano-Cabral, G. Cabral, *Clin. Microbiol. Rev.* **2003**, *16*, 273–307.

[30] F. A. Lesh, *The American Journal of Tropical Medicine and Hygiene* **1975**, *24*, 383–392.

[31] M. Volkonsky, *Archives de Zoologie Experimentale et Generale Paris* **1931**, 317–339.

[32] A. Castellanii, *The American Journal of Tropical Medicine and Hygiene* **1930**, *33*, 160.

[33] M. Douglas, *The American Journal of Tropical Medicine and Hygiene* **1930**, *33*, 258–259.

[34] H.-H. Kong, T. D. Pollard, *Journal of Cell Science* **2002**, *115*, 4993–5002.

[35] A. González-Robles, G. Castañón, V. I. Hernández-Ramírez, L. Salazar-Villatoro, M. González-Lázaro, M. Omaña-Molina, P. Talamás-Rohana, A. Martínez-Palomo, *Experimental parasitology* **2008**, *119*, 411–417.

[36] T. D. Pollard, E. M. Ostap, *Cell structure and function* **1996**, *21*, 351–356.

[37] E. D. Goley, M. D. Welch, *Nature Reviews Molecular Cell Biology* **2006**, *7*, 713–726.

[38] J. M. Schroeder, G. C. Booton, J. Hay, I. A. Niszl, D. V. Seal, M. B. Markus, P. A. Fuerst, T. J. Byers, *Journal of clinical microbiology* **2001**, *39*, 1903–1911.

[39] G. C. Booton, D. J. Kelly, Y.-W. Chu, D. V. Seal, E. Houang, Lam, D. S. C., T. J. Byers, P. A. Fuerst, *Journal of clinical microbiology* **2002**, *40*, 1621–1625.

[40] D. R. Stothard, J. M. Schroeder-Diedrich, M. H. Awwad, R. J. Gast, D. R. Ledee, S. Rodriguez-Zaragoza, C. L. Dean, P. A. Fuerst, T. J. Byers, *The Journal of eukaryotic microbiology* **1998**, *45*, 45–54.

[41] G. Zhao, S. Sun, J. Zhao, L. Xie, *Journal of medical microbiology* **2010**, *59*, 462–466.

[42] N. A. Khan, *FEMS Microbiology Reviews* **2006**, *30*, 564–595.

[43] D. Di Cave, R. Monno, P. Bottalico, S. Guerriero, S. D'Amelio, C. D'Orazi, F. Berrilli, *European journal of clinical microbiology & infectious diseases : official publication of the European Society of Clinical Microbiology* **2009**, *28*, 607–612.

[44] M. Rahdar, M. Niyyati, M. Salehi, M. Feghhi, M. Makvandi, M. Pourmehdi, S. Farnia, *Iranian Journal of Parasitology* **2012**, *7*, 22–26.

[45] A. J. Martinez, K. Janitschke, *Infection* **1985**, *13*, 251–256.

[46] A. Balows, W. J. Hausler, M. Ohashi, A. Turano, E. H. Lennette, *Laboratory Diagnosis of Infectious Diseases: Principles and Practice*, Springer New York, New York, NY **1988**.

[47] L.-L. Chan, J.-W. Mak, Y.-T. Low, T.-T. Koh, I. Ithoi, S. M. Mohamed, *Acta tropica* **2011**, *117*, 23–30.

[48] D. Seal, F. Stapleton, J. Dart, *British Journal of Ophthalmology* **1992**, *76*, 424–427.

[49] A. J. Martinez, G. S. Visvesvara, *Brain Pathology* **1997**, *7*, 583–598.

[50] G. S. Visvesvara, H. Moura, F. L. Schuster, *FEMS immunology and medical microbiology* **2007**, *50*, 1–26.

[51] G. C. Booton, G. S. Visvesvara, T. J. Byers, D. J. Kelly, P. A. Fuerst, *Journal of clinical microbiology* **2005**, *43*, 1689–1693.

[52] M. Hurt, S. Neelam, J. Niederkorn, H. Alizadeh, *Infection and Immunity* **2003**, *71*, 6243–6255.

[53] DPDx - Laboratory Identification of Parasitic Diseases of Public Health Concern 2010, Life Cycle.

[54] F. A. Yousuf, R. Siddiqui, N. A. Khan, *Parasites & vectors* **2013**, *6*, 169.

[55] E. A. G. Elloway, R. A. Armstrong, R. A. Bird, S. L. Kelly, S. N. Smith, *Journal of applied microbiology* **2004**, *97*, 1319–1325.

[56] J. Lorenzo-Morales, C. M. Martín-Navarro, A. López-Arencibia, F. Arnalich-Montiel, J. E. Piñero, B. Valladares, *Trends in parasitology* **2013**, *29*, 181–187.

[57] J. L. Harrison, G. A. Ferreira, E. S. Raborn, A. D. Lafrenaye, F. Marciano-Cabral, G. A. Cabral, *Infection and Immunity* **2010**, *78*, 4001–4011.

[58] S. Piluso, B. Hiebl, S. N. Gorb, A. Kovalev, A. Lendlein, A. T. Neffe, *The International Journal of Artificial Organs* **2011**, *34*, 192–197.

[59] C. J. Kovacs, S. C. Lynch, M. J. Rah, K. A. Millard, T. W. Morris, *Clinical ophthalmology* **2015**, *9*, 1905–1913.

[60] E. Rothe, Contact lens with position stabilisation, EP19900122477, **19.04.1990**.

[61] Spiegel, *Spiegel* **21.05.1979**, *1979*, URL `http://www.spiegel.de/spiegel/print/d-403495`

[62] H. J. Baron, Hydrophilic contact lens, US3698802 A, **29.12.1969**.

[63] Historie der Firma Wöhlk **09.09.2015**, URL `http://www.woehlk.com/historie.html`.

[64] W. D. Bockelmann, In W. D. Bockelmann, Hg., *Auge — Brille — Auto*. Springer Berlin Heidelberg, Berlin, Heidelberg **1987**, 232–243.

[65] P. Oberender, H. Baum, *Marktökonomie: Marktstruktur und Wettbewerb in ausgewählten Branchen der Bundesrepublik Deutschland*, F. Vahlen, München **1989**.

[66] M. B. Abelson, D. Dewey-Mattia, and A. Shapiro, Acanthamoeba: A Dangerous Pathogen: An in-depth look at the organism, how it causes keratitis and how patients can avoid infection. **2008**.

[67] N. Thebpatiphat, K. M. Hammersmith, F. N. Rocha, C. J. Rapuano, B. D. Ayres, P. R. Laibson, R. C. Eagle, E. J. Cohen, *Cornea* **2007**, *26*, 701–706.

[68] A. Patel, K. Hammersmith, *Current opinion in ophthalmology* **2008**, *19*, 302–306.

[69] Y. Kaji, B. Hu, K. Kawana, T. Oshika, *The Lancet. Infectious diseases* **2005**, *5*, 392.

[70] I. V. Maly, G. G. Borisy, *Proceedings of the National Academy of Sciences of the United States of America* **2001**, *98*, 11324–11329.

[71] V. I. Risca, E. B. Wang, O. Chaudhuri, J. J. Chia, P. L. Geissler, D. A. Fletcher, *Proceedings of the National Academy of Sciences of the United States of America* **2012**, *109*, 2913–2918.

[72] F. B. Mallory, *The Journal of experimental medicine* **1900**, *5*, 1–13.

[73] M. Leippe, *Parasitology Today* **1997**, *13*, 178–183.

[74] M. Michalek, F. D. Sönnichsen, R. Wechselberger, A. J. Dingley, C.-W. Hung, A. Kopp, H. Wienk, M. Simanski, R. Herbst, I. Lorenzen, F. Marciano-Cabral, C. Gelhaus, T. Gutsmann, A. Tholey, J. Grötzinger, M. Leippe, *Nature chemical biology* **2013**, *9*, 37–42.

[75] I. D. Bowen, In I. Bowen, R. Lockshin, Hg., *Cell death in biology and pathology*. Springer Netherlands **1981**, 379–444.

[76] N. Guillén, *Nature* **2014**, *508*, 462–463.

[77] K. S. Ralston, M. D. Solga, N. M. Mackey-Lawrence, Somlata, A. Bhattacharya, W. A. Petri, *Nature* **2014**, *508*, 526–530.

[78] G. Gerisch, M. Ecke, D. Wischnewski, B. Schroth-Diez, *BMC cell biology* **2011**, *12*, 42.

[79] D. M. Toney, F. Marciano-Cabral, *The Journal of parasitology* **1998**, *84*, 338–344.

[80] D. I. Dornic, T. Wolf, W. H. Dillon, B. Christensen, C. D. Deem, *Journal of the American Optometric Association* **1987**, *58*, 482–486.

[81] J. K. Stehr-Green, T. M. Bailey, F. H. Brandt, J. H. Carr, W. W. Bond, G. S. Visvesvara, *Journal of the American Medical Association* **1987**, *258*, 57–60.

[82] T. M. Preston, H. Richards, R. S. Wotton, *FEMS Microbiology Letters* **2001**, *194*, 143–147.

[83] B. da Rocha-Azevedo, H. B. Tanowitz, F. Marciano-Cabral, *Interdisciplinary perspectives on infectious diseases* **2009**, *2009*, 251406.

[84] U. Lek-Uthai, R. Passara, K. Roongruangchai, *Journal of the Medical Association of Thailand = Chotmaihet thangphaet* **2009**, *92 Suppl 7*, S156–63.

[85] P. M. Molyneux, S. Kilvington, M. J. Wakefield, J. I. Prydal, N. P. Bannister, *Cornea* **2015**, *34*, 1588–1592.

[86] B. Clarke, A. Sinha, D. N. Parmar, E. Sykakis, *Journal of ophthalmology* **2012**, *2012*, 484892.

[87] R. L. Fernando, S. S. Fernando, A. S.-Y. Leong, *Tropical infectious diseases epidemiology, investigation, diagnostic and management*, Greenwich medical media, London **2001**.

[88] C. E. Oldenburg, N. R. Acharya, E. Y. Tu, M. E. Zegans, M. J. Mannis, B. D. Gaynor, J. P. Whitcher, T. M. Lietman, J. D. Keenan, *Cornea* **2011**, *30*, 1363–1368.

[89] J. S. Seidel, P. Harmatz, G. S. Visvesvara, A. Cohen, J. Edwards, J. Turner, *The New England journal of medicine* **1982**, *306*, 346–348.

[90] S. L. Chang, *Applied and Environmental Microbiology* **1978**, *35*, 368–375.

[91] M. M. Dorsch, A. S. Cameron, B. S. Robinson, *Transactions of the Royal Society of Tropical Medicine and Hygiene* **1983**, *77*, 372–377.

[92] M. Fowler, R. F. Carter, *British medical journal* **1965**, *2*, 740–742.

[93] R. V. Lawande, J. T. Macfarlane, W. R. Weir, C. Awunor-Renner, *The American journal of tropical medicine and hygiene* **1980**, *29*, 21–25.

[94] P. Ma, G. S. Visvesvara, A. J. Martinez, F. H. Theodore, P. M. Daggett, T. K. Sawyer, *Reviews of infectious diseases* **1990**, *12*, 490–513.

[95] D. H. Park, D. A. Palay, S. M. Daya, R. D. Stulting, J. H. Krachmer, E. J. Holland, *Cornea* **1997**, *16*, 277–283.

[96] D. Gupta, G. S. Panda, S. Bakhshi, *Pediatric blood & cancer* **2008**, *50*, 1292–1293.

[97] M. Seijo Martinez, G. Gonzalez-Mediero, P. Santiago, Rodriguez De Lope, A, J. Diz, C. Conde, G. S. Visvesvara, *Journal of clinical microbiology* **2000**, *38*, 3892–3895.

[98] T. H. Dunnebacke, F. L. Schuster, S. Yagi, G. C. Booton, *Microbiology* **2004**, *150*, 2837–2842.

[99] F. L. Schuster, T. H. Dunnebacke, G. C. Booton, S. Yagi, C. K. Kohlmeier, C. Glaser, D. Vugia, A. Bakardjiev, P. Azimi, M. Maddux-Gonzalez, A. J. Martinez, G. S. Visvesvara, *Journal of clinical microbiology* **2003**, *41*, 3175–3180.

[100] A. M. Baig, *Acta tropica* **2015**, *148*, 72–76.

[101] A. J. Martinez, S. M. Markowitz, R. J. Duma, *Journal of Infectious Diseases* **1975**, *131*, 692–699.

[102] K. M. Herrmann, L. M. Weaver, *Annual review of plant physiology and plant molecular biology* **1999**, *50*, 473–503.

[103] F. L. Henriquez, S. J. Campbell, B. K. Sundararaj, A. Cano, S. P. Muench, C. W. Roberts, *Protist* **2015**, *166*, 93–105.

[104] B. K. Jha, H.-J. Jung, I. Seo, H. A. Kim, S.-I. Suh, M.-H. Suh, W.-K. Baek, *Antimicrobial agents and chemotherapy* **2014**, *58*, 6235–6241.

[105] D. E. Discher, P. Janmey, Y.-L. Wang, *Science (New York, N.Y.)* **2005**, *310*, 1139–1143.

[106] A. Engler, L. Bacakova, C. Newman, A. Hategan, M. Griffin, D. Discher, *Biophysical Journal* **2004**, *86*, 617–628.

[107] R. J. Pelham, Y.-L. Wang, *Proceedings of the National Academy of Sciences* **1997**, *94*, 13661–13665.

[108] S. Defrère, M. Mestagdt, R. Riva, F. Krier, A. van Langendonckt, P. Drion, C. Jérôme, B. Evrard, J.-P. Dehoux, J.-M. Foidart, J. Donnez, *Macromolecular bioscience* **2011**, *11*, 1336–1345.

[109] J. G. Alauzun, S. Young, R. D'Souza, L. Liu, M. A. Brook, H. D. Sheardown, *Biomaterials* **2010**, *31*, 3471–3478.

[110] E. Mussig, T. Steinberg, S. Schulz, J. P. Spatz, J. Ulmer, N. Grabe, A. Kohl, G. Komposch, P. Tomakidi, *Advanced Functional Materials* **2008**, *18*, 2919–2929.

[111] J. L. Tan, J. Tien, D. M. Pirone, D. S. Gray, K. Bhadriraju, C. S. Chen, *Proceedings of the National Academy of Sciences of the United States of America* **2003**, *100*, 1484–1489.

[112] A. R. Abate, D. Lee, T. Do, C. Holtze, D. A. Weitz, *Lab on a chip* **2008**, *8*, 516–518.

[113] R. N. Palchesko, L. Zhang, Y. Sun, A. W. Feinberg, *PloS one* **2012**, *7*, e51499.

[114] M.-E. Vlachopoulou, P. S. Petrou, S. E. Kakabakos, A. Tserepi, K. Beltsios, E. Gogolides, *Microelectronic Engineering* **2009**, *86*, 1321–1324.

[115] C.-M. Lo, H.-B. Wang, M. Dembo, Y.-L. Wang, *Biophysical Journal* **2000**, *79*, 144–152.

[116] J. Y. Wong, A. Velasco, P. Rajagopalan, Q. Pham, *Langmuir* **2003**, *19*, 1908–1913.

[117] I. B. Bischofs, U. S. Schwarz, *Proceedings of the National Academy of Sciences of the United States of America* **2003**, *100*, 9274–9279.

[118] E. Sackmann, In H. Haken, L. Rensing, N. I. Jaeger, Hg., *Temporal Order*, Bd. 29 von *Springer Series in Synergetics*. Springer Berlin Heidelberg, Berlin, Heidelberg **1985**, 153–162.

[119] A. J. Engler, S. Sen, H. L. Sweeney, D. E. Discher, *Cell* **2006**, *126*, 677–689.

[120] A. Zemel, F. Rehfeldt, Brown, A E X, D. E. Discher, S. A. Safran, *Nature physics* **2010**, *6*, 468–473.

[121] R. W. Tilghman, C. R. Cowan, J. D. Mih, Y. Koryakina, D. Gioeli, J. K. Slack-Davis, B. R. Blackman, D. J. Tschumperlin, J. T. Parsons, *PloS one* **2010**, *5*, e12905.

[122] A. Raic, L. Rödling, H. Kalbacher, C. Lee-Thedieck, *Biomaterials* **2014**, *35*, 929–940.

[123] S. S. Verbridge, E. M. Chandler, C. Fischbach, *Tissue engineering. Part A* **2010**, *16*, 2147–2152.

[124] X. Liu, P. Ma, *Annals of Biomedical Engineering* **2004**, *32*, 477–486.

[125] Y. Luo, C. Wu, A. Lode, M. Gelinsky, *Biofabrication* **2013**, *5*, 015005.

[126] L. Loeb, *Protoplasma* **1927**, *2*, 512–553.

[127] C. F. A. Pantin, *Journal of the Marine Biological Association of the United Kingdom* **1923**, *13*, 24.

[128] E. Sackmann, *Progress in Biophysics and Molecular Biology* **1996**, *65*, 17.

[129] L. Gebbie, M. Benghezal, S. Cornillon, R. Froquet, N. Cherix, M. Malbouyres, Y. Lefkir, C. Grangeasse, S. Fache, J. Dalous, F. Brückert, F. Letourneur, P. Cosson, *Molecular Biology of the Cell* **2004**, *15*, 3915–3925.

[130] G. Amselem, M. Theves, A. Bae, E. Bodenschatz, C. Beta, *PloS one* **2012**, *7*, e37213.

[131] W. Gutkowski, T. A. Kowalewski, *Mechanics of the 21st Century: Proceedings of the 21st International Congress of Theoretical and Applied Mechanics, Warsaw, Poland, 15-21 August 2004*, Springer, Dordrecht **2005**.

[132] S. S. Rogers, T. A. Waigh, J. R. Lu, *Biophysical Journal* **2008**, *94*, 3313–3322.

[133] W. T. Coakley, D. Gallez, *Bioscience Reports* **1989**, *9*, 675–691.

[134] R. Glaser, D. Gingell, *Biophysics of the Cell Surface*, Bd. 5 von *Springer Series in Biophysics*, Springer Berlin Heidelberg, Berlin, Heidelberg **1990**.

[135] L. Segel, T. Volk, B. Geiger, *Cell Biophysics* **1983**, *5*, 95–104.

[136] O. Nagel, C. Guven, M. Theves, M. Driscoll, W. Losert, C. Beta, *PloS one* **2014**, *9*, e113382.

[137] Y.-J. Liu, M. Le Berre, F. Lautenschlaeger, P. Maiuri, A. Callan-Jones, M. Heuzé, T. Takaki, R. Voituriez, M. Piel, *Cell* **2015**, *160*, 659–672.

[138] M. D. Welch, *Cell* **2015**, *160*, 581–582.

[139] V. Ruprecht, S. Wieser, A. Callan-Jones, M. Smutny, H. Morita, K. Sako, V. Barone, M. Ritsch-Marte, M. Sixt, R. Voituriez, C.-P. Heisenberg, *Cell* **2015**, *160*, 673–685.

[140] C. J. Chan, A. E. Ekpenyong, S. Golfier, W. Li, K. J. Chalut, O. Otto, J. Elgeti, J. Guck, F. Lautenschläger, *Biophysical Journal* **2015**, *108*, 1856–1869.

[141] D. Bansal, P. Ave, S. Kerneis, P. Frileux, O. Boché, A. C. Baglin, G. Dubost, A.-S. Leguern, M.-C. Prevost, R. Bracha, D. Mirelman, N. Guillén, E. Labruyère, *PLoS neglected tropical diseases* **2009**, *3*, e551.

[142] V. Marx, *Nature* **2013**, *496*, 253–258.

[143] G. R. Souza, J. R. Molina, R. M. Raphael, M. G. Ozawa, D. J. Stark, C. S. Levin, L. F. Bronk, J. S. Ananta, J. Mandelin, M.-M. Georgescu, J. A. Bankson, J. G. Gelovani, T. C. Killian, W. Arap, R. Pasqualini, *Nature nanotechnology* **2010**, *5*, 291–296.

[144] G. Charras, E. Sahai, *Nature reviews. Molecular cell biology* **2014**, *15*, 813–824.

[145] F. Lautenschläger, M. Piel, *Current opinion in cell biology* **2013**, *25*, 116–124.

[146] P. Costa, J. E. Gautrot, J. T. Connelly, *Acta biomaterialia* **2014**, *10*, 2415–2422.

[147] S. Mitragotri, J. Lahann, *Nature materials* **2009**, *8*, 15–23.

[148] C. Fischbach, R. Chen, T. Matsumoto, T. Schmelzle, J. S. Brugge, P. J. Polverini, D. J. Mooney, *Nature methods* **2007**, *4*, 855–860.

[149] J. Kim, W. A. Li, W. Sands, D. J. Mooney, *ACS applied materials & interfaces* **2014**, *6*, 8505–8512.

[150] P. X. Ma, R. Zhang, G. Xiao, R. Franceschi, *Journal of Biomedical Materials Research* **2001 Feb**, *54*, 284–293.

[151] J. E. Davies, R. Matta, V. C. Mendes, Perri de Carvalho PS, *Organogenesis* **2010 Jul-Sep**, *6*, 161–166.

[152] C. E. Holy, J. E. Davies, M. S. Shoichet, *Bone Tissue Engineering on Biodegradable Polymers: Preparation of a Novel Poly(lactide-co-glycolide) Foam*, [Distributed by American Institute of Chemical Engineers], [New York, N.Y.] **1997**.

[153] C. M. Madl, M. Mehta, G. N. Duda, S. C. Heilshorn, D. J. Mooney, *Biomacromolecules* **2014**, *15*, 445–455.

[154] J. Kim, S. A. Bencherif, W. A. Li, D. J. Mooney, *Macromolecular rapid communications* **2014**, *35*, 1578–1586.

[155] A. Béduer, T. Braschler, O. Peric, G. E. Fantner, S. Mosser, P. C. Fraering, S. Benchérif, D. J. Mooney, P. Renaud, *Advanced healthcare materials* **2015**, *4*, 301–312.

[156] J. L. Drury, D. J. Mooney, *Biomaterials* **2003**, *24*, 4337–4351.

[157] Y. S. Nam, J. J. Yoon, T. G. Park, *Journal of Biomedical Materials Research* **2000**, *53*, 1–7.

[158] J. J. Yoon, T. G. Park, *Journal of Biomedical Materials Research* **2001**, *55*, 401–408.

[159] J. J. Yoon, J. H. Kim, T. G. Park, *Biomaterials* **2003**, *24*, 2323–2329.

[160] C. E. Holy, M. S. Shoichet, J. E. Davies, *Journal of Biomedical Materials Research* **2000**, *51*, 376–382.

[161] M. Swetha, K. Sahithi, A. Moorthi, N. Srinivasan, K. Ramasamy, N. Selvamurugan, *International journal of biological macromolecules* **2010**, *47*, 1–4.

[162] P. Davidson, C. Denais, M. Bakshi, J. Lammerding, *Cellular and Molecular Bioengineering* **2014**, *7*, 293–306.

[163] A. Kaminski, G. R. Fedorchak, J. Lammerding, *Progress in molecular biology and translational science* **2014**, *126*, 157–203.

[164] K. Wolf, M. Te Lindert, M. Krause, S. Alexander, J. Te Riet, A. L. Willis, R. M. Hoffman, C. G. Figdor, S. J. Weiss, P. Friedl, *The Journal of Cell Biology* **2013**, *201*, 1069–1084.

[165] G. R. Fedorchak, A. Kaminski, J. Lammerding, *Progress in Biophysics and Molecular Biology* **2014**, *115*, 76–92.

[166] C. G. Rolli, H. Nakayama, K. Yamaguchi, J. P. Spatz, R. Kemkemer, J. Nakanishi, *Biomaterials* **2012**, *33*, 2409–2418.

[167] J. F. Reverey, R. Fromme, M. Leippe, C. Selhuber-Unkel, *Contact lens & anterior eye : the journal of the British Contact Lens Association* **2014**, *37*, 262–266.

[168] J. F. Reverey, J.-H. Jeon, H. Bao, M. Leippe, R. Metzler, C. Selhuber-Unkel, *Scientific reports* **2015**, *5*, 11690.

[169] N. Malagnino, G. Pesce, A. Sasso, E. Arimondo, *Optics Communications* **2002**, *214*, 15–24.

[170] D. G. Grier, *Nature* **2003**, *424*, 810–816.

[171] J. Guck, R. Ananthakrishnan, C. C. Cunningham, J. Käs, *Journal of Physics: Condensed Matter* **2002**, *14*, 4843–4856.

[172] M. K. Kreysing, T. Kiessling, A. Fritsch, C. Dietrich, J. R. Guck, J. A. Käs, *Optics express* **2008**, *16*, 16984–16992.

[173] H. Zhang, K.-K. Liu, *Journal of the Royal Society, Interface* **2008**, *5*, 671–690.

[174] S. Mohanty, A. Uppal, P. Gupta, *Biotechnology Letters* **2004**, *26*, 971–974.

[175] S. K. Mohanty, R. Dasgupta, P. K. Gupta, *Appl. Phys. B* **2005**, *81*, 1063–1066.

[176] C. T. Lim, M. Dao, S. Suresh, C. H. Sow, K. T. Chew, *Acta Materialia* **2004**, *52*, 1837–1845.

[177] T. Fine, I. Mey, C. Rommel, J. Wegener, C. Steinem, A. Janshoff, *Soft Matter* **2009**, *5*, 3262.

[178] S. Nawaz, P. Sánchez, K. Bodensiek, S. Li, M. Simons, Schaap, Iwan A T, *PloS one* **2012**, *7*, e45297.

[179] J. J. Yoon, S. H. Song, D. S. Lee, T. G. Park, *Biomaterials* **2004**, *25*, 5613–5620.

[180] Q. Hou, D. W. Grijpma, J. Feijen, *Biomaterials* **2003**, *24*, 1937–1947.

[181] F. Rehfeldt, A. E. Brown, M. Raab, S. Cai, A. L. Zajac, A. Zemel, D. E. Discher, *Integrative biology : quantitative biosciences from nano to macro* **2012**, *4*, 422–430.

[182] S. J. Hollister, *Nature materials* **2005**, *4*, 518–524.

[183] B. Partee, S. J. Hollister, S. Das, *Selective Laser Sintering of Polycaprolactone Bone Tissue Engineering Scaffolds*, Defense Technical Information Center, Ft. Belvoir **2005**.

[184] J. M. Williams, A. Adewunmi, R. M. Schek, C. L. Flanagan, P. H. Krebsbach, S. E. Feinberg, S. J. Hollister, S. Das, *Biomaterials* **2005**, *26*, 4817–4827.

[185] K. Tan, C. Chua, K. Leong, C. Cheah, P. Cheang, M. Abu Bakar, S. Cha, *Biomaterials* **2003**, *24*, 3115–3123.

[186] A. M. Greiner, M. Jäckel, A. C. Scheiwe, D. R. Stamow, T. J. Autenrieth, J. Lahann, C. M. Franz, M. Bastmeyer, *Biomaterials* **2014**, *35*, 611–619.

[187] J. Fischer, M. Wegener, *Optical Materials Express* **2011**, *1*, 614–624.

[188] F. P. W. Melchels, J. Feijen, D. W. Grijpma, *Biomaterials* **2009**, *30*, 3801–3809.

[189] H. Lin, D. Zhang, P. G. Alexander, G. Yang, J. Tan, A. W.-M. Cheng, R. S. Tuan, *Biomaterials* **2013**, *34*, 331–339.

[190] K. Haberstroh, K. Ritter, J. Kuschnierz, K.-H. Bormann, C. Kaps, C. Carvalho, R. Mülhaupt, M. Sittinger, N.-C. Gellrich, *Journal of biomedical materials research. Part B, Applied biomaterials* **2010**, *93*, 520–530.

[191] A. Pfister, R. Landers, A. Laib, U. Hübner, R. Schmelzeisen, R. Mülhaupt, *Journal of Polymer Science Part A: Polymer Chemistry* **2004**, *42*, 624–638.

[192] A. Bandyopadhyay, S. Bose, S. Das, *MRS Bulletin* **2015**, *40*, 108–115.

[193] C. Wu, Y. Luo, G. Cuniberti, Y. Xiao, M. Gelinsky, *Acta biomaterialia* **2011**, *7*, 2644–2650.

[194] T. Serra, J. A. Planell, M. Navarro, *Acta biomaterialia* **2013**, *9*, 5521–5530.

[195] Y. K. Mishra, S. Kaps, A. Schuchardt, I. Paulowicz, X. Jin, D. Gedamu, S. Freitag, M. Claus, S. Wille, A. Kovalev, S. N. Gorb, R. Adelung, *Particle & Particle Systems Characterization* **2013**, *30*, 775–783.

[196] Y. K. Mishra, S. Kaps, A. Schuchardt, I. Paulowicz, X. Jin, D. Gedamu, S. Wille, O. Lupan, R. Adelung, *KONA Powder and Particle Journal* **2014**, *31*, 92–110.

[197] X. Jin, M. Deng, S. Kaps, X. Zhu, I. Hölken, K. Mess, R. Adelung, Y. K. Mishra, *PloS one* **2014**, *9*, e106991.

[198] S. B. Gutekunst, C. Grabosch, A. Kovalev, S. N. Gorb, C. Selhuber-Unkel, *Beilstein journal of nanotechnology* **2014**, *5*, 1393–1398.

[199] Olympus, Confocal Scanning Systems **2015**,
URL `http://www.olympusconfocal.com/theory/confocalscanningsystems.html`.

[200] G. Kronvall, E. Myhre, *Acta Pathologica Microbiologica Scandinavica Section B Microbiology* **1977**, *85B*, 249–254.

[201] L. R. Groden, J. Rodnite, J. H. Brinser, G. I. Genvert, *Cornea* **1990**, *9*, 122–124.

[202] R. Kanungo, R. Srinivasan, R. S. Rao, *Acta ophthalmologica* **1991**, *69*, 750–753.

[203] T. W. Hahn, T. P. O'Brien, W. J. Sah, J. H. Kim, *Japanese journal of ophthalmology* **1998**, *42*, 108–114.

[204] K. L. Johnson, K. Kendall, A. D. Roberts, *Proceedings of the Royal Society A: Mathematical, Physical and Engineering Sciences* **1971**, *324*, 301–313.

[205] C.-H. R. Kuo, J. Xian, J. D. Brenton, K. Franze, E. Sivaniah, *Advanced materials* **2012**, *24*, 6059–6064.

[206] J. Solon, I. Levental, K. Sengupta, P. C. Georges, P. A. Janmey, *Biophysical Journal* **2007**, *93*, 4453–4461.

[207] M. Beil, A. Micoulet, G. v. Wichert, S. Paschke, P. Walther, M. B. Omary, Van Veldhoven, Paul P, U. Gern, E. Wolff-Hieber, J. Eggermann, J. Waltenberger, G. Adler, J. Spatz, T. Seufferlein, *Nature cell biology* **2003**, *5*, 803–811.

[208] B. Trappmann, J. E. Gautrot, J. T. Connelly, Strange, Daniel G. T., Y. Li, M. L. Oyen, Cohen Stuart, Martien A., H. Boehm, B. Li, V. Vogel, J. P. Spatz, F. M. Watt, Huck, Wilhelm T. S., *Nature materials* **2012**, *11*, 742.

[209] J. Stricker, B. Sabass, U. S. Schwarz, M. L. Gardel, *Journal of physics. Condensed matter : an Institute of Physics journal* **2010**, *22*, 194104.

[210] T. Luo, K. Mohan, P. A. Iglesias, D. N. Robinson, *Nature materials* **2013**, *12*, 1064–1071.

[211] M. L. Gardel, B. Sabass, L. Ji, G. Danuser, U. S. Schwarz, C. M. Waterman, *The Journal of Cell Biology* **2008**, *183*, 999–1005.

[212] B. Sabass, M. L. Gardel, C. M. Waterman, U. S. Schwarz, *Biophysical Journal* **2008**, *94*, 207–220.

[213] D. Riveline, E. Zamir, N. Q. Balaban, U. S. Schwarz, T. Ishizaki, S. Narumiya, Z. Kam, B. Geiger, A. D. Bershadsky, *The Journal of Cell Biology* **2001**, *153*, 1175–1186.

[214] Q. Le Duc, Q. Shi, I. Blonk, A. Sonnenberg, N. Wang, D. Leckband, J. d. Rooij, *The Journal of Cell Biology* **2010**, *189*, 1107–1115.

[215] B. D. Hoffman, C. Grashoff, M. A. Schwartz, *Nature* **2011**, *475*, 316–323.

[216] X. Q. Brown, K. Ookawa, J. Y. Wong, *Biomaterials* **2005**, *26*, 3123–3129.

[217] J. N. Lee, C. Park, G. M. Whitesides, *Analytical chemistry* **2003**, *75*, 6544–6554.

[218] A. Eifert, J. Petit, T. Baier, E. Bonaccurso, S. Hardt, *Applied Surface Science* **2015**, *330*, 104–110.

[219] G. C. Lisensky, D. J. Campbell, K. J. Beckman, C. E. Calderon, P. W. Doolan, Rebecca M. Ottosen, A. B. Ellis, *Journal of Chemical Education* **1999**, *76*, 537.

[220] R. Raninga, K. Page, I. P. Parkin, *Chemical communications* **2014**, *50*, 12656–12658.

[221] E. A. Cavalcanti-Adam, T. Volberg, A. Micoulet, H. Kessler, B. Geiger, J. P. Spatz, *Biophysical Journal* **2007**, *92*, 2964–2974.

[222] N. S. Rossen, A. J. Hansen, C. Selhuber-Unkel, L. B. Oddershede, *PloS one* **2011**, *6*, e25196.

[223] K. Saha, A. J. Keung, E. F. Irwin, Y. Li, L. Little, D. V. Schaffer, K. E. Healy, *Biophysical Journal* **2008**, *95*, 4426–4438.

[224] C. Hidaka, C. Cheng, D. Alexandre, M. Bhargava, P. A. Torzilli, *Cell and tissue research* **2006**, *323*, 127–135.

[225] A. Puliafito, L. Hufnagel, P. Neveu, S. Streichan, A. Sigal, D. K. Fygenson, B. I. Shraiman, *Proceedings of the National Academy of Sciences of the United States of America* **2012**, *109*, 739–744.

[226] M. Stöhr, K. Bommert, I. Schulze, H. Jantzen, *Journal of Cell Science* **1987**, *88*, 579–590.

[227] A. Mattana, C. Serra, E. Mariotti, G. Delogu, P. L. Fiori, P. Cappuccinelli, *Eukaryotic cell* **2006**, *5*, 665–671.

[228] D. Lloyd, S. W. Edwards, J. C. Fry, *Proceedings of the National Academy of Sciences of the United States of America* **1982**, *79*, 3785–3788.

[229] T. D. Pollard, E. D. Korn, *Journal of Biological Chemistry* **1973**, *248*, 4682–4690.

[230] W. Pumidonming, M. Koehsler, J. Walochnik, *Parasitology Research* **2010**, *106*, 553–559.

[231] M. H. Olsen, G. M. Hjortø, M. Hansen, Ö. Met, I. M. Svane, N. B. Larsen, *Lab on a chip* **2013**, *13*, 4800–4809.

[232] R. Pankov, *Journal of Cell Science* **2003**, *116*, 947–948.

[233] J. C. Adams, *Methods in cell-matrix adhesion*, Bd. v. 69 von *Methods in cell biology*, Academic Press, San Diego, CA **2002**.

[234] R. Adelung, M. Claus, S. Kaps, Y. K. Mishra, T. Preuße and C. Wolpert, Elastisches Material mit einem auf Partikelebene durch Nanobrücken zwischen Partikeln überbrückten Porenraum, DE102010012385 A1, **22.03.2010**.

[235] R. Adelung, M. Claus, S. Kaps, Y. K. Mishra, T. Preuße, C. Wolpert, A method for generating an elastic material with a bridged to particle level by nano-bridges between particles pore space, DE102010012385 B4, **22.03.2010**.

[236] M. Mecklenburg, A. Schuchardt, Y. K. Mishra, S. Kaps, R. Adelung, A. Lotnyk, L. Kienle, K. Schulte, *Advanced materials* **2012**, *24*, 3486–3490.

[237] M. J. Sawkins, K. M. Shakesheff, L. J. Bonassar, G. R. Kirkham, *Recent Patents on Biomedical Engineering* **2013**, *6*, 3–21.

[238] A. Möhring, Synthese und Charakterisierung mikroporöser Hydrogelmaterialien für dreidimensionale Traction Force Microscopy von Zellen, Masterthesis **2014**.

[239] F. L. Schuster, M. Levandowsky, *The Journal of eukaryotic microbiology* **1996**, *43*, 150–158.

[240] W.-C. Hung, S.-H. Chen, C. D. Paul, K. M. Stroka, Y.-C. Lo, J. T. Yang, K. Konstantopoulos, *The Journal of Cell Biology* **2013**, *202*, 807–824.

[241] M. Leslie, *The Journal of Cell Biology* **2013**, *202*, 721.

[242] K. M. Stroka, H. Jiang, S.-H. Chen, Z. Tong, D. Wirtz, S. X. Sun, K. Konstantopoulos, *Cell* **2014**, *157*, 611–623.

[243] L. S. Dillon, *Ultrastructure, macromolecules, and evolution*, The Evolution and functioning of the genetic mechanism, Plenum Press, New York **1981**.

[244] B. Alberts, A. Johnson, J. Lewis, M. Raff, K. Roberts, P. Walter, *Molecular biology of the cell*, 4. Aufl., Garland Science, NY. **2002**.

[245] S. Elmore, *Toxicologic pathology* **2007**, *35*, 495–516.

[246] B. Bowers, *The Journal of Cell Biology* **1972**, *53*, 681–694.

[247] B. Bowers, T. E. Olszewski, *The Journal of Cell Biology* **1983**, *97*, 317–322.

[248] A. B. Cohen, M. J. Cline, *The Journal of clinical investigation* **1971**, *50*, 1390–1398.

[249] N. Bowden, A. Terfort, J. Carbeck, G. M. Whitesides, *Science* **1997**, *276*, 233–235.

[250] C. W. Shields, S. Zhu, Y. Yang, B. Bharti, J. Liu, B. B. Yellen, O. D. Velev, G. P. López, *Soft Matter* **2013**, *9*, 9219–9229.

[251] C. W. Shields, D. Sun, K. A. Johnson, K. A. Duval, A. V. Rodriguez, L. Gao, P. A. Dayton, G. P. López, *Angewandte Chemie (International ed.)* **2014**, *53*, 8070–8073.

[252] E. D. Korn, R. A. Weisman, *The Journal of Cell Biology* **1966**, *34*, 219–227.

[253] J. R. Stewart, *The Journal of Cell Biology* **1972**, *52*, 117–130.

[254] H. H. Sim, Fluorescent marker comprising double bond ester group and method for marking and detecting the same, WO2007037586 A1, **22.08.2005**.

[255] S. Klein, V. Manoharan, D. Pine, F. Lange, *Colloid and Polymer Science* **2003**, *282*, 7–13.

[256] W. C. Griffin, *J. Soc. Cosmetics Chemist* **1949**, 311–326.

[257] R. W. Behrens, W. C. Griffin, *Soap Sanit. Chem.* **1951**.

[258] W. C. Griffin, *J. Soc. Cosmetics Chemist* **1954**, 249–256.

[259] P. M. Kruglyakov, *Hydrophile - Lipophile Balance of Surfactants and Solid Particles: Physicochemical aspects and applications*, Studies in Interface Science, Elsevier Science **2000**.

[260] M. Rieger, L. D. Rhein, *Surfactants in Cosmetics, Second Edition*, Surfactant Science, Taylor & Francis **1997**.

[261] A. Grubenmann, H. Mollet, *Formulation technology: Emulsions : suspensions : solid forms*, Wiley-VCH, Weinheim **2001**.

[262] J. T. DAVIES, Hg., *A quantitative kinetic theory of emulsion type, I. Physical chemistry of the emulsifying agent* **1957**.

[263] D. Schuster, *Encyclopedia of Emulsion Technology: Basic Theory, Measurement, Applications*, Encyclopedia of Emulsion Technology, Taylor & Francis **1987**.

[264] A. Fahr, *Voigt Pharmazeutische Technologie: Für Studium und Beruf*, Wissen und Praxis, 12. Aufl., Deutscher Apotheker Verlag, Stuttgart **2015**.

[265] H. H. J. Hager, F. v. Bruchhausen, *Hagers Handbuch der pharmazeutischen Praxis*, 5. Aufl., Springer, Berlin **1990-2000**.

[266] K. Ziani, J. Oses, V. Coma, J. I. Maté, *LWT - Food Science and Technology* **2008**, *41*, 2159–2165.

[267] J.-W. Janiesch, M. Weiss, G. Kannenberg, J. Hannabuss, T. Surrey, I. Platzman, J. P. Spatz, *Analytical chemistry* **2015**, *87*, 2063–2067.

[268] Grundlagen Partikelgrößen- und Formberechnung durch Bildanalyse **2015**, URL `https://www.sympatec.com/DE/ImageAnalysis/Fundamentals.html`.

[269] J. Guck, R. Ananthakrishnan, H. Mahmood, T. J. Moon, C. C. Cunningham, J. Käs, *Biophysical Journal* **2001**, *81*, 767–784.

[270] M. Dao, C. T. Lim, S. Suresh, *Journal of the Mechanics and Physics of Solids* **2003**, *51*, 2259–2280.

[271] M. J. Padgett, J. E. Molloy, D. McGloin, Hg., *Optical tweezers: Methods and applications*, Series in optics and optoelectronics, CRC Press/Taylor & Francis, Boca Raton, Fla **2010**.

[272] A. S. Urban, S. Carretero-Palacios, A. A. Lutich, T. Lohmüller, J. Feldmann, F. Jäckel, *Nanoscale* **2014**, *6*, 4458–4474.

[273] P. Mulser, *Journal of the Optical Society of America B* **1985**, *2*, 1814.

[274] J. Kepler, *De cometis libelli tres*, typis Andreae Apergeri, Augustae Vindelicorum **1619**.

[275] P. Apian, *Ein kurtzer bericht der observation unnd urtels des jüngst erschinnen cometen im Weinmon und wintermon dises XXXII. jars*, Apian, Ingolstadt **1532**.

[276] L. Euler, *I. Solutio Problematis Mechanici De Motu Corporum Tubis Mobilibus Inclusorum. II. Nova Tabulæ Astronomicæ Motuum Solis Ac Lunæ. III. Nova Theoria Lucis Et Colorum. IV. De Perturbatione Motus Planetarum A Resistentia Ætheris Orta. V. Enodatio Quæstionis: An Materiæ Facultas Cogitandi Tribui Possit? VI. Recherches Sur La Nature Des Moindres Particules Des Corps*, Bd. [1] von *L. Euleri Opuscula Varii Argumenti*, sumtibus Ambr. Haude & Jo. Carol Speneri, Berolini **1746**.

[277] Casper Hakfoort, In *Optics in the age of Euler*. Cambridge University Press **1995**, 72–116.

[278] W. Crooks, *Philos. Trans. R. Soc. London* **1874**, 501–527.

[279] P. N. Lebedev, *Ann. Phys.* **1901**, 433–458.

[280] E. F. Nichols, G. F. Hull, *Phys. Rev.* **1901**, 307–320.

[281] E. F. Nichols, G. F. Hull, *Phys. Rev.* **1903**, 557–559.

[282] R. C. Carrington, *Mon. Not. R. Astron. Soc.* **1859**, *20*, 13–15.

[283] L. Biermann, *Zeitschrift für Astrophysik* **1951**, *29*, 274–286.

[284] L. Biermann, B. Brosowski, H. U. Schmidt, *Solar Physics* **1967**, *1*, 254–284.

[285] J. C. Maxwell, *A treatise on electricity and magnetism. Vol. 2*, Clarendon press (Oxford) **1873**.

[286] A. Bartoli, Il calorico raggiante e il secondo principio di termodynamica **1884**.

[287] R. G. Gould, In *The Ann Arbor Conference on Optical Pumping: The University of Michigan*, 128.

[288] P. A. Franken, R. H. Sands, *The Ann Arbor Conference on Optical Pumping: The University of Michigan, June 15 Through June 18, 1959*, The Ann Arbor Conference **1959**.

[289] A. Ashkin, *Physical Review Letters* **1970**, *24*, 156–159.

[290] A. Ashkin, J. M. Dziedzic, J. E. Bjorkholm, Steven Chu, *Opt. Lett.* **1986**, *11*, 288–290.

[291] A. Ashkin, J. Dziedzic, *Science* **1987**, *235*, 1517–1520.

[292] M. D. Wang, H. Yin, R. Landick, J. Gelles, S. M. Block, *Biophysical Journal* **1997**, *72*, 1335–1346.

[293] M. Streichfuss, F. Erbs, K. Uhrig, R. Kurre, A. E.-M. Clemen, Böhm, Christian H J, T. Haraszti, J. P. Spatz, *Nano Letters* **2011**, *11*, 3676–3680.

[294] Scot C. Kuo, *Microscop. Microanal.* **1995**, *1*, 65–74.

[295] G. Mie, *Annalen der Physik* **1908**, *330*, 377–445.

[296] K. Svoboda, S. M. Block, *Annual review of biophysics and biomolecular structure* **1994**, *23*, 247–285.

[297] T. Winther, L. Xu, K. Berg-Sørensen, S. Brown, L. B. Oddershede, *Biophysical Journal* **2009**, *97*, 1305–1312.

[298] TechNote 203: Washing Microspheres **18.March.2013**.

[299] J. Arlt, V. Garces-Chavez, W. Sibbett, K. Dholakia, *Optics Communications* **2001**, *197*, 239–245.

[300] V. Bingelyte, J. Leach, J. Courtial, M. J. Padgett, *Applied Physics Letters* **2003**, *82*, 829.

[301] L. G. Simonson, A. E. Liberta, A. Richardson, *Applied microbiology* **1975**, *30*, 855–861.

[302] Einzeller des Jahres 2012 **2012**.

[303] J. A. Champion, S. Mitragotri, *Proceedings of the National Academy of Sciences of the United States of America* **2006**, *103*, 4930–4934.